Native expression of voltage-gated potassium channels in the mouse striatum and their plasticity in models of Parkinson's and Alzheimer's diseases

This thesis is submitted in partial fulfilment of the requirements for the award of the degree of Doctor of Philosophy of the University of Portsmouth

Babajide Otuyemi, PhD

April 2020

For my wife, Motunrayo, and kids, Tiolulope, Adegbuyi and Ireayo.

Abstract

Disruption of the normal patterns of expression, localisation and function of potassium channels in brain neurons has emerged as a likely pathophysiological basis for stress-induced mental illnesses, Parkinson's and Alzheimer's disease, with the striatum as a particular brain region of interest. Among the major classes of potassium channels, voltage-gated potassium channels are known to play a major role in regulating neuronal excitability. However, expression of voltage-gated potassium channel subtypes in the striatum have not been well established. In this research, a mouse model of early life stress was used for chronic stress while SNCH-OVX and APP-PSEN1 transgenic mouse models were used to model Parkinson's and Alzheimer's disease respectively and compared to their wild type littermates as controls to investigate how the native expression patterns of different voltage-gated potassium channel sub-families within the mouse striatum changes in response to stress and pathology associated with Parkinson's and Alzheimer's disease. This led to the characterisation of the expression patterns of different voltage-gated potassium channel subtypes and the neurochemical inputs they integrate in the striatum. Furthermore, the data indicated voltage-gated potassium channels to be highly plastic in response to life experience, provided insights into the earliest functional changes in Parkinson's disease, and showed the resilience of striatal neurochemicals to Alzheimer's disease pathology. Therefore, psychosocial stress and neurodegenerative disease pathology alters the expression of specific voltage-gated potassium channels in distinct cell types of the striatum. The

expected changes in neuronal excitability arising from such changes could contribute to pathology of such conditions.

Summary of Findings

The broad aims of my PhD project were to determine the native expression patterns of different voltage-gated potassium channels (K_v) sub-families, their cellular and subcellular localisation within the mouse striatum, the neurochemical inputs they integrate and how these changes in response to stress or pathology associated with Parkinson's disease (PD) and Alzheimer's disease (AD). The importance of this work is founded on the central role that K_v play in contributing to the diversity of neuronal activity patterns across different populations of neurons and the need for neurons to express chemicals to integrate inputs from different brain regions. Whilst K_v subfamilies have been extensively characterised in many regions of the brain such as the hippocampus and cortex, relatively less is known about K_v expression in the striatum. This represents an important gap in the scientific literature since a range of debilitating brain disorders are associated with altered neuronal activity of striatal neurons. Given the major roles that K_v serve in regulating neuronal activity, identifying the native expression in this brain region will provide a platform for understanding their potential roles, and thus suitability as therapeutic targets, in such medical conditions. In my PhD research, I therefore have firstly provided the first high resolution immunolocalisation of the native expression patterns for different K_v subtypes. I then investigated whether such expression patterns are susceptible to life experience, or pathology relating to specific neurodegenerative diseases, namely Alzheimer's and Parkinson's.

My main findings were:

1. RT-PCR revealed that the mouse striatum expresses mRNA for $K_v1.1$, $K_v1.2$, $K_v1.3$, $K_v1.4$, $K_v1.5$, $K_v1.6$, $K_v2.1$, $K_v2.2$, $K_v3.1$, $K_v3.3$, $K_v3.4$, $K_v4.2$, $K_v5.1$, $K_v7.1$, $K_v7.2$, $K_v7.3$ and $K_v7.4$ (**Chapter three**).

2. Immunohistochemistry and confocal microscopy revealed that different sub-families of K_v are targeted to different striatal cell types. For example, $K_v2.1$ and 4.2 were exclusively expressed on the principal cells of the striatum, called medium spiny neurons (MSNs), whereas $K_v3.1$ and 4.3 were only expressed on inhibitory interneurons (**Chapter three**).

3. Immunohistochemistry and confocal microscopy revealed that different sub-families of K_v are targeted to different sub-cellular compartments. For example, members of the K_v1 family were exclusively expressed on neurochemically diverse axons, originating from other brain region, and innervate MSNs. Furthermore, $K_v2.1$ signal was restricted to the cell body and proximal dendritic regions of MSNs whilst the $K_v4.2$ was targeting to their distal dendrites. (**Chapter three**).

4. Immunohistochemistry and confocal microscopy revealed that different sub-families of K_v are targeted to non-neuronal cells within the striatum. For example, $K_v1.6$ was exclusively expressed on immune modulating

microglia, whereas K_v1.5 was expressed on oligodendrocyte precursor cells (**Chapter three**).

5. Quantitative immunohistochemistry revealed that in response to early life stress, there was significant decrease in the expression of K_v2.1 in the ventral striatum but not the dorsal striatum, K_v4.2 both in the ventral and dorsal striatum, and IBA1, a marker of inflammation, both in the ventral and dorsal striatum (**Chapter three**).

6. Immunohistochemistry with confocal microscopy revealed that in a mouse model of PD (OVX), alpha-synuclein, a key molecule in PD pathology, was associated with glutamatergic axons originating from the cortex as well as axon terminals from local GABAergic interneurons, together with dopaminergic and noradrenergic axons (**Chapter four**).

7. Quantitative reverse transcription polymerase chain reaction (qRT-PCR) of WT and OVX mice revealed changes in the expression of genes encoding for diverse axonal inputs, namely tyrosine hydroxylase (TH), tryptophan hydroxylase 1 (TPH1) and K_v4.3 at the mRNA level, with TH and K_v4.3 being increased significantly while TPH1 was decreased significantly in the striatum of OVX mice (**Chapter four**).

8. Quantitative immunohistochemistry with confocal microscopy revealed that in OVX mice, there were significant decrease in the expression of

dopamine- and cyclic-AMP-regulated phosphoprotein of molecular weight 32 kDa (DARPP-32), a protein responsible for regulating the phosphorylation of dopamine receptors, the inflammation marker IBA1, and K_v2.1, 4.2 and 4.3. (**Chapter four**).

9. Using immunohistochemistry with confocal microscopy, I demonstrated that amyloid beta, a pathological feature of AD is expressed in sub-populations of MSNs, cholinergic interneurons and parvalbumin containing GABAergic interneurons (**Chapter five**).

10. qRT-PCR and quantitative immunoreactivity revealed that neurochemicals within the striatum are resilient to AD pathology with only a decrease in K_v4.3 expression being observed (**Chapter five**).

Table of Contents

Declaration

Whilst registered as a candidate for the above degree, I have not been registered for any other research award. The results and conclusions embodied in this thesis are the work of the named candidate and have not been submitted for any other academic award.

Word count: 28,844

Table of Figures

Chapter one

Chapter two

Chapter three

Chapter four

Chapter five

Table of Tables

Chapter two

Chapter three

List of Abbreviations

Aβ	Amyloid beta
Aβ40	Aβ with 40 amino acids
Aβ42	Aβ with 42 amino acids
AβO	Amyloid beta oligomer
AChE	Acetylcholinesterase
AD	Alzheimer's disease
AIS	Axon initial segment
α-syn	Alpha-synuclein
APP	Aβ precursor protein
ATP	Adenosine triphosphatase
BACE1	β-site APP-cleaving enzyme 1
BK_{Ca}	Large conductance Ca^{2+}-activated potassium channel
Ca	Calcium
CA	Cornu Ammonis
cDNA	Complementary Deoxyribonucleic acid
ChAt	Choline acetyltransferase
CNS	Central nervous system
CRH	Corticotrophin-releasing hormone
DARPP-32	Dopamine- and cyclic-AMP-regulated phosphoprotein of molecular weight 32 kDa
DAT	Dopamine transporter
DBH	Dopamine β-hydroxylase
DNA	Deoxyribonucleic acid
D1R	Dopamine 1 receptor

D2R	Dopamine 2 receptor
ELS	Early life stress
GABA	γ-aminobutyric acid
GIRK	G protein-gated inwardly-rectifying potassium channel
GOI	Gene of interest
GPi	Internal globus pallidus
GPe	External globus pallidus
HPA	Hypothalamic-pituitary-adrenocortical
HUGO	Human Genome Organisation
I_A	A-type potassium current
IBA1	Ionized calcium binding adaptor molecule 1
IK_{Ca}	Intermediate conductance Ca^{2+}-activated potassium channel
K	Potassium
KCh	Potassium channel
K_{Ca}	Ca^{2+}-activated potassium channel
K_{ir}	Inwardly-rectifying potassium channel
K_{2P}	Two-pore potassium channel
K_v	Voltage-gated potassium channel
LB	Lewy bodies
L-DOPA	L-3,4-dihydroxyphenylalanine
MAP-2	Microtubule associated protein
mRNA	Messenger ribonucleic acid
MSN	Medium spiny neuron
Na	Sodium
NAC	Non-amyloid- β component

NADPH	Nicotinamide adenine dinucleotide phosphate
NFT	Neurofibrillary tangle
NG2	Neuron-glial antigen 2
NOS	Nitric oxide synthase
OPC	Oligodendrocyte precursor cells
OVX	Over-expresses alpha-synuclein
PD	Parkinson's disease
PFA	Paraformaldehyde
PKA	cAMP-dependent protein kinase
pS	Picosiemens
PV	Parvalbumin
qRT-PCR	Quantitative reverse transcription polymerase chain reaction
RNA	Ribonucleic acid
RT-PCR	Reverse transcription polymerase chain reaction
SK_{Ca}	Small conductance Ca^{2+}-activated potassium channel
SLC6A4	Serotonin transporter gene
SNc	substantia nigra pars compacta
SNCA	Synuclein alpha
SNr	Substantia nigra pars reticulata
TALK	TWIK-related alkaline pH-activated K_{2P}
TASK	TWIK-related acid-sensitive K_{2P}
TG	Transgenic
TH	Tyrosine hydroxylase
THIK	tandem pore halothane-inhibited K_{2P}
TPH	Tryptophan hydroxylase

TRAAK	TWIK-related and arachidonic acid stimulated K_{2P}
TRESK	TWIK-related spinal cord K_{2P}
TWIK	tandem pore, weak inwardly rectifying K_{2P}
VAchT	Vesicular acetylcholine transporter
VGAT	Vesicular γ-aminobutyric acid transporter
VGLUT1-2	Vesicular glutamate transporter 1 and 2
VMAT2	Vesicular monoamine transporter 2
WT	Wild-type

Acknowledgements

Foremost, I want to give thanks to God Almighty for the grace and strength given me throughout my doctoral training. To my supervisor and coach, Dr Jerome Swinny, I am eternally grateful for assisting me in the face of challenges and directing my research path. Your enthusiasm and dedication to scientific discovery shaped me to become a better scientist throughout my doctoral training. Thank you. I would also like to thank my co-supervisors, Dr Marisa Van Der Merwe and Dr Paul Cox for their encouragement and support.

I appreciate the support of the past and present members of SwinnyLab™ whose graciousness and warmth have been of great value. I would also like to thank the occupants of SM 5.12 for making the office sociable.

To my wonderful family: my parents, Mr and Mrs T.O Otuyemi; my siblings, Adeniyi, Olalekan and Oluwakemi; and my in-laws, Mr and Mrs B.A Adeyemi. Your encouragement and support helped me throughout.

Finally, I would like to thank my nearest and dearest: my wife, Motunrayo and my kids; Tiolulope, Adegbuyi, and Ireayo. Your love, companionship and support throughout greatly enhanced the experience.

Dissemination

Conference presentations

Oral presentation

University of Portsmouth Science Together Postgraduate Research Conference- Portsmouth, June 2017.

Poster presentations

1. The UK PharmSci Conference, University of Strathclyde- Glasgow, September 2016.
2. Global Experts Meeting on Frontiers in Alzheimer's Disease and Dementia- Rome, October 2019.

Chapter One

General introduction

Ion channels

Ion channels are macromolecules, embedded within biological lipid bi-layer membranes, for the primary purposes of allowing the flow of ions across cellular compartments, with high degree of specificity (Viviani, Gardoni and Marinovich, 2007). As such, they are integral to various intracellular and extracellular processes, from single cell to multicellular organisms, and organs system. In the organ that forms the focus of my PhD research, the mammalian brain, various ion channels classes regulate various aspects of development via cell adhesion and cell migration as well as cellular (neurons and glia) communication, (Kumar, Kumar, Jha, Jha and Rashmi K Ambasta, 2016). The cardinal properties of ion channels are ion selectivity and gating. Selectivity refers to the ability of some channels to discriminate between ion species. This is achieved through a physical–chemical interaction between the ion and various amino acid residues lining the channel. Gating is the process of transition between the open and closed states (Viviani, Gardoni and Marinovich, 2007).

Ion channels allow the flow of ions down their electrochemical gradient from one side of a membrane to the other and form a very diverse group of proteins found in the cell membrane as well as in the membrane of intracellular compartments (Vizcaya-ruiz and Camacho, 2010). They also activate enzymes linked to cellular signalling pathways, serve as cell adhesion

molecules or components of the cytoskeleton, and their activity can alter the expression of specific genes (Kaczmarek, 2006).

Ion channels can be classified based on the main ion to which they are selective under physiological conditions. These include sodium, chloride, calcium and potassium.

Potassium channels are the focus of my PhD research and will therefore restrict my assessment to this class.

Overview of potassium channels and their contribution to neuronal activity

Potassium (K^+) channels are multipass transmembrane polypeptides that contain the K^+ selective pore that selectively conduct K^+ across cell membrane as well as the domains that allow them to respond to diverse stimuli (Trimmer and Rhodes, 2004). They are found in both excitable and non-excitable cells that are involved in diverse cellular processes including cell proliferation, apoptosis, hormone secretion, K^+ homeostasis, neurotransmitter release and modulation of the action potential (Bauer and Schwarz, 2001) (Burg, Remillard and Yuan, 2006). For the purposes of this chapter, I will focus on K^+ channels (KCh) and their roles in neuronal function.

KCh are synthesized in the endoplasmic reticulum and specifically transported to their functional site of action, which in neurons, is predominantly the plasma membrane. Once KCh reach their final place, the ion channel complex is retained either by interaction with other signalling proteins or by scaffolding mechanisms. The selective localisation of KCh into different cell types and subcellular compartments is crucial for their primary role in brain function,

which is the maintenance and physiological regulation of normal neuronal activity through contributing to the membrane potential of individual neurons (Andrea Lorincz and Nusser, 2008) (Trimmer, 2015).

At rest, neuronal membranes are polarised, due to the unequal distribution of charge, in the form of ions, across their surfaces (Fig 1.1).

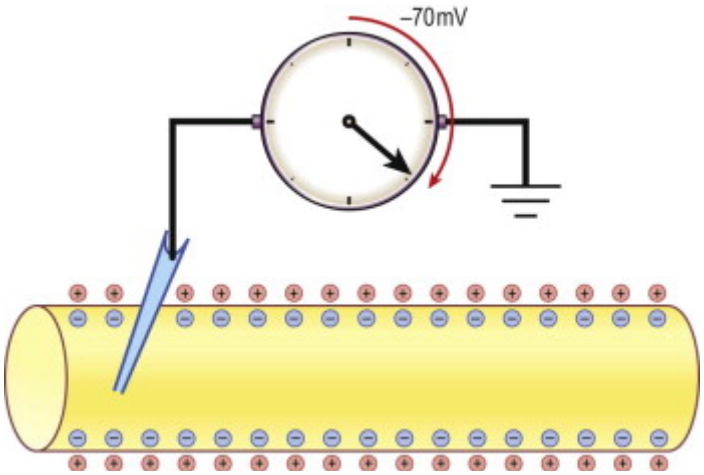

Figure 1.1. Schematic depiction of the polarised neuronal membrane (Tigner and Cornell, 2014).

Sodium (Na) and K ions make the major contribution to this charge differential, with the extracellular compartments concentrated with Na, and intracellular compartments enriched with K, via the sodium-potassium adenosine triphosphatase (ATPase) exchange pump (Fig 1.2).

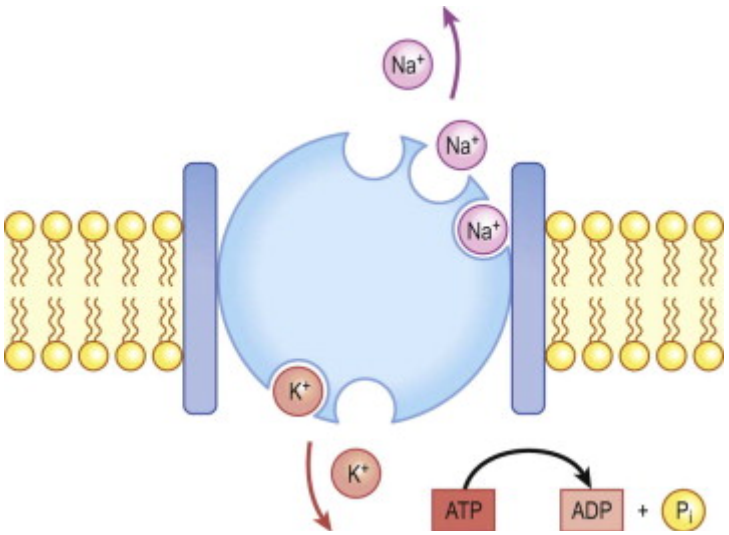

Figure 1.2. Schematic depiction of the unequal distribution of Na and K ions across neuronal membranes via the Na-K ATPase pump (Tigner and Cornell, 2014).

The primary purpose of KCh in neurons is to dampen their excitability by facilitating hyperpolarisation. Therefore, they are principally involved in counteracting phases of excitability, or depolarisation, especially following an action potential (Fig 1.3).

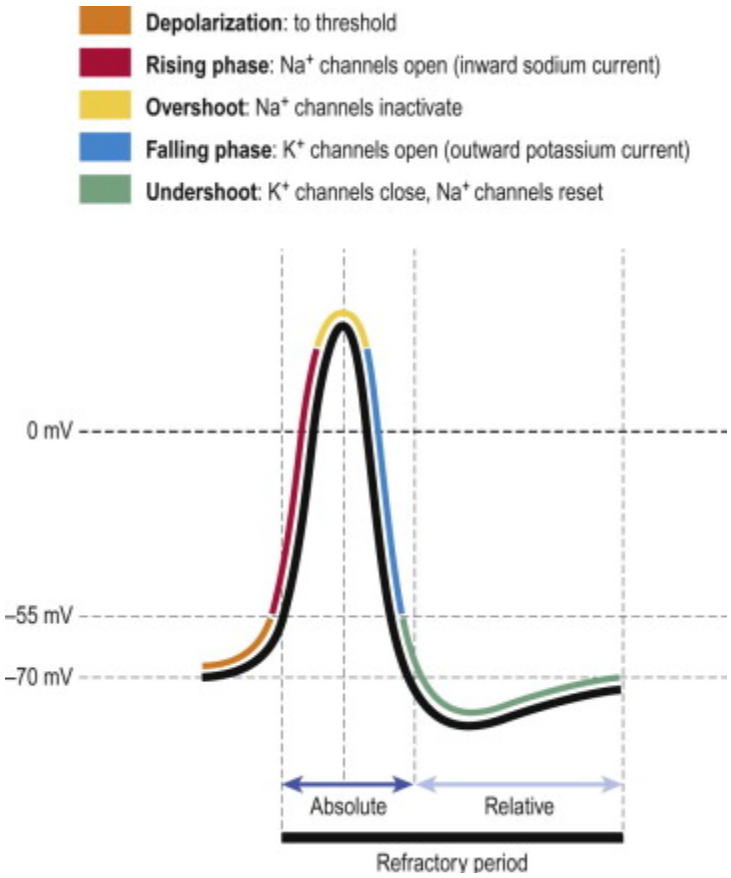

Figure 1.3. Schematic depiction of the role of KCh in counteracting neuronal activity by facilitating the hyperpolarising phase of the action potential (Tigner and Cornell, 2014).

KCh are made up of α subunits and are classified based on the number of transmembrane domains in the α subunit and the mode of activation. KCh have been grouped into the following classes: six transmembrane domains, formed by the voltage-activated and Ca^{2+} activated KCh; four transmembrane domains, formed by the two-pore KCh; and two transmembrane domains, formed by the inward-rectifying KCh (Gutman *et al.*, 2005). Thus, the four major classes of KCh are: Ca^{2+}-activated KCh (K_{Ca}), Inwardly-rectifying KCh

(K_{ir}), Two-pore KCh (K_{2P}) and Voltage-gated KCh (K_v) (Vizcaya-ruiz and Camacho, 2010) (Fig 1.4).

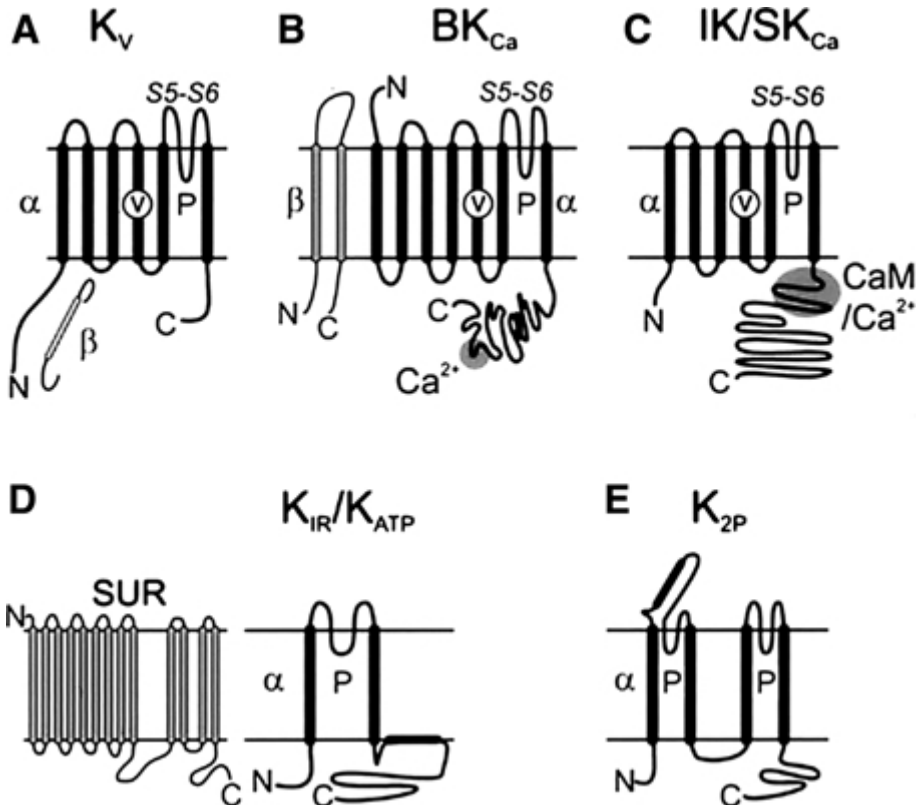

Figure 1.4. Schematic representation of the four classes of potassium channels: (A) K_v, (B) BKCa, (C) IK/SKCa, (D) KIR/KATP, (E) K2P channels. Pore-forming α subunits are highlighted in the grey boxes. Pores are identified as "P" and voltage sensor as "V". C-terminal Ca2+ binding domains are depicted for BKCa and IK/SKCa channels (Burg, Remillard and Yuan, 2006).

Ca^{2+}-activated KCh (K_{Ca})

Molecular structure

Each α subunit of K_{Ca} consists of six transmembrane-spanning domains with both amino and carboxyl termini on the intracellular side of the membrane and a pore domain formed by the last two transmembrane domains (Wei *et al.*, 2005). K_{Ca} are subcategorized into large conductance (>200 pS) K_{Ca} (BK_{Ca}), intermediate conductance (50-200 pS) K_{Ca} (IK_{Ca}) and small conductance (2-15 pS) K_{Ca} (SK_{Ca}) based on single channel conductance. BK_{Ca} channel α subunits have an additional N-terminus segment, which allows for interaction

with membrane-spanning regulatory β subunits. SK_{Ca} and IK_{Ca} have fewer positive residues in the voltage sensor (S4 transmembrane domain) than BK_{Ca}. BK_{Ca} and IK/SK_{Ca} channel subunits assemble as tetramers, with β subunits in the case of BK_{Ca} (Burg, Remillard and Yuan, 2006). Each α subunit of K_{Ca} consists of six transmembrane-spanning domains with both amino and carboxyl termini on the intracellular side of the membrane and a pore domain formed by the last two transmembrane domains (Wei *et al.*, 2005).

Biophysical properties and expression patterns

α subunits of K_{Ca} channels assemble in the plasma membrane forming homo- or heterotetrameric structures. Auxiliary β subunits can also co-assemble, thereby influencing channel expression and modulating the biophysical properties of the channels. Functionally, K_{Ca} are involved in the regulation of neuronal firing properties, blood flow and cell proliferation.

K_{Ca} are present in excitable and non-excitable cells and open on activation by low concentrations of Ca^{2+}, resulting in hyperpolarization of the membrane potential and changes in cellular excitability. (Luján, 2010). K_{Ca} have also been found in secretory cells in which their activation results in the closing of voltage-dependent Ca channels thus providing a negative feedback to regulate Ca entry (Rudy, 1988).

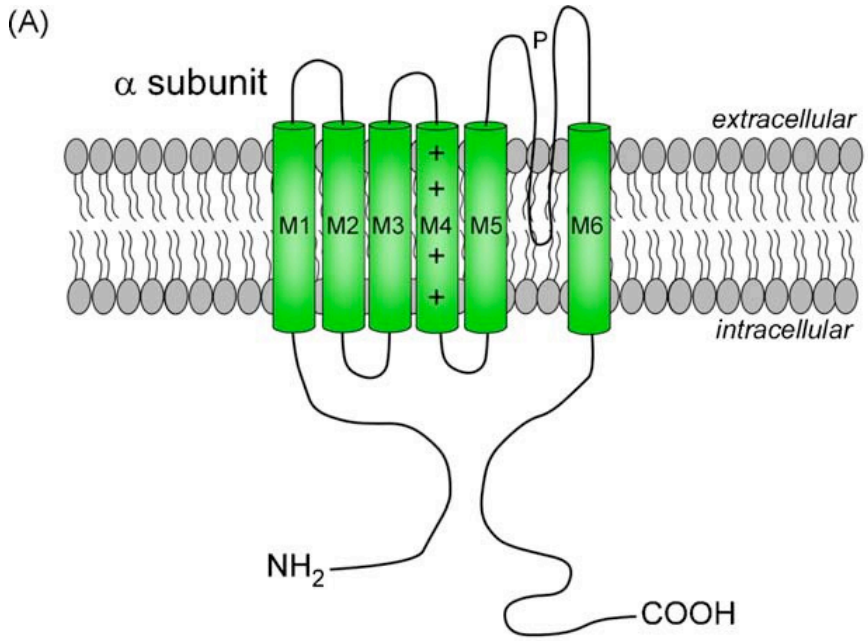

(B)

Channel	Gene	Other names	Subcellular localization
$K_{Ca}1.1$	*KCNMA1*	Slo1, MaxiK, BK	Somata, dendrites, axon terminals
$K_{Ca}2.1$	*KCNN1*	$SK_{Ca}1$, SK1	Dendrites, spines, axon terminals
$K_{Ca}2.2$	*KCNN2*	$SK_{Ca}2$, SK2	Dendrites, spines, axon terminals
$K_{Ca}2.1$	*KCNN3*	$SK_{Ca}3$, SK3	Somata, dendrites, spines, axon terminals
$K_{Ca}3.1$	*KCNN4*	$IK_{Ca}1$, IK	Mainly absent in brain
$K_{Ca}4.1$	*KCNT1*	Slo2.2, Slack	Somata, dendrites, axon terminals
$K_{Ca}4.2$	*KCNT2*	Slo2.1, Slick	Somata, dendrites, axon terminals
$K_{Ca}5.1$	*KCNU1*	Slo3	Mainly absent in brain

Figure 1.5. Subunit composition of K_{Ca} principal subunits in mammalian central neurons. (A) Schematic representation of a single K_{Ca} α subunit. The K_{Ca} are composed of four α subunits each containing six transmembrane segments (M1–M6) and a conducting pore (P) between M5 and M6, and a voltage sensor (positive charge of amino acid residues) located at M4. (B) Classification, genetic nomenclature, and well-characterized subcellular localization of K_{Ca} α subunits (Luján, 2010).

Inwardly-rectifying KCh (K_{ir})

Molecular structure

K_{ir} have two membrane-spanning domains and a conserved pore-forming loop domain or P region and also assemble as tetramers. An additional membrane-bound cytoplasmic α helix, the slide helix, can move laterally to displace the inner helix and is involved in K_{ir} channel gating. The large C-terminal domain is also believed to contribute to pore structure formation. In the closed state, the K_{ir} C-terminus covers the cytoplasmic side of the pore and causes

conformational changes that preclude K^+ permeation (Burg, Remillard and Yuan, 2006).

Biophysical properties and expression patterns

K_{ir} are characterized by their inward-rectifying current–voltage relationship. Inward rectification refers to an increased K^+ conductance upon hyperpolarization and a decreased conductance upon depolarization. Under physiological conditions, K_{ir} allow the outward flow of K^+ only when cells are near their resting potential, but these channels are blocked when the cells are depolarized. Thus, K_{ir} modulate cell excitability and are involved in the repolarization of action potentials, setting the resting potential of the neuron, and contributing to K^+ homeostasis. K_{ir} are widely expressed in excitable and non-excitable cells, generated by the homo- or heterotetrameric arrangement of α subunits, and are often associated with additional β subunits. Each α subunit consists of two transmembrane-spanning domains with both amino and carboxyl termini on the intracellular side of the membrane, a re-entrant P loop, and a pore domain located between the two transmembrane domains. K_{ir} are formed by at least sixteen subunits subdivided into seven subfamilies ($K_{ir}1$–$K_{ir}7$) with different functional properties. Among the seven K_{ir} channel subfamilies, the $K_{ir}3$ subfamily, also known as G protein-gated K_{ir} (GIRK) are widely expressed in the CNS and are a key determinant of membrane excitability because they mediate the postsynaptic inhibitory effect of many neurotransmitters (Luján, 2010). K_{ir} have also been found in skeletal muscle, cardiac muscle, eggs of many animals and several vertebrate and invertebrate neurons (Rudy, 1988).

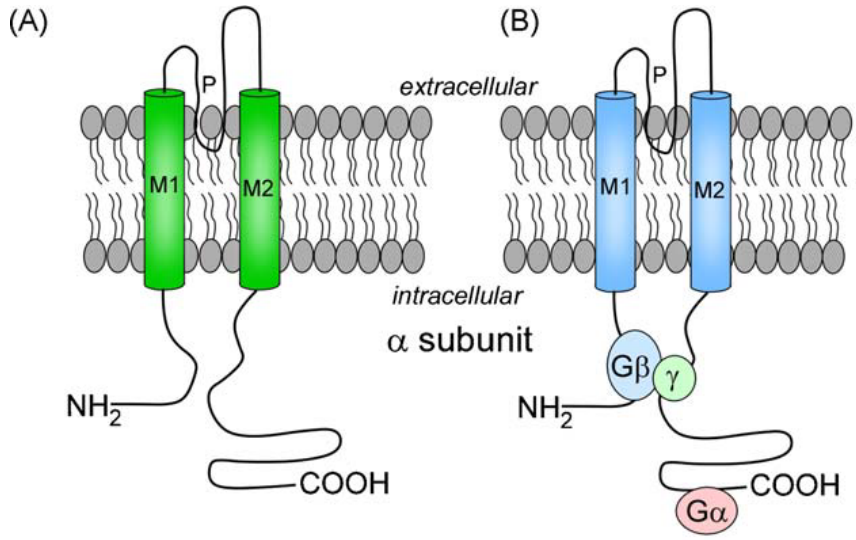

(C)

Channel	Gene	Other names	Subcellular localization
Kir1.1	*KCNJ1*	ROMK, ROMK1	Somata, dendrites
Kir2.1	*KCNJ2*	IRK1	Somata, dendrites
Kir2.2	*KCNJ12*	IRK2, hIRK	Somata, dendrites
Kir2.3	*KCNJ4*	IRK3, hIRK2	Somata, dendrites, synaptic
Kir2.4	*KCNJ14*	IRK4	Somata, dendrites
Kir3.1	*KCNJ3*	GIRK1, KGA	Somata, dendrites, axon terminals
Kir3.2	*KCNJ6*	GIRK2	Somata, dendrites, synaptic, axon terminals
Kir3.3	*KCNJ9*	GIRK3	Somata, dendrites, synaptic, axon terminals
Kir3.4	*KCNJ5*	GIRK4	Somata, dendrites, axon terminals
Kir4.1	*KCNJ10*	K_{AB}-2, BIR10	Glia
Kir4.2	*KCNJ15*	Kir1.3, IRKK	Unknown
Kir5.1	*KCNJ16*	BIR 9	Glia
Kir6.1	*KCNJ8*	uKATP-1	Axon terminals
Kir6.2	*KCNJ11*	BIR	Axon terminals
Kir7.1	*KCNJ13*	Kir1.4	Unknown

Figure 1.6. Subunit composition of K_{ir} principal subunits in mammalian central neurons. (A) Schematic representation of a single K_{ir} α subunit. The K_{ir} are composed of four subunits each containing two transmembrane segments (M1 and M2) and a P loop (P) located in between these two segments. (B) Schematic representation of the Kir3 α subunit, showing the association of the G protein subunits (α, β and γ) with the N- and C termini of the channel. (C) Classification, genetic nomenclature, and well-characterized subcellular localization of K_{ir} α subunits (Luján, 2010).

Two-pore KCh (K_{2P})

Molecular structure

K_{2P} have four transmembrane domains and two ion-conducting pores. Functional K_{2P} exist as homo- or hetero-dimers. There are six structural and functional groups of K_{2P} which include: tandem pore, weak inwardly rectifying K_{2P} (TWIK), TWIK-related acid-sensitive K_{2P} (TASK), TWIK-related and arachidonic acid stimulated K_{2P} (TRAAK), TWIK-related alkaline pH-activated

K_{2P} (TALK), tandem pore halothane-inhibited K_{2P} (THIK), and TWIK-related spinal cord K_{2P} (TRESK) (Burg, Remillard and Yuan, 2006).

Biophysical properties and expression patterns

Activation of K_{2P} is associated with a strong membrane hyperpolarization (Burg, Remillard and Yuan, 2006). The activity of K_{2P} contributes significantly to the background leak K^+ currents that form and maintain the resting membrane potential of living cells (Goldstein *et al.*, 2005) (Luján, 2010).

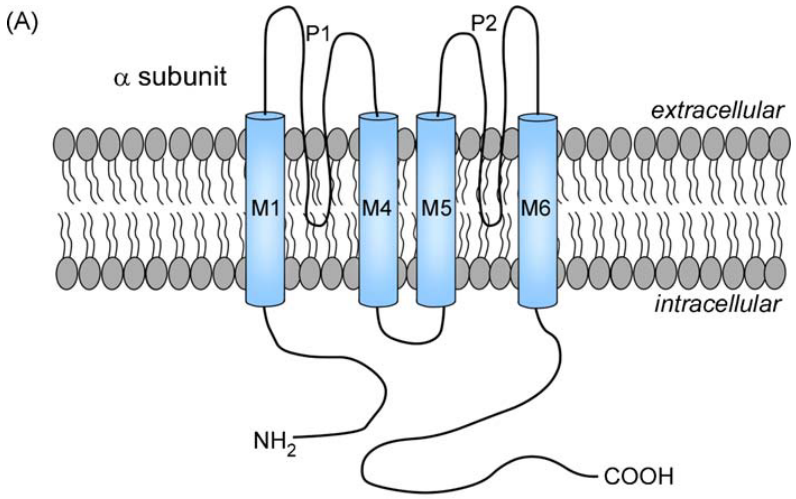

(B)

Channel	Gene	Other names
K_{2P}1.1	*KCNK1*	TWIK-1, hOHO
K_{2P}2.1	*KCNK2*	TREK-1, TPKC1
K_{2P}3.1	*KCNK3*	TASK-1, TBAK-1, OAT-1
K_{2P}4.1	*KCNK4*	TRAAK
K_{2P}5.1	*KCNK5*	TASK-2
K_{2P}6.1	*KCNK6*	TWIK-2, TOSS
K_{2P}7.1	*KCNK7*	kcnk8
K_{2P}9.1	*KCNK9*	TASK-3
K_{2P}10.1	*KCNK10*	TREK-2
K_{2P}12.1	*KCNK12*	THIK-2
K_{2P}13.1	*KCNK13*	THIK-1
K_{2P}15.1	*KCNK15*	TASK-5, KT3.3
K_{2P}16.1	*KCNK16*	TALK-1
K_{2P}17.1	*KCNK17*	TASK-4, TALK-2
K_{2P}18.1	*KCNK18*	TRESK-1, TRESK-2

Figure 1.7. Subunit composition of K_{2P} principal subunits in mammalian central neurons. (A) Schematic representation of a single K_{2P} α subunit. The K_{2P} are composed of four subunits each containing four transmembrane segments (M1, M2, M3 and M4) and two P loops (P1 and P2). (B) Classification and genetic nomenclature of K_{2P} α subunits (Luján, 2010).

Voltage-gated KCh (K_v)

Molecular structure

K_v exist as homo- or hetero-tetramers of pore-forming α subunits associated with regulatory β subunits. This association of regulatory K_v β subunits with functional K_v α subunits contributes to the diversity of K_v. K_v α subunits have six transmembrane domains (M1–M6) and cytoplasmic N- and C- termini. The M5–M6 region constitutes the channel's conduction pore (P-region) and K^+ selectivity filter while the M4 domain contains a positively charged voltage sensor (Burg, Remillard and Yuan, 2006). The first four transmembrane domains form the voltage-sensing domain, whereas the last two transmembrane domains, in conjunction with a re-entrant P loop, form the pore region of the channel. cDNAs encoding multiple members of each of the corresponding mammalian gene families have now been isolated and expressed. This include: Shaker/K_v1/KCNA; Shab/K_v2/KCNB; Shaw/K_v3/KCNC; Shal/K_v4/KCND; K_v5/KCNF; K_v6/KCNG; K_v7/KCNQ; K_v8/KCNV; K_v9/KCNS; K_v10/KCNH; K_v11/KCNH; andK_v12/ KCNH). The most widely expressed families in the CNS are the K_v1–K_v4 (Gutman *et al.*, 2005)(Luján, 2010)

Biophysical properties and expression patterns

K_v determines a neuron's intrinsic electrical excitability. Following depolarization of the plasma membrane, K_v open rapidly (<1 ms) allowing K^+ to flow passively down their electrochemical gradients. K_v remain closed when the intracellular compartment of a neuron is at a negative voltage relative to the extracellular site (Luján, 2010).

K_v have been found in nerve and muscle cells, neuronal cells as well as in many non-excitable cells (Rudy, 1988).

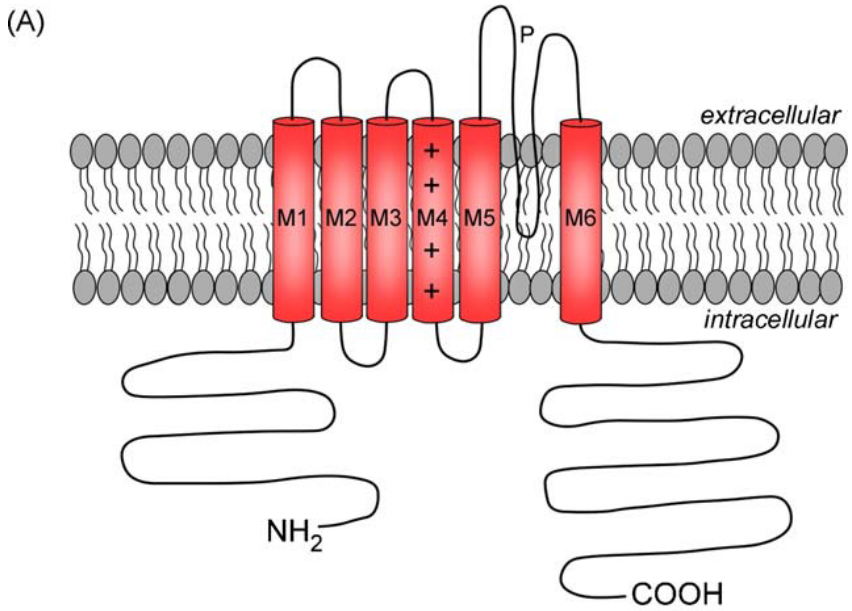

(B)

Channel	Gene	Channel	Gene	Channel	Gene
$K_v1.1$	*KCNA1*	$K_v4.1$	*KCND1*	$K_v8.1$	*KCNV1*
$K_v1.2$	*KCNA2*	$K_v4.2$	*KCND2*	$K_v8.2$	*KCNV2*
$K_v1.3$	*KCNA3*	$K_v4.3$	*KCND3*	$K_v9.1$	*KCNV1*
$K_v1.4$	*KCNA4*	$K_v5.1$	*KCNF1*	$K_v9.2$	*KCNV2*
$K_v1.5$	*KCNA5*	$K_v6.1$	*KCNG1*	$K_v9.3$	*KCNV3*
$K_v1.6$	*KCNA6*	$K_v6.2$	*KCNG2*	$K_v10.1$	*KCNH1*
$K_v1.7$	*KCNA7*	$K_v6.3$	*KCNG3*	$K_v10.2$	*KCNH5*
$K_v1.8$	*KCNA10*	$K_v6.4$	*KCNG4*	$K_v11.1$	*KCNH2*
$K_v2.1$	*KCNB1*	$K_v7.1$	*KCNQ1*	$K_v11.2$	*KCNH6*
$K_v2.2$	*KCNB2*	$K_v7.2$	*KCNQ2*	$K_v11.3$	*KCNH7*
$K_v3.1$	*KCNC1*	$K_v7.3$	*KCNQ3*	$K_v12.1$	*KCNH8*
$K_v3.2$	*KCNC2*	$K_v7.4$	*KCNQ4*	$K_v12.2$	*KCNH3*
$K_v3.3$	*KCNC3*	$K_v7.5$	*KCNQ5*	$K_v12.3$	*KCNH4*
$K_v3.4$	*KCNC4*				

Figure 1.8. Subunit composition of K_v principal subunits in mammalian central neurons. (A) Schematic representation of a single K_v α subunit. The K_v are composed of four α subunits each containing six transmembrane segments (M1–M6) a conducting pore (P) between M5 and M6 and a voltage sensor (positive charge of amino acid residues) located at M4. (B) Classification and genetic nomenclature of K_v α subunits (Luján, 2010).

K_vs are the focus of this work and will therefore restrict the remainder of my chapter to this KCh subtype, and their roles in the brain, in health and disease.

K_v in the brain

Neurons express a wide variety of K_v that can contribute to diverse aspects of neuronal signalling, depending on the functional characteristics, abundance, subunit composition, distribution, cellular and subcellular localisation of the channel subtypes (Trimmer and Rhodes, 2004).

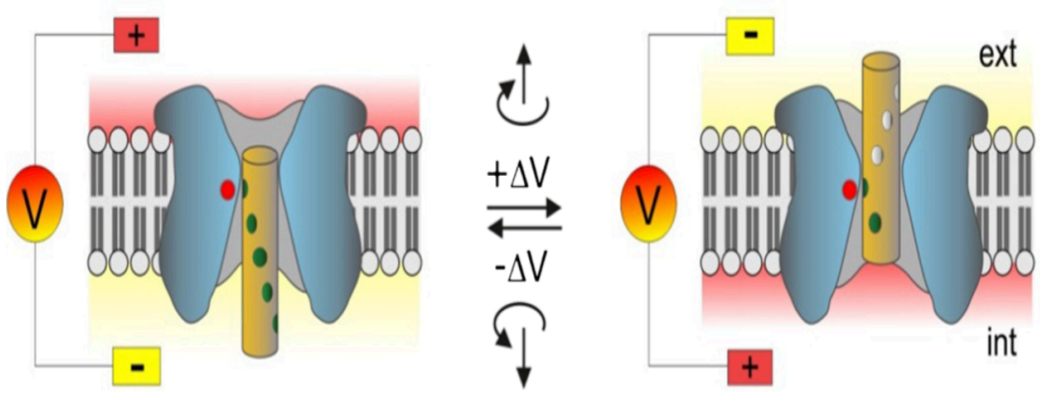

Figure 1.9. Drawing illustrating the sliding helix model of voltage- dependent gating of K_v channels. Upon depolarization, the electrostatic force keeping the voltage sensor, the sliding helix, fully inward (left sketch) is relieved, letting it slide outward along a helicoidal path (right sketch) such that positive charges (green) on the sliding helix establish in succession ion pairs with negative charges (red) present in the neighbouring segments of the voltage sensor domain. Only one of the four sliding helices/voltage sensors of K_v channels is shown in the figure (Catacuzzeno, Sforna and Franciolini, 2020).

A parallel nomenclature for K_v subunit genes was established by the HUGO Gene Nomenclature Committee. Genes encoding the four original K_v1–K_v4 subfamilies of α subunits were named KCN, and assigned the letters A–D (i.e., K_v1–K_v4 is KCNA–KCND) and the specific gene numbers following the K_v nomenclature (e.g., $K_v1.1$ is KCNA1, $K_v1.4$ is KCNA4, $K_v2.1$ is KCNB1, etc.). K_v5–K_v12 subfamilies were assigned KCNF (K_v5), KCNG (K_v6), KCNQ (K_v7), KCNV (K_v8), KCNS (K_v9), and KCNH (K_v10-12) (Vacher, Mohapatra and Trimmer, 2008).

Cellular distribution of k_v

Many studies have reported the regional and cellular localisation of the members of the K_v1–K_v4 and K_v7 subfamily (Trimmer and Rhodes, 2004) (Vacher, Mohapatra and Trimmer, 2008), However, members of the K_v subfamilies K_v5, K_v6, and K_v8–K_v12 have been far less characterized.

K_v1 family

The K_v1 channels are mostly expressed in the brain, especially in axons, soma, synaptic terminals and proximal dendrites, but they can also be found in non-excitable cells such as lymphocytes (Foust *et al.*, 2011). The three most abundant K_v1 subunits expressed in the brain, $K_v1.1$, $K_v1.2$, and $K_v1.4$, are members of the heteromeric channel complexes. However, the subunit composition of channels containing the three subunits depends upon the brain region. $K_v1.1$ and $K_v1.4$ are found in the globus pallidus and substantia nigra pars reticulata (SNr). $K_v1.1$ and $K_v1.2$ are also found in cerebellar basket cell terminals. In the hippocampus, $K_v1.4$ are found in the mossy fiber terminals and axon terminals associated with the perforant pathway, and in the cerebellum are found in the pinceau structures associated with Purkinje cells (Rhodes *et al.*, 1997) (Luján, 2010).

The K_v1 subfamily regulates different neuronal electrical properties, including action potential amplitude and duration, the cell resting membrane potential, the frequency of cell firing and the kinetics and amount of neurotransmitter release (Villa *et al.*, 2020). K_v1 channels at the distal axon initial segment (AIS) play prominent roles in determining the properties of action potentials, and in repolarizing the distal AIS, the site of spike initiation, after an action potential

has been fired (Trimmer, 2015). $K_v1.1$, $K_v1.2$ and $K_v1.3$ interferes with the demyelinating process of axons. $K_v1.1$ is involved in repolarisation of axons (Kumar, Kumar, Jha, Jha and Rashmi K. Ambasta, 2016).

K_v2 family

The K_v2 family members are widely distributed in the CNS. $K_v2.1$ is highly expressed and has an extensive distribution throughout the brain. In spite of its widespread expression, $K_v2.1$ is especially prominent in the cortical pyramidal cells in layers II/III and V, as well as in the principal cells and interneurons of the hippocampus. $K_v2.2$ is highly expressed in neurons of the olfactory bulb and pyramidal cells of the cortex, and in general it is expressed in many of the same cells that express $K_v2.1$. In general, K_v2 channels are found predominantly at postsynaptic sites on somata and dendrites and are not detected in axons and axon terminals (Du *et al.*, 1998)(Luján, 2010).

K_v2 channels are the major constituents of the somatic delayed rectifier K^+ current (Villa *et al.*, 2020), and are also found at/near sites of intracellular Ca^{2+} release, which may influence their modulation by Ca^{2+}-regulated protein kinases and phosphatases (Trimmer, 2015).

K_v3 family

The K_v3 family is composed of four subunits, with some of them composed of several isoforms. Three of the subunits ($K_v3.1$, $K_v3.2$, and $K_v3.3$) are expressed mainly in the CNS, whereas $K_v3.4$, although also present in the CNS, is more abundant in skeletal muscle. In situ hybridisation studies have shown that $K_v3.1$, $K_v3.2$, $K_v3.3$ and $K_v3.4$ are expressed in distinct

subpopulations of projecting neurons and interneurons in the cerebral cortex, hippocampus, caudate-putamen and midbrain auditory. In general, each of the four subunits have a unique expression pattern in the CNS, although $K_v3.1$, $K_v3.3$, and $K_v3.4$ do exhibit expression patterns similar to each other, but completely distinct from $K_v3.2$ channels. For example, regions that express high levels of $K_v3.1$, $K_v3.3$ and $K_v3.4$ mRNAs such as the cerebellar cortex, the spinal cord, the reticular thalamic nucleus, the inferior colliculus, and many nuclei in the brainstem, express little or no $K_v3.2$ (Weiser *et al.*, 1994)(Luján, 2010).

The K_v3 channels are among the most brain specific of all known K channels being involved in the rapid repolarization of the action potential in neurons with a key role in the fast-spiking neuronal phenotype (Yanagi *et al.*, 2014). High-threshold K_v3 channels play a critical role in repolarization of mossy fibres axons and terminals (Trimmer, 2015). K_v3 family members have unique functional characteristics, including fast activation at voltages positive to -10 mV and very fast deactivation rates. These properties are thought to facilitate sustained high-frequency firing, and K_v3 subunits are highly expressed in fast-spiking neurons, such as neocortical and hippocampal interneurons as well as midbrain auditory neurons (Vacher, Mohapatra and Trimmer, 2008). Kv3.3 mediates the voltage-dependent K^+ permeability of excitable membranes (Kumar, Kumar, Jha, Jha and Rashmi K. Ambasta, 2016).

K_V4 family

The K_V4 channels are expressed in a wide range of tissues, with high levels in the brain and in the heart. This channel is abundant in the dendrites of CA1 pyramidal neurons of the hippocampus and expressed in membranes of soma, dendrites, and spines of pyramidal cells and GABAergic neurons (Villa *et al.*, 2020). The three subunits of the K_V4 family are differentially distributed in the CNS. While K_V4.1 is expressed at very low levels, K_V4.2 and K_V4.3 are widely expressed throughout the brain. Although the regional and cellular expression of K_V4.2 and K_V4.3 is complementary, they can also co-express in some neuronal populations. In the hippocampus, K_V4.2 is highly expressed in principal cells, whereas K_V4.3 is primarily found in a subset of principal cells and in many interneurons (Trimmer and Rhodes, 2004)(Luján, 2010).

K_V4.2 represents the key component of the A-type K^+ current (I_A) in the CNS which is involved in several physiological processes, including the regulation of membrane excitability, the control of the firing pattern and action potential propagation (Kerti, Lorincz and Nusser, 2012).

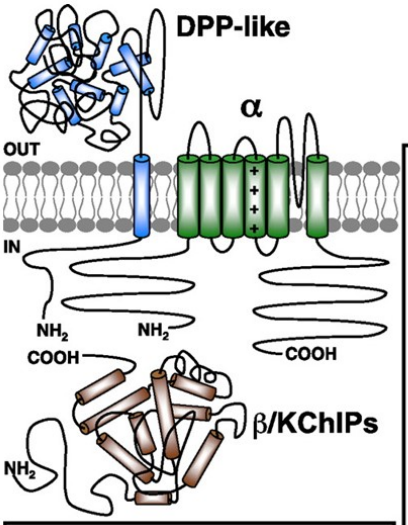

Auxiliary Subunits

Type	Name	Effects on α function
$K_v\beta$	$K_v\beta1$	gating, kinetics
	$K_v\beta2$	trafficking,
	$K_v\beta3$	gating, kinetics
KChIP	KChIP1-4	trafficking, kinetics
DPP-like	DPPx, DPP1-10	trafficking, kinetics

Principal Subunits

Channel	Gene	Subcellular Localization
$K_v1.1$	*KCNA1*	axon, some dendritic
$K_v1.2$	*KCNA2*	axon
$K_v1.3$	*KCNA3*	axon
$K_v1.4$	*KCNA4*	axon
$K_v1.6$	*KCNA6*	axon
$K_v2.1$	*KCNB1*	soma, proximal dendrites
$K_v2.2$	*KCNB2*	soma, dendrites
$K_v3.1$	*KCNC1*	axon (Kv3.1b) somatodendritic (Kv3.1a)
$K_v3.2$	*KCNC2*	soma, dendrites
$K_v3.3$	*KCNC3*	axon
$K_v3.4$	*KCNC4*	axon
$K_v4.1$	*KCND1*	soma, dendrites
$K_v4.2$	*KCND2*	soma, dendrites
$K_v4.3$	*KCND3*	soma, dendrites
$K_v7.2$	*KCNQ2*	axon
$K_v7.3$	*KCNQ3*	axon, soma, dendrites
$K_v7.5$	*KCNQ5*	soma, dendrites

Principal Subunits (unknown brain localization)

Channel	Gene
$K_v1.5$	*KCNA5*
$K_v1.8$	*KCNA10*
$K_v5.1$	*KCNF1*
$K_v6.1$	*KCNG1*
$K_v6.2$	*KCNG2*
$K_v6.3$	*KCNG3*
$K_v6.4$	*KCNG4*
$K_v8.1$	*KCNV1*
$K_v9.1$	*KCNS1*
$K_v9.2$	*KCNS2*
$K_v9.3$	*KCNS3*
$K_v10.1$	*KCNH1*
$K_v10.2$	*KCNH5*
$K_v11.1$	*KCNH2*
$K_v11.2$	*KCNH6*
$K_v11.3$	*KCNH7*
$K_v12.1$	*KCNH8*
$K_v12.2$	*KCNH3*
$K_v12.3$	*KCNH4*

Figure 1.10. Cellular distribution of K_v channels (Vacher, Mohapatra and Trimmer, 2008).

K_v7 family

The K_v7 family, which is chiefly responsible for the slowly activating and non-inactivating M current, is composed of five subunits referred to as $K_v7.1$–$K_v7.5$. $K_v7.1$ is expressed mainly in the heart, whereas $K_v7.2$–$K_v7.5$ are distributed throughout both the central and peripheral nervous systems (Gutman *et al.*, 2005). Immunohistochemical studies have shown that immunoreactivity for $K_v7.5$ is especially strong in the auditory brainstem nuclei, including the cochlear nucleus, superior olivary complex, nuclei of the lateral lemniscus, and inferior colliculus (Luján, 2010).

K_v7 are low-threshold activated voltage-gated K^+ channel which determine the neuron resting membrane potential and regulate their excitability (Brown and Passmore, 2009). Neuronal K_v7 suppresses neuronal firing in many types of brain neurons and suppression of M current by muscarinic modulation

enhances neuronal excitability (Vacher, Mohapatra and Trimmer, 2008). K_v7.2 and K_v7.3 are involved in repolarization activity of axons while K_v7.4 plays a crucial role in the regulation of neuronal excitability in association with K_v7.3 (Kumar, Kumar, Jha, Jha and Rashmi K. Ambasta, 2016). K_v7.5 expressed in calyx of Held nerve terminals is an important determinant of the resting membrane potential, and as such plays a key role in determining glutamate release probability (Trimmer, 2015).

Immunohistochemical analyses of the precise subcellular localisation of K_v5, K_v6, K_v8, K_v9, K_v10, K_v11 and K_v12 subunit have not been fully established (Luján, 2010).

K_v subfamilies have been well characterized in many regions of the brain. However, its expression in the striatum have not been well established. Therefore, I will focus further on K_v expressed in the striatum.

The striatum and its contribution to brain function

The striatum is part of the basal ganglia which comprise the striatum, the globus pallidus (internal-GPi and external-GPe segments), the subthalamic nucleus and the substantia nigra (pars reticulata-SNr and pars compacta-SNc). Together, these subcortical areas process sensorimotor information to allow proper movement generation, including action selection, planning, execution and orientation of locomotion (Albin *et al.*, 1989). The basal ganglia are a group of interconnected subcortical nuclei spanning the telencephalon, diencephalon, and midbrain. The primary afferent structure of the basal ganglia is the striatum which consists of the medial caudate and lateral

putamen (Albin *et al.*, 1989). The striatum receives afferents from all of the isocortex (Kemp and Powell, 1970) and projects upon the SNc, which in turn, receives a substantial projection from the SNc putamen. The primary neurotransmitter of the striatal, pallidal, and SNr projection neurons is γ-aminobutyric acid (GABA) while the neurotransmitter of SNc neurons is dopamine (Albin *et al.*, 1989).

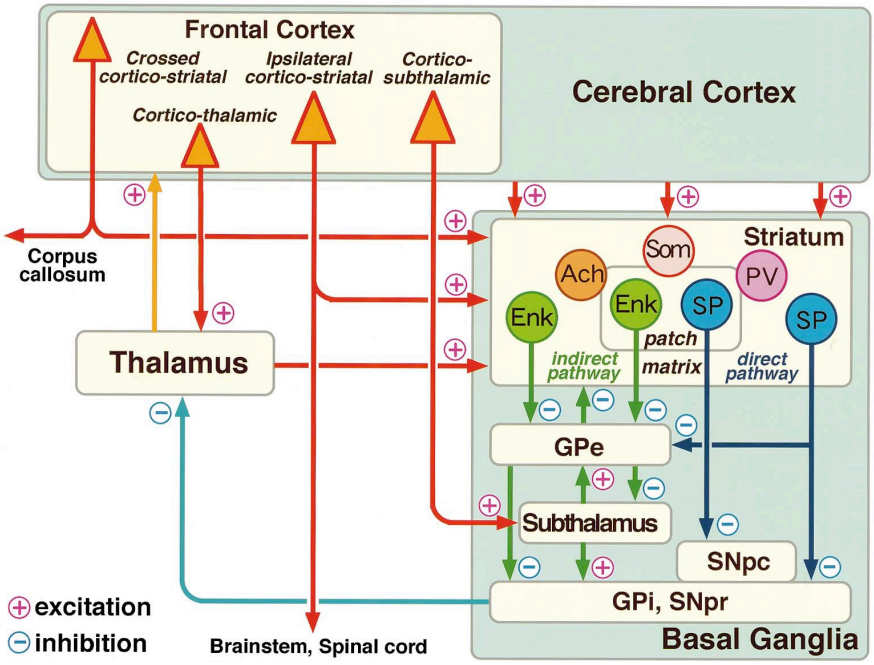

Figure 1.11. Basic neural connections among the cerebral cortex, basal ganglia and thalamus (Kawaguchi *et al.*, 1995).

The striatum is divided into: ventral striatum which consists of the nucleus accumbens and olfactory tubercule important for reward system; and the dorsal striatum which consists of the caudate nucleus and the putamen. These compartments have distinct chemical compositions and connections (Holt, Graybiel and Saper, 1997). Studies of the ventral striatum suggests the accumbens are associated with locomotor and incentive– reward effects (Zahm, 2000) while the dorsal striatum coordinates neuronal signals from multiple cortical and subcortical regions and plays a critical role in voluntary movements, motor learning, cognition, and emotion (Guo *et al.*, 2015).

Cell types of the striatum

The mammalian striatum contains two different types of cells: 1) medium spiny neurons (MSNs) also called projection neurons because their axons generally exit the striatum and project to the target regions of the striatum. They represent about 74% of the total striatal neuronal population; 2) interneurons, whose axons target only MSNs, and account for the remaining 26% of striatal neurons. MSNs, morphologically, are distinguished by the presence of spines on their dendrites. These small protuberances significantly increase the surface area of neurons and are the sites of excitatory synapses. MSNs send their axons to the internal and external segments of the globus pallidum and to the SNr. In contrast, interneurons do not contain dendritic spines and exert a powerful control over MSNs (Gime and Berna, 2012).

The principal neurons: MSN

The MSN are medium sized neurons and are the major cell type of the neostriatum (Ell, 1971), MSN utilize GABA as their major neurotransmitter (Albin *et al.*, 1989)., and have somatic diameters of about 20 μm (Wilson and Groves, 1980). MSN are subdivided into two major populations based on their projection region, pattern of axonal collateralisation and their neurochemical content - dopamine D1 and D2 receptors (Wilson and Groves, 1980). D1 receptor cells projects to the output nuclei of the basal ganglia and expresses GABA, substance P, dynorphin and dopamine D1 receptors while D2 receptor cells projects almost exclusively to the globus pallidus and expresses enkephalin and dopamine D2 receptors (Graybiel, 1990).

Interneurons

Four major classes of interneurons have been identified using cytochemical, physiological and morphological methods. They are: the large cholinergic neurones, which are identifiable by the presence of choline acetyltransferase (ChAt); GABAergic interneurons that contain parvalbumin; GABAergic interneurons that contain calretinin; and a class of interneurons that contain somatostatin, NADPH-diaphorase, and nitric oxide synthase (NOS) (Kawaguchi, 1997).

i. Cholinergic interneurons

Early biochemical studies showed that the biosynthetic enzyme ChAt was present in large amounts in the striatum along with the degradative enzyme acetylcholinesterase (AChE) (McGeer *et al.*, 1971). These was confirmed by immunohistochemistry when large aspiny ChAt immunoreactive cells were shown to comprise 2-3% of striatal cells with widespread processes distributed throughout the striatum (Wainer *et al.*, 1984). Cholinergic interneurons have large somata, widespread dendritic trees, subtending a region much larger than that of the projection neurons. Thus, these cells are capable of integrating synaptic inputs over relatively large regions. Similarly, their axonal fields are very extensive compared with those of most of the other striatal neurons (Wilson, Chang and Kitai, 1990).

ii. Parvalbumin-containing GABAergic interneurons

This group of interneurons in the striatum stain positively for parvalbumin, a calcium binding protein (Kawaguchi *et al.*, 1995). Parvalbumin-containing cells

constitute between 3-5% of striatal cells and are slightly larger than the MSN. They have varicose dendrites that arborize within 200-300μm of the cell body, and a dense arborization of local axonal collaterals. Parvalbumin-positive GABAergic interneurons receive powerful excitation from the cerebral cortex. Because of the potentials seen in projection neurons after afferent stimulation, it has been proposed that the parvalbumin-positive neurons are responsible for most of the inhibition seen in experimental studies of striatal projection cells (Kawaguchi, 1997). They provide a feed forward inhibitory circuit in which they receive excitatory inputs (mostly from cortex) and inhibit both spiny output cells and interneurons including those containing somatostatin (Emson *et al.*, 1993) (Cowan *et al.*, 1990)

iii. Calretinin-containing GABAergic interneurons

Calretinin, is a calcium-binding protein containing four calcium binding domains and believed to bind calcium over the physiological range of concentration of intracellular calcium. Calretinin may function as calcium buffers, but the precise physiological roles have not been established (Baimbridge, Celio and Rogers, 1992). Electron microscopic studies shows calretinin to be aspiny neurons with indented nuclei (Bennett and Bolam, 1993).

iv. Somatostatin (neuropeptide Y, nitric oxide synthase)-containing interneurons

These are medium-sized aspiny interneurons that contains the neuropeptide Y, somatostatin and nitric oxide synthase (Emson *et al.*, 1993). Somatostatin-

containing interneurons are aspiny cells 12-25 μm in diameter, which represent 1-2% of striatal neurons. In comparison with cholinergic and parvalbumin-positive cells, Somatostatin-containing interneurons have fewer dendritic branches (Kawaguchi *et al.*, 1995).

Main inputs and projection patterns of the striatum

The striatum is the main recipient of inputs to the basal ganglia and major excitatory inputs from cortex and cortical-like structures such as the amygdala and subiculum of the hippocampus. Information entering the striatum from other parts of the brain can either stimulate activity in the striatum (known as an "excitatory input") or alter existing excitatory inputs (Hunnicutt *et al.*, 2016). Striatal neurons receive convergent excitatory inputs from the cerebral cortex, the intralaminar thalamus, the SNc and the dorsal raphe nucleus (Zahm, 2000).

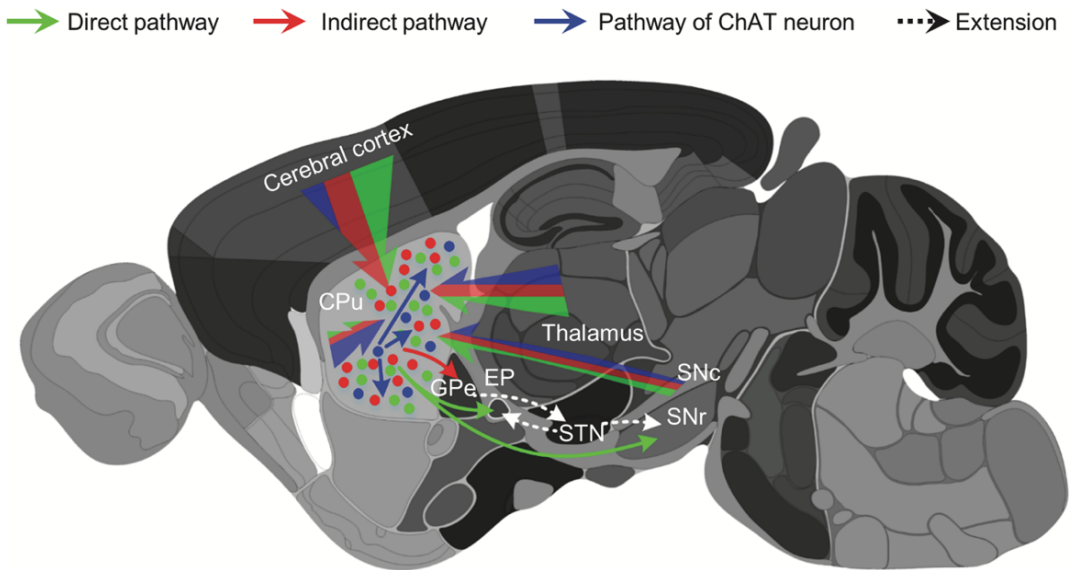

Figure 1.12. Inputs to the dorsal striatum cholinergic interneurons and D1/D2 projection neurons. Blue, green, and red lines indicate monosynaptic inputs to striatal ChAt, D1, and D2 neurons, respectively. Thickness of the lines represents proportional input strength (cell numbers) from given brain areas. Abbreviations: CPu, caudate putamen; GPe, external globus pallidus; GPi/EP, internal globus pallidus/entopeduncular nucleus; SNc, substantia nigra, compact part; SNr, substantia nigra, reticular part; STN, subthalamic nucleus (Guo *et al.*, 2015).

Inputs are neurochemically diverse, all releasing different messengers that synapse on different types of neurons in the striatum and as such have an impact on the excitability of striatal neurons. Therefore, the striatal neurons themselves need to express chemicals to integrate such inputs, in order to ensure coordinated activity. K_vs will be central to integrating such inputs in a coordinated way because they regulate the neurons. Whilst neurotransmitter receptors have been widely explored, we currently know very little about which particular K_v is expressed on specific cells in proximity to specific inputs. Therefore, it is important to characterise the native expression patterns of K_v within the striatum and determine whether such expression patterns evolve with different life experiences or diseases. For my thesis, I focussed on psychosocial stress as a life experience that impacts on the striatum, and Parkinson's and Alzheimer's as diseases that impact on this brain region.

The striatum and psychosocial stress

Exposure to stressors results in the initiation of a host of central and peripheral physiological processes. These physiological responses to stressors are essential survival mechanisms which allow the individual to contend with such challenges throughout one's lifetime. However, exposure to stressors can also manifest in maladaptive physiological responses which predispose individual to developing a host of diseases either of the CNS or peripheral systems. When the brain detect a stressful experience (stressor), corticotrophin-releasing hormone (CRH) is activated resulting in the activation of hypothalamic-pituitary-adrenocortical (HPA) axis (De Kloet, Joëls and

Holsboer, 2005). The activation of the HPA axis results in widespread hormonal, neurochemical, and physiological alterations (Mcrae, 2003).

Within the CNS, there is a complex CRH circuitry that serves to coordinate the stress response between different brain regions (De Kloet, Joëls and Holsboer, 2005). A CRH pathway within striatum has been demonstrated to have a profound role in altering neuronal activity within this brain region, and associated behaviours which may be deleterious for health (Lemos *et al.*, 2012). However, the effect of stress on K_v expression in the striatum, or anywhere in the brain for that matter, is poorly explored. Such changes could represent novel therapeutic targets for such conditions. Therefore, for the first results chapter, the first high resolution native expression pattern of K_v would be characterised within the striatum and investigated for changes following exposure to stress.

An animal model of early life stress (ELS) in mice would be used because ELS has been shown to impart the most severe negative consequences in individuals due to the underdevelopment of the body's stress system at this time (Rice *et al.*, 2008)(Gunn *et al.*, 2013). Experimental studies have shown that ELS have an effect on animals later in life resulting in elevated level of inflammation (Danese and J Lewis, 2017) and decreased indices of approach motivation and responsiveness to reward. Since the striatum is important for the reward system, I believe it would be instructive to characterise the changes in brain neurochemistry in the striatum following exposure to ELS.

Parkinson's disease (PD)

Clinical presentations of PD

PD is a progressive, neurodegenerative disorder characterized by severe motor symptoms, including static tremor, postural imbalance, bradykinesia and muscle rigidity. It is a disease classified as protein-misfolding disorder (Zeng *et al.*, 2018). The onset of PD is considered to commence at least 20 years prior to detectable motor abnormalities, when a variety of non-motor symptoms can be observed. This period is referred to as the prodromal phase where patients experience a range of non-motor symptoms including constipation, olfactory dysfunction (hyposmia), sleep disturbance, obesity and depression (Hawkes, Del Tredici and Braak, 2010). This phase of PD is followed by degenerative cell loss, alteration of the expression levels of a range of proteins involved in synaptic transmission in the prefrontal and cingulate cortex, and substantia nigra (Dijkstra *et al.*, 2015).

Mechanisms of neuronal cell death in PD

The deaths of dopaminergic neurons mainly occur in the SNc, in which the neurotransmitter dopamine is normally synthesized and pumped into movement-regulating brain regions. Though up to 70% of dopaminergic neurons in SNc die during the development of PD, symptoms are not noticed immediately because the striatum downstream can compensate. However, the continuous death of neurons in the striatum continues resulting in development of PD symptoms. Dopamine metabolism, oxidative stress and mitochondrial dysfunction, endoplasmic reticulum stress, impairment of protein degradation systems, neuroinflammation and mutations of the genes

α-synuclein, LRRK2, PINK1, Parkin, DJ-1, VPS35 and GBA1 have been shown to be involved in the loss of dopaminergic neurons in SNc (Zeng *et al.*, 2018).

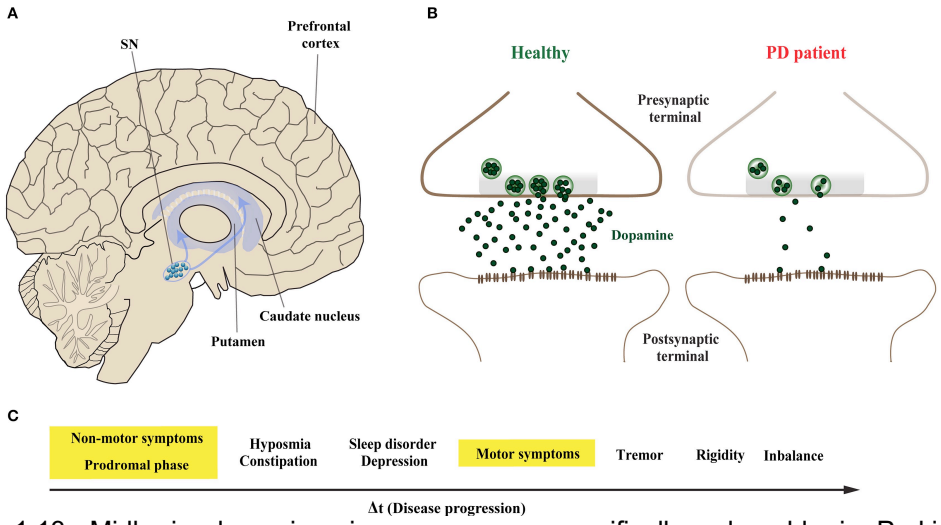

Figure 1.13. Midbrain dopaminergic neurons are specifically vulnerable in Parkinson's disease. (A) The predominant symptoms of Parkinson's disease (PD) are caused by loss of dopaminergic neurons in the substantia nigra. According to the dying-back hypothesis, the degeneration of dopaminergic neurons is preceded by dysfunction and in turn degeneration of the nigrostriatal pathway, which innervates the caudate nucleus and the putamen that together form the striatum. (B) Compared to healthy controls (left), nigrostriatal degeneration results in the depletion and ultimate loss of the neurotransmitter dopamine on synaptic terminals of striatal neurons (right). (C) The resulting motor symptoms, among others, are usually diagnosed when approximately 30–60% of striatal dopaminergic neurons are already lost. However, PD patients can experience non-motors symptoms 20 years before the onset of motor abnormalities in the so-called prodromal phase; these include olfactory dysfunction, sleep disturbances and depression (Jessika C Bridi and Hirth, 2018).

Pathology

In 1817, an English physician, Dr. James Parkinson, firstly described shaking palsy. The pattern was eventually called "PD" by Charcot and Vulpian in 1862. Intraneuronal proteinaceous inclusions called Lewy bodies (LBs) and Lewy neurites (LNs) plays a main role in PD and are predominantly formed of misfolded and aggregated forms of the presynaptic protein, alpha-synuclein (α-syn), which can result to loss of dopaminergic neurons in the substantia nigra (Osterhaus *et al.*, 1997). The reduction of striatal dopamine triggers a range of motor symptoms including bradykinesia, uncontrollable tremor at rest, postural impairment, and rigidity which together characterise PD as a

movement disorder. Recent studies have shown the correlation of genetic mutation of PD in genes such as Parkin, DJ-1, UCHL-1, LRRK2, PINK1 (PTEN-induced kinase1), NURR1, VPS35 (vacuolar protein sorting 35), and HtrA2 (Truban *et al.*, 2017). However, among the identified PD-related genes, SNCA encoding the presynaptic protein α-syn remains the most underlying factor of PD (Huang, Chan and Halliday, 2007). α-syn is the main component of LB which has been shown to have a central pathogenic role in both familial and sporadic PD (Satake *et al.*, 2009).

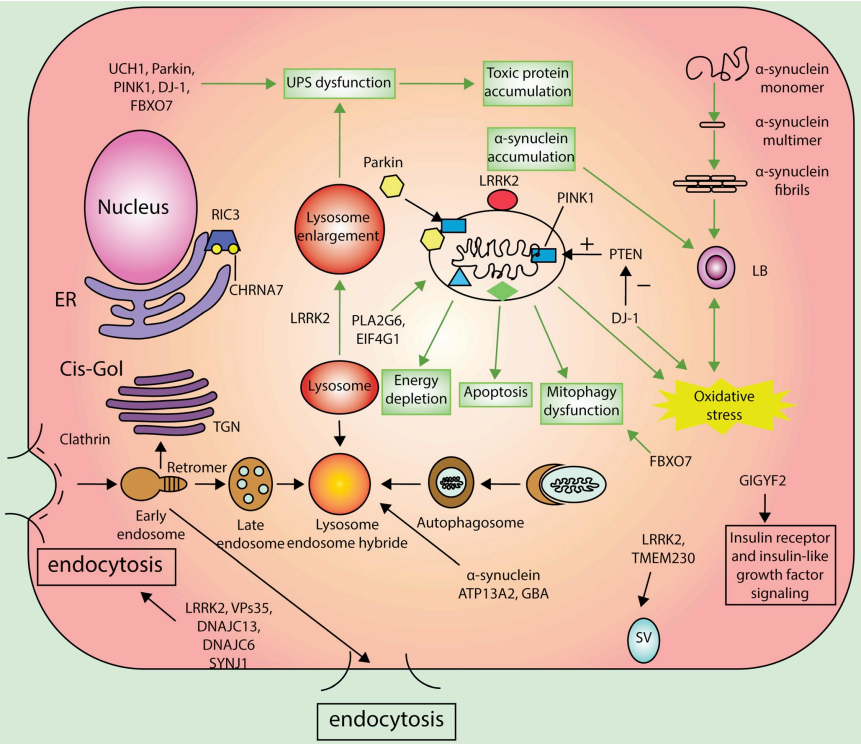

Figure 1.14. Main molecular pathways related to PD pathogenesis. Abbreviations: UPS, ubiquitin-proteasome system; LB, Lewy body; TGN, trans-Golgi network; SV, synaptic vesicle; ER, endoplasmic reticulum; UPSCHRNA7, neuronal nicotinic acetylcholine receptor subunit α-7 (Jamebozorgi *et al.*, 2018).

Alpha-synuclein

α-syn is a small soluble cytoplasmic protein of 140 amino acid that comprises an amphipathic region, non-amyloid- β component (NAC) domain and an acidic tail (Jessika C Bridi and Hirth, 2018). α-synuclein together with β-synuclein and ɣ-synuclein belong to the synuclein protein family (Maroteaux,

Campanelli and Scheller, 1988) (Fig 1.15). All three are highly expressed in the human brain. However, α-syn is the only protein of the synuclein family to be found in LB and to be implicated in PD pathogenesis (Goedert, Jakes and Spillantini, 2017). The biological role of α-syn is not fully understood. However, there is strong evidence that α-syn is involved in regulating and maintaining dopamine homeostasis within the cytoplasm (Perez *et al.*, 2002). Also, α-syn has been shown to function primarily as a protein within axon terminals to regulate the release of neurotransmitters (Jessika C. Bridi and Hirth, 2018).

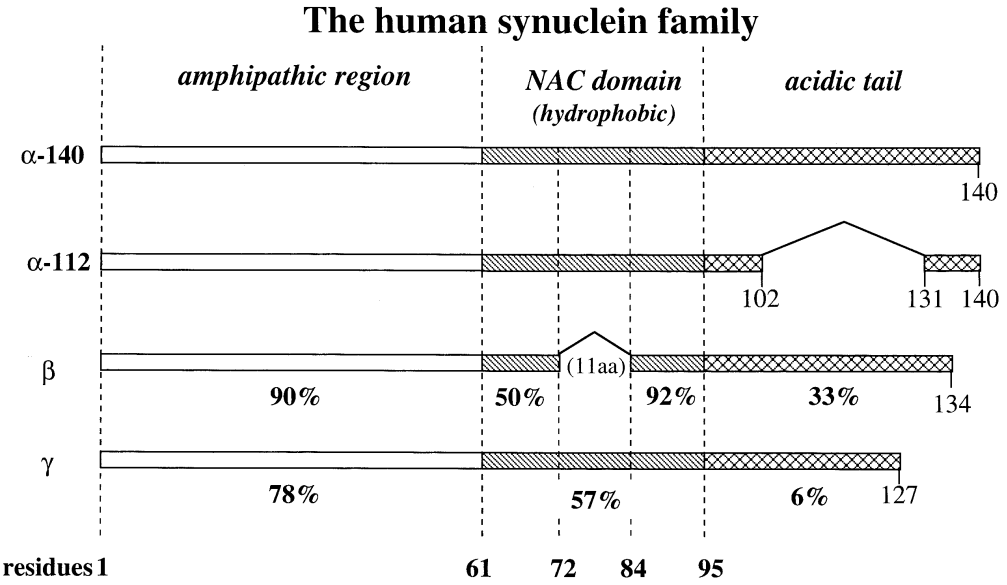

Figure 1.15. The human synuclein family. The different synucleins are represented as a bar. Amino acid positions are indicated at the bottom. The N-terminal amphipathic region, the hydrophobic NAC region, and the acidic tail are separated by vertical dashed lines and are differently hatched. The α-112 splice variant of α-synuclein (lacking 28 amino acids within the acidic tail) as well as β- and ɣ-synuclein are shown. The NAC region of β-synuclein lacks 11 central amino acids (residues 73–83). The degree of amino acid identity compared to α-synuclein, according to cross-species consensus sequences, is given as a percentage below each domain (Brice, 2000).

α-syn aggregation

The aggregation of α-syn into small oligomers and protofibrils that elongate into mature fibrils is believed to occur via a nucleation dependent pathway (Wood *et al.*, 1999). This involves an initial conformational change of α-syn monomers into a partially folded conformation that undergoes a series of unfavourable self-associations to form a highly unstable nucleus during a lag

phase. The formation of the nucleus is followed by a more favourable growth phase (elongation) where the nucleus rapidly grows into fibrils by the addition of monomers (Harper and Lansbury, 1997).

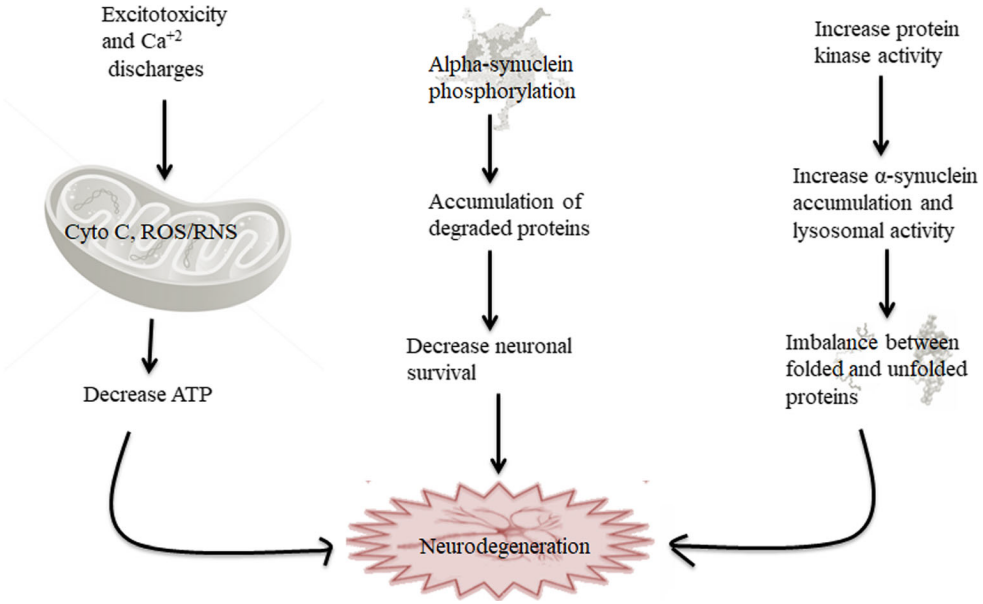

Figure 1.16. α-synuclein aggregation and neurodegeneration (Kaur, Mehan and Singh, 2018).

Changes in brain chemistry

PD affects brain chemistry causing changes in ion channels and neurotransmitters. Tyrosine hydroxylase (TH), responsible for producing dopamine through conversion of L-tyrosine to L-3,4-dihydroxyphenylalanine (L-DOPA), activity was found to be reduced in mouse models overexpressing α-syn (Jessika C Bridi and Hirth, 2018). Thus α-syn is a negative modulator of dopamine synthesis by interplay with the rate-limiting enzyme TH. Studies also show α-syn to impair transport and uptake of dopamine by altering the activity of the vesicular monoamine transporter 2 (VMAT2) and the dopamine transporter (DAT), respectively (Lotharius and Brundin, 2002). This is thought to be vital for dopaminergic neuron susceptibility observed in PD. Also, α-syn disruption of VMAT2 and DAT activity and their function in regulating dopamine levels in the synaptic terminal have been shown to fuel the formation

of soluble α-syn oligomers that are considered to be toxic species (Jessika C Bridi and Hirth, 2018).

Alzheimer's disease (AD)

Clinical presentations of AD

AD is a form of dementia mainly characterized by cognitive dysfunction, memory loss, and neuronal death (Castellani, Rolston and Smith, 2011). The focal hallmark of AD includes amyloid beta (Aβ) accumulation, tau hyper phosphorylation and mutations in the catalytic domain of γ secretase (Zhao and Zhao, 2013). Studies in transgenic mice have shown that Aβ produced at the onset of AD disrupts synaptic function and contributes to cognitive impairment early in the disease process (Hsiao *et al.*, 1996). Clinical symptoms of AD include mild to severe memory loss, problems with cognition and behaviour, and gradual losses in the activities of daily living (Castellani, Rolston and Smith, 2011).

Pathology

The main pathological features in the Alzheimer's brain are progressive depositions of amyloid protein plaques between nerve cells and neurofibrillary tangles within the nerve cells (Mattson, 1997). Aβ plaques are generated by sequential proteolytic cleavage of Aβ precursor protein (APP) by β-site APP-cleaving enzyme 1 (BACE1) and the γ-secretase complex (Villa *et al.*, 2020). Amyloid plaques are made up of small, aggregated peptides called beta amyloid (Aβ). They are extracellular accumulations principally composed of abnormally folded Aβ with 40 or 42 amino acids (Aβ40 and Aβ42), two by-

products of APP metabolism. Aβ42 is more abundant than Aβ40 within plaques due to its higher rate of fibrillization and insolubility (Lane, Hardy and Schott, 2018). The extracellular deposition of Aβ in the brain could trigger a cascade of pathological events, including microglia-mediated inflammation, mitochondrial dysfunctions, excess in mitochondrial reactive oxygen species generation, increased oxidative stress, dysfunction of neurotransmission and brain networks, and loss of synapses (Villa *et al.*, 2020).

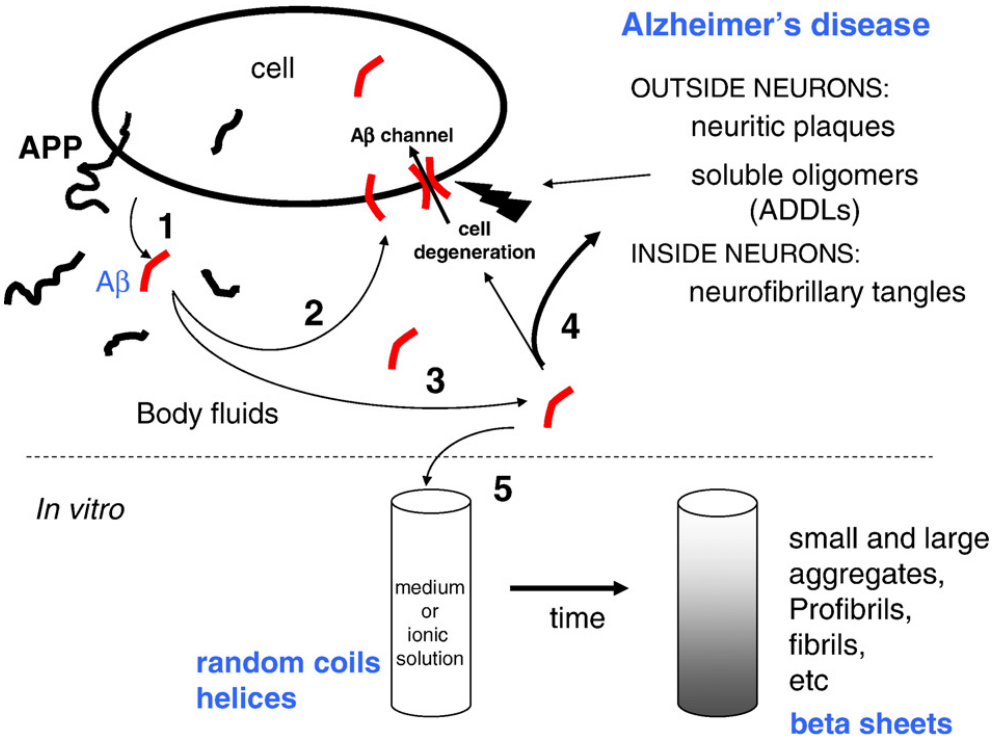

Figure 1.17. Schematic of major steps in the life of the enzymatically liberated Aβ peptide and its action on cells. (1) Physiologically, the Aβ peptide is released from the precursor protein, APP, into the medium. (2) Some of the extracellular Aβ could be taken up into the cell. (3) Most Aβ remains in the medium in the non-toxic non-aggregated state. (4) However, in Alzheimer's disease brain the Aβ released into the extracellular fluid aggregates to form neuritic plaques, soluble oligomers and structures that can form ion channels in cells. (5) In vitro, when Aβ is added to cell culture media or ionic solutions, the basically random coil and helices structures, characteristic of the non-aggregated state of Aβ, are converted into small and large aggregates, protofibrils and fibrils enriched of β sheet structures (Arispe, Diaz and Simakova, 2007).

Whilst fibrillar amyloid within dense core plaques was originally thought to be critical to the development of AD, it is now thought that soluble Aβ oligomers (AβO) may be the most pathological forms. Studies showed that oligomers purified from AD brains and applied to neurons in vitro inhibit long-term

potentiation, cause synaptic dysfunction, damage dendritic spines and cause neuronal death (Forloni *et al.*, 2016). Human oligomers also induce hyperphosphorylation of tau at AD-relevant epitopes and cause neuritic dystrophy in cultured neurons. Plaques may therefore act as a reservoir from which amyloid oligomers diffuse or may even act as a protective mechanism sequestering toxic Aβ series until they reach a physiological saturation point (Hardy and Selkoe, 2002). Neurofibrillary tangles (NFTs) are primarily composed of paired helical filaments consisting of hyperphosphorylated Tau. Tau pathology typically begins in the allocortex of the medial temporal lobe (entorhinal cortex and hippocampus) before spreading to the associative isocortex (Serrano-Pozo *et al.*, 2011).

In addition to the cardinal features of Alzheimer's pathology (amyloid plaques and NFTs), neuropil threads, dystrophic neurites, associated astrogliosis and microglial activation are also seen, and cerebral amyloid angiopathy frequently coexists (Serrano-Pozo *et al.*, 2011). The consequences of these pathological processes include neurodegeneration with synaptic and neuronal loss (John R.Giudicessi, BA.Michael J.Ackerman., 2008).

Several mechanisms proposed to explain the underlying pathology of AD include:

The cholinergic hypothesis

The development of the cholinergic hypothesis was due to a significant and selective loss of ChAt activity in different parts of AD brain samples (cortex, hippocampus and amygdala) complemented with the finding that neurons in

the basal part of the brain were selectively degenerated in AD (Whitehouse *et al.*, 1981).

Amyloid cascade hypothesis

The amyloid hypothesis of AD is based on abnormal processing of the APP, leading to production of Aβ. Secretase enzymes cleave APP and aberrancy of this process, specifically mutations in gamma and beta- secretases, can lead to the abnormal production of Aβ which can then trigger a cascade leading to synaptic damage and neuron loss, and ultimately to the pathological hallmarks of AD with resulting neurodegeneration (Murphy and Levine, 2010).

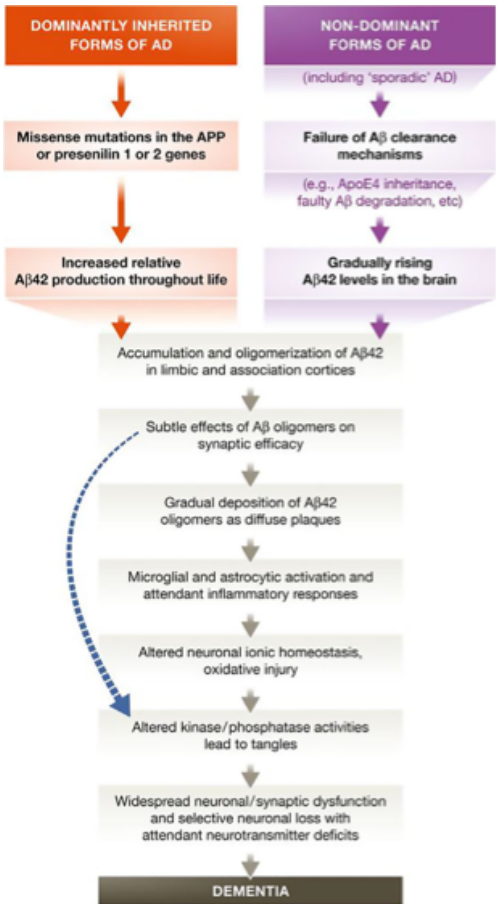

Figure 1.18. An overview of the major pathogenic events leading to Alzheimer's disease as proposed by the amyloid hypothesis. The curved blue arrow indicates that Aβ oligomers may directly cause synaptic and neuritic damage and induce tau hyperphosphorylation, in addition to activating damaging inflammatory cascades (Lane, Hardy and Schott, 2018).

Tau hypothesis

Tau is a protein expressed in neurons that normally functions in the stabilisation of microtubules in the cell cytoskeleton. Hyperphosphorylation causes it to accumulate into NFT masses inside nerve cell bodies. These tangles then aberrantly interact with cellular proteins, preventing them from executing their normal functions (Bloom, 2014).

Changes in brain chemistry

AD affects brain chemistry causing changes in ion channels. Increased $K_v1.4$ and $K_v2.1$ expression has been observed in the hippocampus of Aβ-injected animals (Shah and Aizenman, 2014). $K_v1.4$ was then reported to play a role in AD in which increased $K_v1.4$ levels was observed in the hippocampus of Aβ-treated rats (Villa *et al.*, 2020). $K_v1.3$ and $K_v1.5$ have also been found to be associated with toxic Aβ and have been implicated in AD (Kumar, Kumar, Jha, Jha and Rashmi K. Ambasta, 2016). Some evidences reported that oxidative stress occurring during early stages of AD acts as negative modulator of $K_v2.1$-dependent K^+ currents (Cotella *et al.*, 2012). A dysregulation of the $K_v3.1$ and $K_v3.4$ channels has been found to be associated with glial and neuronal alterations occurring during AD pathogenesis. Increased levels of $K_v4.2$ transcript and protein were found in the cerebral cortex after Aβ-injection in rats, suggesting that an upregulation of this channel in Aβ-induced cognitive impairment may be involved in AD pathogenesis (Villa *et al.*, 2020). A link between Aβ deposition and K_v7 channels has also been demonstrated by some studies in which a reduced $K_v7.2$ expression was found in different brain areas in response to an impaired neuron activity after the exposure of Aβ

peptide injected into the hippocampus of live rats (Durán-González *et al.*, 2013). Some research has been carried out to link K_v changes to AD pathology. However, AD-associated changes in K_v expression are yet to be demonstrated in the striatum.

Whilst the attention of many studies has been focussed on neurotransmitter changes, less is known about ion channels. More importantly, when ion channels have been looked at, it has mainly been in the cortex or hippocampus, with very little known about the striatum and definitely not about K_v in the striatum.

Aims

The overall aims of my PhD research were to characterise the native expression patterns of different K_v sub-families within the mouse striatum and how these changes in response to stress or pathology associated with PD and AD.

Objectives

1. Characterise the native expression of K_v within the striatum, at the gene and protein levels, and determine the plasticity of such expression profiles following exposure to stress, using reverse transcription polymerase chain reaction (RT-PCR), immunohistochemistry, microscopy and animal models of stress. (Chapter three).
2. Determine how PD-associated pathology alters striatal neurochemistry and K_v expression, using quantitative reverse transcription polymerase chain reaction (qRT-PCR), immunohistochemistry, microscopy and an animal model of PD. (Chapter four).
3. Determine how AD-associated pathology alters striatal neurochemistry and K_v expression, using qRT-PCR, immunohistochemistry, microscopy and an animal model of AD. (Chapter five).

Chapter Two

Materials and methods

Animals and animal procedures

Ethics

All procedures involving experimental animals were approved by the Animal Welfare and Ethical Review Board of the University of Portsmouth. I performed this work under the auspices of my supervisor Dr Jerome Swinny's Project Licence (PPL 70/8459), and in accordance with the Animals (Scientific Procedures) Act 1986 and the European Directive 2010/63/EU on the protection of animals used for scientific purposes.

Animal husbandry

Adult male mice (*Mus musculus*) were used throughout this project. Animals were bred in-house by University of Portsmouth Bioresources Centre, and housed in a temperature and humidity-controlled environment under 12-hour light-dark cycle, with free access to standard food and water.

The background wild-type (WT) strain used throughout was C57/BL6J.

Mouse model of Alzheimer's disease (AD)

To model AD, a mouse model expressing a chimeric mouse/human amyloid precursor protein (Mo/HuAPP695swe) and a mutant human presenilin 1 (PS1-dE9) was exploited. This will be referred to throughout as transgenic (TG). These mutations result in the increased expression of amyloid precursor

protein and accelerated deposition of Aβ plaques (Borchelt *et al.*, 1997), which is a key pathological feature of AD. The development of Aβ plaques is age and brain region dependent, with most presenting from 5-7 months of age, mainly in the cortex. The characterisation of striatal neurochemistry has not been examined, especially at young ages. I therefore used mice aged ~ 5 months in order to capture the earliest changes that might occur in this brain region. Breeding pairs were obtained from The Jackson Laboratory (strain number34829-JAX) and bred on a C57/BL6 background. WT littermates were used as controls.

Mouse model of Parkinson's disease (PD)

A pathological hallmark of PD is the increased expression of the synaptic protein α-syn (Maroteaux, Campanelli and Scheller, 1988) and its aggregation into Lewy bodies (Osterhaus *et al.*, 1997). To model such pathology, a transgenic mouse line that over-expresses α-syn at disease relevant levels, termed OVX was used (Janezic *et al.*, 2013). Studies have shown that the phenotype and age-related profile of PD-related motor deficits are closely replicated in this model with age-dependent loss of dopamine neurons and motor impairments characteristic of PD presenting at ~14 months of age. However, changes in striatal neurochemistry have yet to be explored in young adulthood. OVX breeding pairs were obtained from collaborators at the Oxford Parkinson's Disease Centre and bred on a C57/Bl6 background with WT used as control.

Mouse model of chronic psychosocial stress

Stress can either be acute or chronic. In order to assess the impact of stress on striatal K_v, chronic stress would be more ideal since it is persistent and will allow for the detection of any changes, at any time point. An animal model of early life stress (ELS) was employed because it has been shown to robustly and reliably result in a hyper-stress phenotype throughout adulthood. The ELS paradigm is based on a model of fragmented maternal care within the first week of life (Rice *et al.*, 2008)(Gunn *et al.*, 2013). Briefly, the dam and pups are provided with limited nesting and bedding between postnatal days 2-9. This results in the dam frequently leaving the nest in search of additional nesting material. Whilst this does not alter the amount of time she spends with the pups, it does manifest in a fragmented dam-pup relationship which impoverishes the quality of maternal care. Controls were raised as normal. Such impaired maternal care has been shown to impact a stress hyper-responsive phenotype in adulthood evidenced by elevated levels of circulating cortisone (Rice *et al.*, 2008). All ELS and control animals were used at 5 months of age.

Experimental procedures

Immunohistochemistry

Tissue preparation

The tissue was perfusion-fixed as follows: anaesthesia was induced with isoflurane and maintained with pentobarbitone (1.25 mg/kg of bodyweight, IP). The animals were perfused transcardially with 0.9% saline solution for 2 min, followed by 10 min fixation with a fixative consisting of 1% paraformaldehyde

(PFA) and 15% v/v saturated 1% picric acid in 0.1 M phosphate buffer (PB), pH 7.4. The picric acid was included in the fixative to neutralise the pH so as to facilitate PFA bond formation with proteins. 1% PFA was used because the majority of the targeted epitopes were integral membrane proteins; relevant epitopes of such proteins may be masked by formaldehyde cross-linking, which is minimised by a less concentrated fixative solution compared to the standard 4% paraformaldehyde protocol (Eyre *et al.*, 2012) (Lorincz and Nusser, 2013). After the perfusion, the brains were carefully dissected from the skull and placed over night at room temperature in the fixative. The following day, the brains were rinsed in 0.1M PB, after which 60 µm sections, either in the sagittal or coronal planes, depending on the brain region, were prepared using a vibrating microtome (VT 1000, Leica, Wetzlar, Germany). The sections were thoroughly washed in 0.1M PB to remove any residual fixative and then stored in a solution containing 0.1 M PB and 0.05% w/v sodium azide until further processing.

Antigen retrieval

Proteolytic antigen retrieval method originally described by Watanabe et al (Watanabe *et al.*, 1998) was used due to experience in the lab. The method is as follows: Tissue sections were incubated for 10 minutes at 37°C in 0.1M PB in a shaking incubator. The PB was removed and replaced with a solution containing 1mg/ml pepsin (Sigma Aldrich, St Louis, MI, USA) dissolved in 0.2M HCL for 10 minutes. After which, sections were washed three times for 10 minutes in 50mM TRIS-buffered saline solution containing 0.3 % w / v Triton-X-100 (TBS-Tx).

Blocking of non-specific secondary antibody binding

Secondary antibodies may bind non-specifically to native immunoglobulin within the specimen, resulting in poor signal-to-noise, and labelling that does not represent target antigen binding. To mitigate this, tissue sections were preincubated in a solution containing 20% normal horse serum (Vector Laboratories, Burlingame, CA, USA) in TBS-Tx for two hours at room temperature on a horizontal shaker.

Incubation of primary and secondary antibodies

After incubation in the blocking solution, tissue sections were incubated with a cocktail of primary antibodies diluted in TBS-Tx for 4°C overnight on a horizontal shaker. Details of the primary antibodies used are given in **Table 2.1**. The following day, tissue sections were washed in TBS-Tx three times for 10 minutes to remove unbound antibodies. Tissue sections were then incubated in a cocktail containing appropriate secondary antibodies, targeted at the fragment crystallizable (Fc) region of the primary antibodies used, for 2 hours at room temperature on a horizontal shaker. Secondary antibodies were all raised in donkey, and conjugated to either Alexa Fluor™488, indocarbocyanine (Cy3) or DyLight549™, or DyLight649™ (Jackson Immunoresearch, West Grove, PA, USA), for 2 hours. Sections were then washed three times for 10 minutes in TBS-Tx to remove unbound antibodies, and mounted on glass microscope slides, air dried, and sealed with glass coverslips using Vectashield™ antifade mounting medium (Vector Laboratories).

Antibody specificity

All antibodies used in this thesis have had their specificity fully characterised prior to the collection of data. This was achieved through confirmation of specific labelling cross-referenced with reports in the literature, or, in the case of certain antibodies, the lack of specific signal appropriate for gene-deleted mice. Details for specificity testing are referenced in **Table 2.1**. Method specificity was tested for as follows: The same immunohistochemistry protocol was run under identical conditions, but primary antibodies were omitted in the reaction sequence; this was used to confirm the specificity of secondary antibodies. In the case of double and triple immunolabelling experiments, confirmation of the lack of cross-reactivity by secondary antibodies was tested by reacting a single primary antibody with the full complement of secondary antibodies.

Table 2.1. Details of the primary antibodies used in this study. Rb: Rabbit; Rt: Rat; Ch: Chicken; Go: Goat; GP; Guinea Pig; Ms: Mouse; Sh: Sheep.

Primary Antibody	Species	Dilution Factor	Supplier (Product code)	Specificity/Reference
Alpha-synuclein	Ms	1:1000	BIOLEGEND (SIG-39720-20)	(Larson *et al.*, 2012)
Amyloid beta	Ms	1:2000	The GENETICS company (02-250204)	Labelling identical to previously published reports
Amyloid beta oligomer- NU1	Ms	1:10000	A generous donation from our collaborator William Klein,	(Lambert *et al.*, 2007)

			Northwestern University, USA	
Amyloid beta oligomer- NU2	Ms	1:10000	A generous donation from our collaborator William Klein, Northwestern University, USA	(Lambert *et al.*, 2007)
AnkyrinG	Go	1:250	Santa Cruz Biotechnology Sc-31778 (10806)	Labelling identical to previously published reports
Calretinin	Ch	1:1000	Synaptic systems (214106)	Labelling identical to previously published reports
ChAt	Go	1:250	MILLIPORE AB1441 (2010060)	(Härtig *et al.*, 2007)
DARPP-32	Rb	1:4000	Frontier Institute (DARPP-Rb-Af400)	(Yang, You and Levison, 2008)
DARPP-32	Go	1:250	Santa Cruz Biotechnology Sc-8483 (H2409)	(Yang, You and Levison, 2008)
IBA1	Rb	1:4000	Wako PTP5154 (019-19741)	(Yang, You and Levison, 2008)
K_v1.1	Ms	1:500	UC DAVIS/NIH NeuroMab Facility Antibodies Incorporated K36/15 75-105 (440-5HK- 57c)	Specificity tested using knockout mice, UC DAVIS/NIH NeuroMab Facility

K_v1.2	Ms	1:500	UC DAVIS/NIH NeuroMab Facility Antibodies Incorporated K14/16 75-008 (443-1KS- 37)	Specificity tested using knockout mice, UC DAVIS/NIH NeuroMab Facility
K_v1.3	Ms	1:500	UC DAVIS/NIH NeuroMab Facility Antibodies Incorporated L23/27 75-009 (413-5RR- 07)	Specificity tested using knockout mice, UC DAVIS/NIH NeuroMab Facility
K_v1.4	Ms	1:500	UC DAVIS/NIH NeuroMab Facility Antibodies Incorporated K13/31 75-010 (440-5HK- 05)	Specificity tested using knockout mice, UC DAVIS/NIH NeuroMab Facility
K_v1.5	Ms	1:500	UC DAVIS/NIH NeuroMab Facility Antibodies Incorporated K7/45 75-011 (413-7RR- 33)	Specificity tested using knockout mice, UC DAVIS/NIH NeuroMab Facility
K_v1.6	Ms	1:500	UC DAVIS/NIH NeuroMab Facility Antibodies Incorporated K19/36 75-012 (413-9RR- 31)	Specificity tested using knockout mice, UC DAVIS/NIH NeuroMab Facility

K_v2.1	Ms	1:500	UC DAVIS/NIH NeuroMab Facility Antibodies Incorporated K89/34 75-014 (449-3AK- 78E)	Specificity tested using knockout mice, UC DAVIS/NIH NeuroMab Facility
K_v2.2	Ms	1:500	UC DAVIS/NIH NeuroMab Facility Antibodies Incorporated K37/89 75-015 (443-1KS- 100)	Specificity tested using knockout mice, UC DAVIS/NIH NeuroMab Facility
K_v3.1	Ms	1:500	UC DAVIS/NIH NeuroMab Facility Antibodies Incorporated N16b/8 75-041 (443. 2KS. 14)	Specificity tested using knockout mice, UC DAVIS/NIH NeuroMab Facility
K_v3.4	Ms	1:500	UC DAVIS/NIH NeuroMab Facility Antibodies Incorporated N72/16 75-112 (440-5HK- 77)	Specificity tested using knockout mice, UC DAVIS/NIH NeuroMab Facility
K_v4.2	Ms	1:500	UC DAVIS/NIH NeuroMab Facility Antibodies Incorporated K57/1 75-016 (428-9JH- 88)	Specificity tested using knockout mice, UC DAVIS/NIH NeuroMab Facility

K_v4.3	Ms	1:500	UC DAVIS/NIH NeuroMab Facility Antibodies Incorporated K75/41 75-017 (444-1LC- 26)	Specificity tested using knockout mice, UC DAVIS/NIH NeuroMab Facility
Map-2	Ch	1:500	Aves labs, Inc. (MAP7777983)	Labelling identical to previously published reports
NG2	Rb	1:500	MILLIPORE AB1529 (2290214)	(Jiang *et al.*, 2013)
NOS	Sh	1:1000	MILLIPORE AB1529 (2290214)	(Cauli *et al.*, 2004)
Parvalbumin	Go	1:500	Swant (PVG 214)	(Vereczki *et al.*, 2016)
Parvalbumin	Rb	1:500	Swant	(Härtig *et al.*, 2007)
Parvalbumin	Ch	1:500	Synaptic systems (195006)	Labelling identical to previously published reports
Picolo	Rb	1:500	Abcam Ab20664-100 (352575)	Labelling identical to previously published reports
Somatostatin	Rt	1:1000	MILLIPORE (NMM1638322)	(Dimitrov and Usdin, 2010)
Spinophyllin	Rb	1:10000	MILLIPORE AB5669 (2061438)	(Aigelsreiter *et al.*, 2013)
Substance P	Gp	1:500	Abcam	(Myöhänen *et al.*, 2008)

			Ab10353 (GR3195542-9)	
TH	Ch	1:1000	Aves labs, Inc. (TYH1205)	(Muzerelle *et al.*, 2016)
VAChT	Go	1:500	Abcam Ab43875-50 (634637)	Labelling identical to previously published reports
VGAT	Go	1:3000	Frontier Institute (VGAT-Go-Af620)	(Miura *et al.*, 2006)
VGAT	GP	1:2000	Synaptic systems (131004)	(Schock *et al.*, 2012)
VGluT1	Go	1:4000	Frontier Institute (VgluT1-Gt-Af310)	(Miyazaki *et al.*, 2003)
VGluT1	GP	1:3000	Frontier Institute (VgluT1-GP-Af570)	(Miyazaki *et al.*, 2003)
VGluT2	GP	1:3000	Frontier Institute (VgluT2-GP-Af810)	(Miyazaki *et al.*, 2003)

Microscopy

Tissue samples were examined with a confocal laser-scanning microscope (LSM 880 with AiryScan or LSM 710; Zeiss, Oberkochen, Germany) using either a Plan Apochromat 20x (NA 0.8) (pixel size 0.42 um) objective, Plan Apochromat 40x DIC oil objective (NA 1.3) (pixel size 0.29 um), Plan Apochromat 63x DIC oil objective (NA 1.4) (pixel size 0.13 um) objective or a Plan Apochromat 100x DIC oil objective (NA 1.46) (pixel size 0.08 um). Detection was with either PMT or AiryScan detectors. All images presented represent a single optical section. Images were acquired using sequential acquisition of the different channels to avoid crosstalk between fluorophores.

Pinholes were adjusted to 1.0 Airy unit for PMT scans, or optimal settings in the case of AiryScan capture. In all cases where multiple images were captured from the same immunohistochemical reaction, laser power, pinhole, and exposure settings were captured once on tissue from a representative control section and maintained throughout imaging. Images were processed with the software Zen (Zeiss) and exported into bitmap images for processing in Adobe Photoshop (Adobe Systems, San Jose, Ca, USA). Only brightness and contrast were adjusted for the whole frame, and no part of any frame was enhanced or modified in any way.

Quantification analysis of fluorescence intensity

To quantify the fluorescence intensity, ImageJ Particle Analysis tool (Open source, https://fiji.sc/) was employed. The choice to use this method was based on previous experience within the lab. The procedure is as follows: A representative micrograph acquired from confocal microscope was selected and analysed. Fluorescence intensity from ten images representing ten separate fields of view ranging from the ventral to dorsal striatum were measured and averaged to create a fluorescence intensity value for one animal.

Statistical analysis of immunohistochemical quantification

Statistical analysis was performed using GraphPad Prism (Graphpad Software, La Jolla, CA, USA). Unpaired Student's t-test was performed, and a P value of < 0.05 was considered statistically significant. N values represent

the number of animals used. A representative graph was acquired to illustrate the mean intensity.

Gene expression analyses

Sample preparation for gene expression analyses

Animals were killed by cervical dislocation and tissue homogenates prepared. In order to prevent degradation of nucleic acid in samples, fresh tissue was dissected and immediately submerged in liquid nitrogen. Total RNA was isolated from the samples using a RNeasy Mini kit (Qiagen, Venlo, Netherlands) according to the manufacturer's protocol. Briefly, tissue samples were submerged in a lysis buffer and homogenised. Samples were then centrifuged, and supernatants extracted. The supernatants were then mixed with equal volumes of 70% ethanol to prepare ribonucleic acid (RNA) binding to centrifugation columns. Samples were then added to centrifugation columns and washed by centrifugation with two wash buffers. Finally, RNA was eluted by addition of nuclease-free water and centrifuged. Samples were stored at -80°C. The quality and quantity of the extracted RNA in each tissue was examined with spectrophotometry (Thermo Scientific™ NanoDrop™) (figure 2.1), and reverse-transcribed to provide cDNA templates for polymerase chain reaction (PCR) and quantitative PCR (qPCR) reactions.

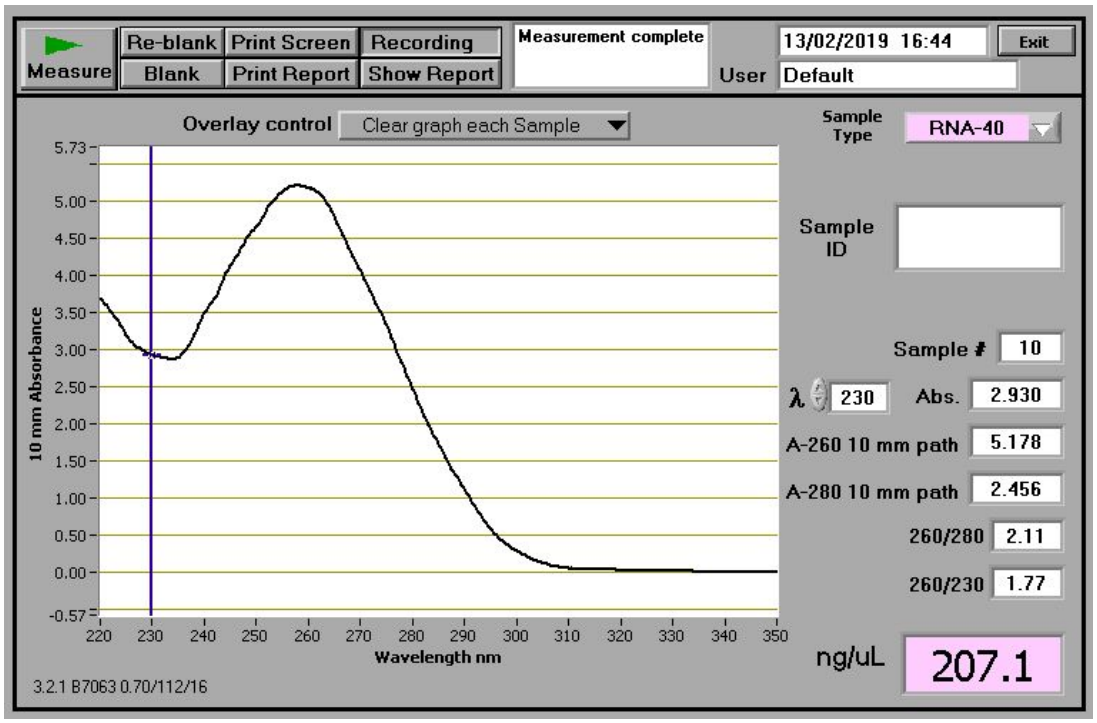

Figure 2.1. Example of absorbance spectrum for RNA samples.

Polymerase chain reaction

Reverse-transcription was achieved by incubating RNA isolates for 2 hours at 37°C in a cocktail containing: 200ng RNA 10% reverse transcription buffer (Biolabs), 5% of Oligo (dT) primers (ThermoFisher Scientific), 5% dNTPS (ThermoFisher Scientific), 2.5% M -MulV reverse transcriptase (Applied Biosystems), and 2.5% Ribolock RNase inhibitor (ThermoFisher Scientific) made up to 20µl with nuclease-free water.

PCR was performed in a cocktail containing: Taqman-specific master mix (Roche, Burgess Hill, UK); forward and reverse primers (Table 2.2) and performed using a LightCycler® 96 system (Roche). The cycling conditions were: 95°C for 300s, followed by 40 Cycles of 95°C for 15s, 60°C for 30s, 72°C for 30s and 60°C for 600s.

Gel electrophoresis was carried out as follows. A gel cast was set comprising of 4g agarose in 200mL of 0.02% TAE buffer and 4µl of SYBr safe DNA gel

stain. 20 tooth combs were inserted to define loading wells. The gel and apparatus were then submerged in TAE buffer. Sample cocktails and a protein ladder of known molecular weights (PageRuler^{TM} prestained protein ladder, Thermo Fisher) were transferred to wells and the gel was electrophoresed at 120V until the loading dye reached the end of the gel. The electrophoresed gel was then analysed on a gel documentation system.

Table 2.2. primer sequences used for PCR in this study (Li *et al.*, 2015).

Gene	**Accession numbers**	**Forward Primer Sequence**	**Reverse Primer Sequence**
K_v1.1	NM_010595.3	AGGGCTCCCGTAGTGTTC	TTTGCTGCTCCTTGGCTC
K_v1.2	NM_008417.5	CTCCTCAAGTCGTGGTGC	GGTCTGCCTCTGGGTCAT
K_v1.3	NM_008418.2	GTGTCAGTGCTGGTCATTCTC	CTGCCCATTACCTTGTCGT
K_v1.4	NM_021275.4	TTCGGAGAACCTTGACTT	GACGCAGTTCCAGCAGAG
K_v1.5	NM_145983.2	GTCACCCATCAAAGTCCG	CACTCGTCAGCCATAAGAATA
K_v1.6	NM_013568.6	GTGGATGATGTAACCGTGTC	CTCCTTCTCCTCCTCTGG
K_v2.1	NM_008420.4	AGGAGCAGATGAACGAGG	AGTGACAGGGCAATGGTG

K_v2.2	NM_001098568.2	GCGACTGTAACAC TCACG	AGCAATGGTGGAA AGAAC
K_v3.1	NM_001112739.2	TCGCTCACATCCT GAACTAT	CGTTCTCGATTTCG GTCT
K_v3.2	NM_001025581.1	TTGATATTCGCTA CGATG	TTCTGGAGGTGAT AATGG
K_v3.3	NM_001290682.1	GAGGCACTGGAC TCTTTCG	CACCGTCTTGTTG CTGATGT
K_v3.4	NM_145922.2	GAATCGCCCATTT ACTGC	GCCTTCTTGTTTCT GTCCC
K_v4.2	NM_019697.3	TCTCAAGGGCTG CGTATA	TTCGTTTGTCTGCT CGTT
K_v4.3	NM_021275.4	CAGGAAACGGTA GGAATC	GGAGTTCAGGGAT GAT
K_v5.1	NM_201531.3	TGCCTCCTCTTCA CATTTC	CTGGGCTTGGTCT TCTATT
K_v6.2	NM_001190373	TGGAAACAGCCG AGAACAA	GCTGCGGTCGAAG AAGAA
K_v7.1	NM_008434.2	ACTTCACCGTCTT CCTCATT	TGGCGAACACTTG TCCTT
K_v7.2	NM_010611.2	CTCAAGGTGGGC TTCGTG	GCAATGGAGGCAA TCAGC
K_v7.3	NM_152923.2	CTGGGCTCGGCT ATCTGT	GTGCTTCTGACGG TGCTG

K_v7.4	NM_001081142.1	TTGTCGCTACAGA GGATGGC	CAGGAAAGAGGCA AAGATGAG

Quantitative polymerase chain reaction

Reverse-transcription was achieved by incubating RNA isolates for 2 hours at 37°C in a cocktail containing: 200ng RNA 10% reverse transcription buffer (Biolabs), 5% of Oligo (dT) primers (ThermoFisher Scientific), 5% dNTPS (ThermoFisher Scientific), 2.5% M -MulV reverse transcriptase (Applied Biosystems), 2.5% Ribolock RNase inhibitor (ThermoFisher Scientific) made up to 20µl with nuclease-free water, and standard curve containing serial dilutions of RNA concentration.

qRT-PCR amplification was performed in 96-well plates in a cocktail containing a Taqman-specific master mix (Roche, Burgess Hill, UK), and Taqman probes (Table 2.3) and performed using a LightCycler® 96 system (Roche). The cycling conditions were: 95°C for 600s, followed by 40 Cycles of 95°C for 15s and 60°C for 60s. Samples were loaded containing probes for the gene of interest and *Gapdh*, which was used as a reference gene for relative mRNA quantification calculations. A standard curve of serial dilutions of known concentration were prepared alongside every sample set and loaded onto the 96-well microplate. All samples were loaded in 10µL duplicates to reduce technical variability. Standard curves were graphically analysed for reaction efficiency of each primer as well as between gene of interest (GOI) and reference gene, and for pipetting consistency. Assays in which the reaction efficiency was within 90-120%, and similar between GOI and reference genes were analysed. Linear regression of the line produced by a graph of C_t against

RNA concentration was performed and the relative concentration calculated using the following formulae:

$$\alpha = e\text{^}((C_t\text{-}m)/c)$$

$$\alpha(GOI)/\alpha(\textit{Gapdh}) = X$$

Where **α** is the product of the linear regression, ***e*** is Euler's constant (2.718281828), ($\mathbf{C_t}$) is the cycle number at which the qRT-PCR machine detects fluorescence over a pre-defined threshold, **m** is the gradient of the standard curve line, **c** is the intercept, and **x** is the level of mRNA relative to *Gapdh* levels in the sample. This technique was chosen as it allowed extra quality control steps to be performed and reduce any inter- experiment variability. qRT-PCR assays were duplicated using samples from separate cohorts of animals and numerical data pooled for statistical analyses.

Table 2.3. TaqMan probes used for qRT-PCR gene expression assays in this study

Mouse Gene	**Encoding protein**	**Reference (Life Technologies)**
ChAt	ChAt	Mm01221882-m1
DBH	DBH	Mm00460472-m1
Gapdh	GAPDH	Mm99999915_g1
Kcna2	Kv1.2	Mm00434584-s1
Kcnb1	Kv2.1	Mm00492791-m1
Kcnd2	Kv4.2	Mm01161732-m1
Kcnd3	Kv4.3	Mm01302126-m1
PV	PV	Mm00443100-m1

Slc6a4	SERT	Mm00447557-m1
TH	TH	Mm00447557-m1
TPH1	TPH1	Mm01202614-m1
TPH2	TPH2	Mm00557715-m1

Chapter Three

Characterisation of the native expression of K_v in the striatum and their plasticity in response to stress

Summary and importance

Background

Functionally and molecularly diverse classes of K_v provide unique contributions to the regulation of neuronal excitability, and therefore overall brain function. A considerable body of evidence indicates that the expression of different K_v within the brain varies according to different sub-cellular domains such as cell bodies, axons dendrites, cell types such as excitatory principal and inhibitory neurons, and brain regions such as the hippocampus and cerebellum. This contributes to the diversity of neuronal activity patterns across different populations of neurons, different brain regions, and the resultant behaviours that arise from such complex activity. Characterising such native expression and functional patterns for different classes of K_v has been instrumental in understanding diseases associated with such areas. However, almost all focus on K_v brain expression and function has been restricted to cortical regions. As a result, we currently know significantly less about classes of K_v expressed in sub-cortical brain regions such as the striatum. This is a serious impediment to identifying their potential contribution to the myriad of brain disorders associated with the striatum. Important amongst these are stress-induced psychiatric disorders such as addiction and apathy, and motor deficits related to neurodegenerative diseases. Therefore,

the aim of this chapter is to provide the first comprehensive characterisation of the cell type and domain specific expression patterns of individual K_v subtypes within the mouse striatum and determine whether a form of stress, that has been shown to alter striatum neuronal excitability, alters such expression patterns.

Methods

WT mice aged 8-10 weeks were used to investigate the native expression of K_v within the striatum. RT-PCR was used to determine the expression of K_v subtypes at the mRNA level. Immunohistochemistry with confocal microscopy was used to provide a high-resolution localisation of the protein expression patterns of K_v within the different classes of cells in the striatum, alongside their inputs from different brain regions. A model of early life stress (ELS), which has been shown to induce striatal neuronal activity, was used to assess stress-induced plasticity of K_v expression.

Results

RT-PCR revealed mRNA expression for 1, 2, 3, 4, 5, 6 and 7 families of K_v families within the striatum, which closely correlated with expression patterns in the brain region used as a positive control, namely the hippocampus. Immunohistochemistry revealed that the protein expression of specific K_v sub-classes was distinct to other brain regions. Indeed, whilst K_v1.2 has been shown to be enriched in the axon initial segment of hippocampal neurons, it was located in axonal terminals in the striatum. Furthermore, whilst K_v1.6 has been shown to be located in the axon initial segment of hippocampal neurons,

it was located in microglia of the striatum, which are the brain's resident immune cells. Different classes of K_v were selectively expressed by specific striatal cell types. Indeed, while K_v2.1 and 4.2 were exclusively expressed by principal projection cells, or medium spiny neurons (MSNs), K_v3.1 and 4.3 were exclusively expressed by parvalbumin-expressing local inhibitory interneurons. An added level of complexity was that individual cell types targeted different K_v to different sub-cellular domains. For example, MSNs expressed K_v2.1 exclusively on their proximal dendrites, and K_v4.2 on their distal dendrites. Finally, stress in early life resulted in significant decrease in the expression levels of K_v2.1, K_v4.2 as well as immune cells.

Importance

The data demonstrate that striatal neurons exhibit K_v expression patterns that are distinct from other brain regions. This might contribute to the patterns of neuronal activity that distinguish striatal-related brain functions and behaviours. The implication is that potential therapeutics for striatal-related disorders, that target various K_v, are likely to have contrasting functional roles, across different brain regions. Furthermore, life experience, in the form of ELS, had a significant effect on the expression levels of specific K_v. Since K_v expression directly determine neuronal activity, these data reveal a potentially novel mechanism, and therapeutic strategy, for stress-related disorders associated with the striatum.

Results

3.1. Characterisation of cell types, sub-cellular compartments and neurochemically diverse input to the mouse striatum

In other brain regions, different K_v have been shown to be expressed divergently across different types of cells and sub-cellular compartments. In order to interpret the immunoreactivity patterns for individual K_v within the striatum and assess whether they mirror those in other regions or are unique to the striatum, it was essential to first fully immunohistochemically characterise the different cell types and axonal input to the striatum.

The principal cells within the striatum are known as medium spiny neurons (MSN) and provide GABAergic projections to a range of other brain regions (Kemp, J.M., and Powell, 1971). They are distinctive within the striatum by their expression of Dopamine- and cyclic-AMP-regulated phosphoprotein of molecular weight 32 kDa (DARPP-32). Throughout this chapter, DARPP-32 immunoreactivity was therefore used to identify MSNs and the striatum overall (Fig 3.1 A). There are also 2 classes of MSNs, distinguished by their expression of either dopamine 1 receptor (Fig 3.1 B1) or dopamine 2 receptor (Fig 3.1 B2).

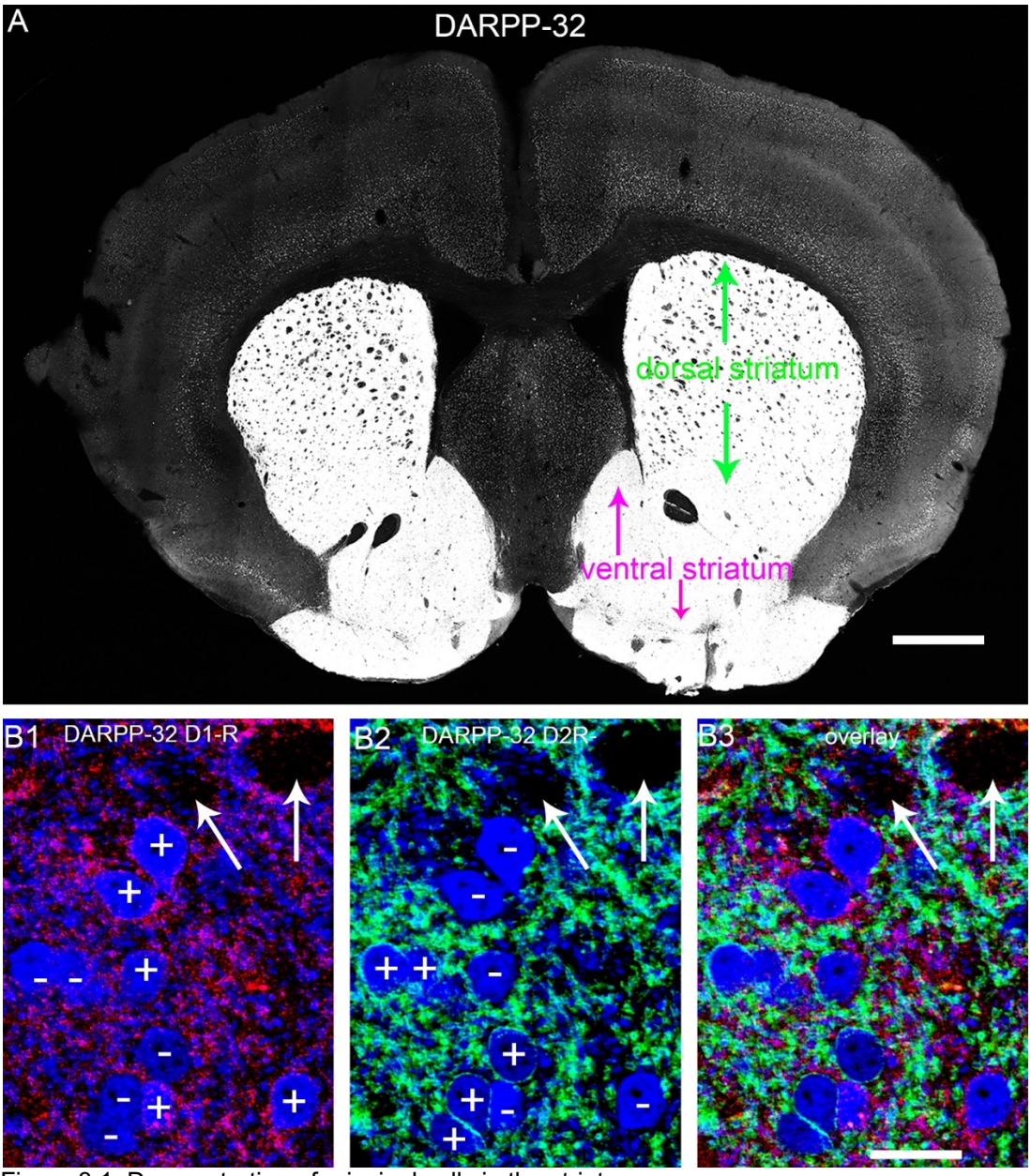

Figure 3.1. Demonstration of principal cells in the striatum.
(A) is a low power overview of the mouse brain showing the location of the striatum, identified with immunoreactivity for DARPP-32, a protein expressed exclusively in cells that express dopamine receptors. All principal cells in the striatum express DARPP-32, thereby demonstrating the distribution of the main cells within this brain region.
(B1) shows immunoreactivity for the dopamine 1 receptor (D1R) and how it is expressed by a select population of DARPP-32 immunopositive (+) whilst others are immunonegative (-). (B2) shows immunoreactivity for the dopamine 2 receptor (D2R) and how it is expressed by a select population of DARPP-32 immunopositive (+) whilst others are immunonegative (-). (B3) is an overlay of both (B1 and B2) demonstrating that all DARPP-32 cells express either D1R or D2R. Note that some cells are immunonegative for DARPP-32 (arrows) and most likely represent interneurons.
Scale bars: (A) 2 mm; (B1-3) 20 μm.

A range of marker proteins were used to identify the sub-cellular compartments of MSNs. Microtubule associated protein (MAP-2) is a cytoskeletal protein enriched in dendrites (Dehmelt and Halpain, 2005) and

was used to delineate MSNs dendritic branches (Fig 3.2 A). Spinophilin is an actin binding protein enriched in dendritic spines (Feng *et al.*, 2000). It was used to identify the sub-compartment of dendrites that are postsynaptic compartments of glutamatergic synaptic axons (Fig 3.2 B). AnkyrinG is a protein that links integral membrane proteins, such as ion channels, to the actin cytoskeleton (Michaely *et al.*, 2002). In neurons, it is enriched in the axon initial segment (Yang *et al.*, 2019), which is the first segment of the axon and the site of action potential generation (Fig 3.2 C). Piccolo is a protein that is part of the presynaptic cytoskeletal matrix (Fenster *et al.*, 2000) and is thus a marker of all presynaptic axon terminals (Fig 3.2 D).

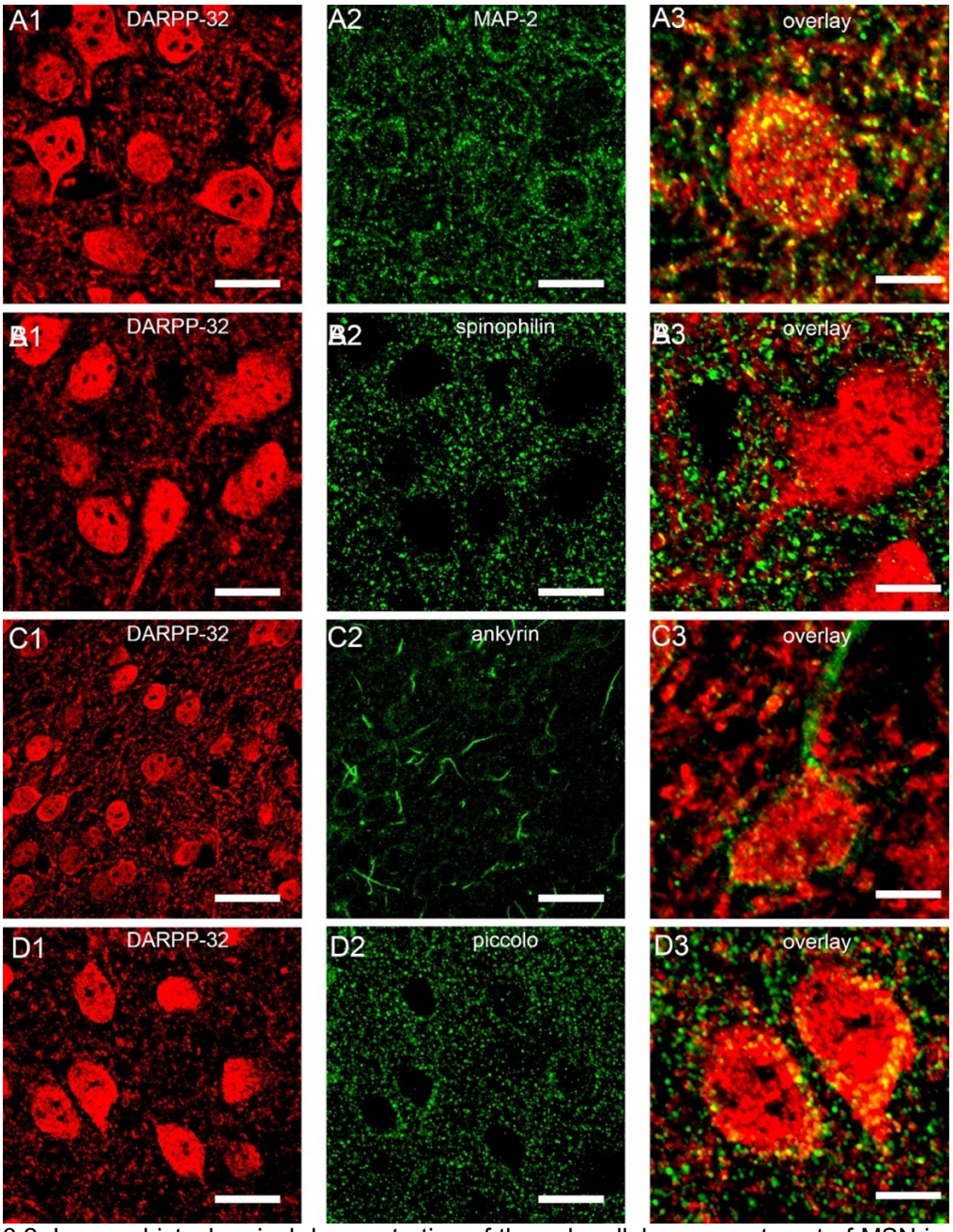

Fig 3.2. Immunohistochemical demonstration of the sub-cellular compartment of MSN in the striatum.

(A1) shows the principal cell in the striatum, MSN, identified with immunoreactivity for DARPP-32. (A2) shows, in the same field of view, immunoreactivity for dendrites, identified by Map-2, a protein enriched in dendrites. (A3) is an enlarged overlay of both (A1 and A2) demonstrating the dendrites of MSNs. As with (A1), (B1) shows the MSN. (B2) shows, in the same field of view, immunoreactivity for dendritic spines, identified by spinophilin, a protein enriched in dendritic spines. (B3) is an enlarged overlay of both (B1 and B2) demonstrating the dendritic spines of MSNs. As with (A1), (C1) shows the MSN. (C2) shows, in the same field of view, immunoreactivity for axon initial segment, identified by ankyrinG, a protein enriched in the axon initial segment. (C3) is an enlarged overlay of both (C1 and C2) demonstrating the axon initial segment of MSNs. As with (A1), (D1) shows the MSN. (D2) shows, in the same field of view, immunoreactivity for presynaptic axon terminals, identified by picolo, a protein that is part of the presynaptic cytoskeletal matrix. (D3) is an enlarged overlay of both (D1 and D2) demonstrating the presence of presynaptic axon terminals on MSNs.

Scale bars: (A1-2, B1-2; D1-2) 10 μm; (A3, B3, D3) 5 μm; (C1-2) 30 μm; (C3) 5 μm.

In other brain regions, some classes of K_v have been shown to be expressed in inhibitory interneurons. In order to interpret any such potential labelling patterns in the striatum, experimental techniques were optimised in order to confirm that the expression of various classes of interneurons known to be located in the striatum can be replicated. Under the experimental conditions, It was possible to localise all major classes of striatal interneurons (Muñoz-Manchado *et al.*, 2018) including cholinergic neurons, using immunoreactivity for the acetylcholine synthesising enzyme choline acetyl transferase (Fig 3.3 A), GABAergic interneurons distinguished by their expression of the calcium binding proteins calretinin (Fig 3.3 B) and parvalbumin (Fig 3.3 C), the neuropeptide somatostatin (Fig 3.3 D) and interneurons utilising neuronal nitric oxide as a messenger, identified by the NO synthesising enzyme nitric oxide synthase (NOS) (Fig 3.3 E).

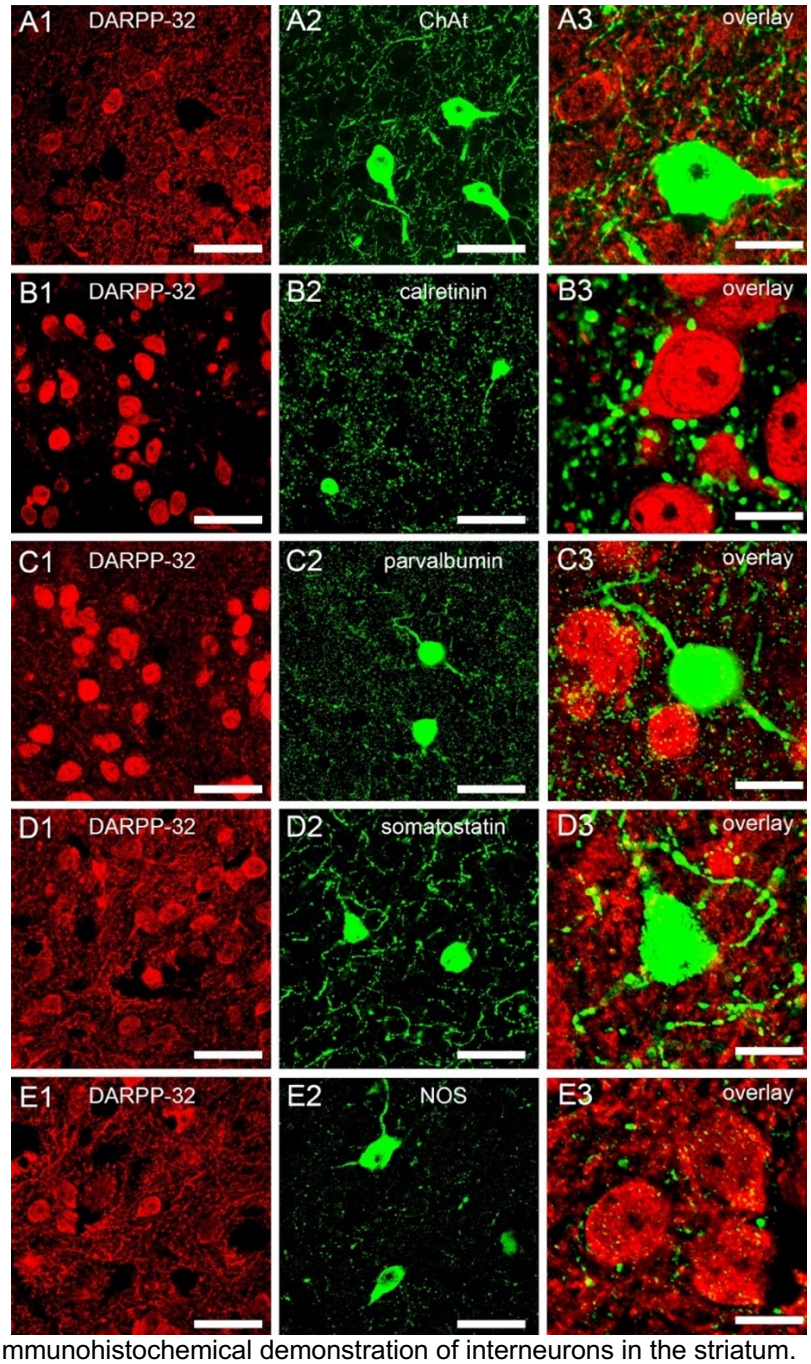

Figure 3.3. Immunohistochemical demonstration of interneurons in the striatum.
(A1-2) shows immunoreactivity for DARPP-32 (A1) and cholinergic interneurons (A2) in the same field of view. (A3) is an enlarged overlay of both (A1 and A2) demonstrating specific labelling of the cholinergic interneuron, identified with choline acetyl transferase (ChAt), an enzyme that synthesise acetylcholine which is exclusively expressed on cholinergic interneurons. (B1-2) shows immunoreactivity for DARPP-32 (B1) and GABAergic interneurons that expresses calretinin (B2) in the same field of view. (B3) is an enlarged overlay of both (B1 and B2) demonstrating specific labelling of the GABAergic interneuron expressing calretinin. As with (B1-3), (C1-3) also demonstrates specific labelling of GABAergic interneuron, however, expressing parvalbumin. (D1-2) shows immunoreactivity for DARPP-32 (D1) and interneurons expressing the neuropeptide, somatostatin in the same field of view. (D3) is an enlarged overlay of both (D1 and D2) demonstrating specific labelling of the interneuron expressing somatostatin. (E1-2) shows immunoreactivity for DARPP-32 (E1) and interneurons utilising nitric oxide (E2) identified by nitric oxide synthase (NOS) in the same field of view. (E3) is an enlarged overlay of both (E1 and E2) demonstrating specific labelling of the interneurons utilising nitric oxide (NO).
Scale bars: (A-E 1-2) 30 µm; (A-E 3) 10 µm.

Since K_v regulate neuronal activity, and MSN activity is influenced by synaptic transmission from a variety of axonal inputs, the location of neurochemically diverse inputs was next characterised in order to interpret the potential relevance of the prospective K_v immunoreactivity patterns. Excitatory neurotransmission via glutamate-containing axons provides one of the major drives of MSN activity, and thus striatal function. Glutamatergic axons that synapse on MSNs originate from a variety of other brain regions (Britt *et al.*, 2012). The sources of such inputs can be distinguished by the expression of the vesicular glutamate transporters 1 and 2 (VGLUT 1-2). The majority of the VGLUT1-containing axons originate from the cortex, hippocampus and amygdala, carry information related to emotion and cognition and synapse on MSN dendritic spines (Fig 3.4 A1, 3). While VGLUT2-containing axons also synapse on MSN dendritic spines (Fig 3.4 A2, 3), they originate primarily from the thalamus and relay sensory related information to the striatum. While excitatory synapses target dendritic spines, inhibitory synapses, containing GABA released by local interneurons and identified by immunoreactivity for the vesicular γ-aminobutyric acid transporter (VGAT), contact MSN cell bodies as well as dendritic shafts (Fig 3.4 B). Monoaminergic inputs, such as noradrenaline and dopamine, identified by immunoreactivity for the synthesising enzyme tyrosine hydroxylase (TH), contact both the dendrites and cell bodies of MSNs (Fig 3.4 C). Finally, axon terminals from local cholinergic interneurons, identified by immunoreactivity for the vesicular acetylcholine transporter (VAchT), also contact MSN somata and dendrites (Fig 3.4 D).

Thus, having replicated the core cell biology and neurochemistry of the striatum under my experimental conditions, I was in place to critically analyse the immunoreactivity patterns of K_v within such neural circuitry.

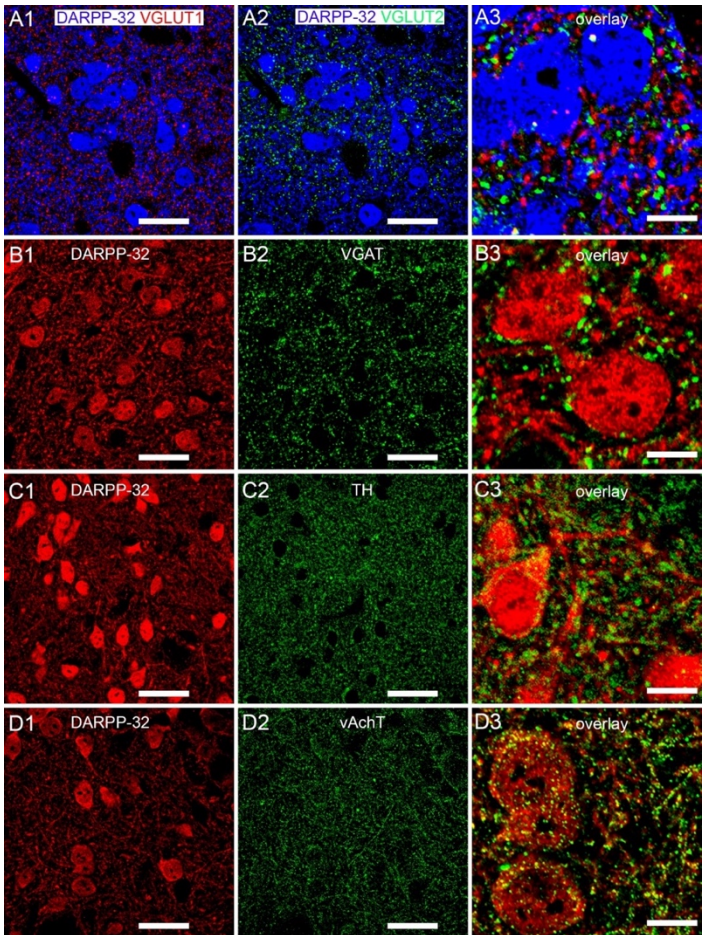

Figure 3.4. Immunohistochemical demonstration of neurochemical inputs in the striatum.
(A1-2) shows the association between MSN identified by immunoreactivity with DARPP-32 and excitatory synapses identified by immunoreactivity with vesicular glutamate transporter 1 (VGLUT1) and vesicular glutamate transporter 2 (VGLUT2) in the same field of view. (A3) is an enlarged overlay of both (A1 and A2) showing that both VGLUT1 and 2 synapses on MSN dendritic spines. Note that VGLUT1-containing axons originate from the cortex, hippocampus and amygdala, while VGLUT2-containing axons originate primarily from the thalamus. (B1-2) shows immunoreactivity for MSN (B1) and inhibitory synapses, containing GABA (B2) identified by vesicular γ-aminobutyric acid transporter (VGAT) in the same field of view. (B3) is an enlarged overlay of both (B1 and B2) demonstrating that local interneurons release inhibitory synapse that contact MSN cell bodies as well as dendritic shafts. (C1-2) shows immunoreactivity for MSN (C1) and monoaminergic inputs (C2) identified by tyrosine hydroxylase (TH) in the same field of view. Immunoreactivity for TH is used to identify monoaminergic inputs, such as noradrenaline and dopamine. (C3) is an enlarged overlay of both (C1 and C2) demonstrating that monoaminergic inputs contact MSN cell bodies and dendrites. Monoaminergic inputs, such as noradrenaline originates from the locus coeruleus; while dopamine originates from the ventral tegmental area, substantia nigra and hypothalamus. (D1-2) shows immunoreactivity for MSN (D1) and axon terminals from cholinergic interneurons (D2), identified by vesicular acetylcholine transporter (VAChT). (D3) is an enlarged overlay of both (D1 and D2) demonstrating that local cholinergic interneurons axon terminals contact MSN somata and dendrites.
Scale bars: (A-D 1-2) 20 μm; (A-D 3) 10 μm.

3.2. Expression of K_v subtypes at the mRNA level in the striatum and hippocampus

Since the overall aims of my PhD research was to characterise the native expression patterns of different K_v sub-families within the mouse striatum, I characterised all the K_v sub families in the striatum at the mRNA level to identify which of them is expressed in the striatum. Studies have shown the regional and cellular localisation of the members of the K_v1–K_v7 subfamily (Trimmer and Rhodes, 2004) and primer sequences have been developed to investigate them at the mRNA level (Li *et al.*, 2015). To this end, I performed RT-PCR using homogenates from the striatum and hippocampus of WT mice. Gel electrophoresis images of cDNA amplicons showed that $K_v1.1$, $K_v1.2$, $K_v1.3$, $K_v1.4$, $K_v1.5$, $K_v1.6$, $K_v2.1$, $K_v2.2$, $K_v3.1$, $K_v3.3$, $K_v3.4$, $K_v4.2$, $K_v5.1$, $K_v7.1$, $K_v7.2$, $K_v7.3$ and $K_v7.4$ were expressed in the striatum (Fig 3.5). The expression pattern was similar when compared with the K_v subtypes expressed in the hippocampus. The gel electrophoresis images from the RT-PCR didn't show the expression of $K_v4.3$ both in the striatum and hippocampus even though studies have shown $K_v4.3$ to be expressed throughout the brain (Trimmer and Rhodes, 2004). Thus, further investigation was carried out using immunohistochemical reactions to ascertain the expression of $K_v4.3$.

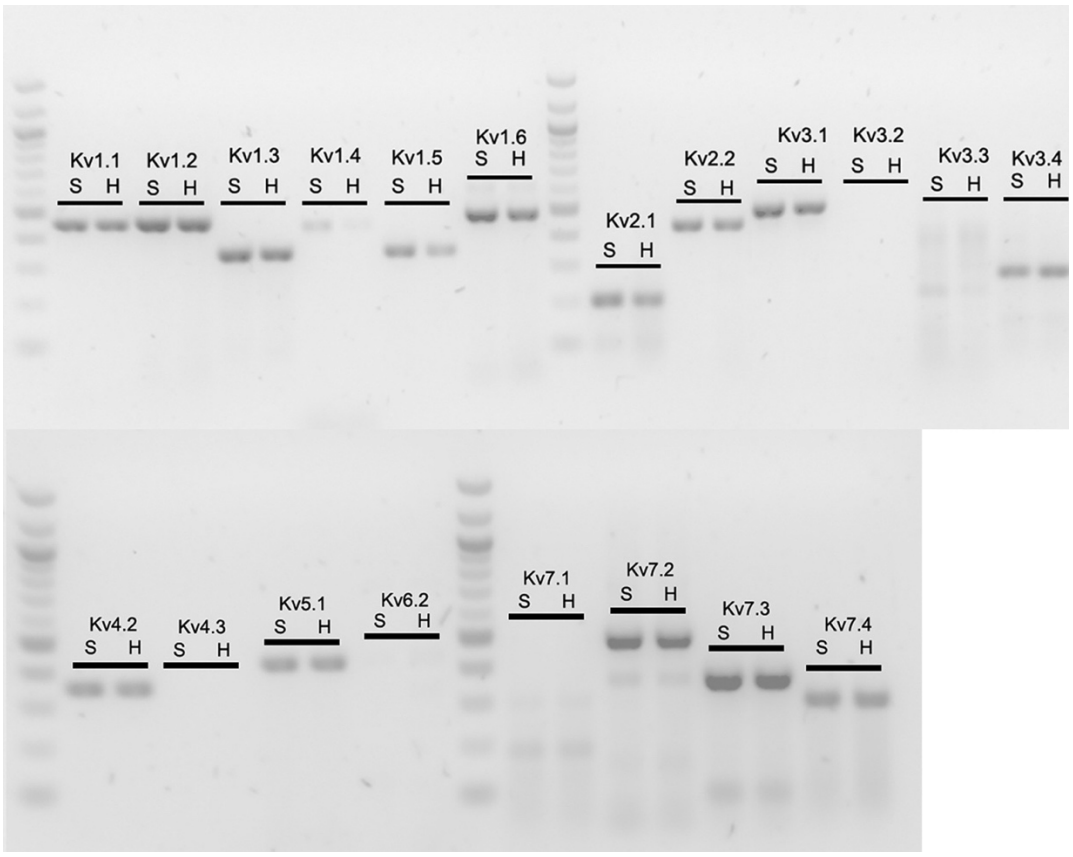

Figure 3.5. Demonstration of the native expression of K_v sub-family at the mRNA level in the striatum.

Tissue homogenates of mouse striatum were extracted for RNA and reverse-transcribed to provide cDNA templates for polymerase chain reaction (PCR) of K_v1- K_v7 subfamily. Gel electrophoresis images shows that $K_v1.1$, $K_v1.2$, $K_v1.3$, $K_v1.4$, $K_v1.5$, $K_v1.6$, $K_v2.1$, $K_v2.2$, $K_v3.1$, $K_v3.3$, $K_v3.4$, $K_v4.2$, $K_v5.1$, $K_v7.1$, $K_v7.2$, $K_v7.3$ and $K_v7.4$ are expressed in the striatum (S). The RT-PCR of hippocampus (H) homogenates were used as a positive control.

3.3. Immunochemical characterisation of the location of K_v subtypes in the striatum

Guided by the mRNA expression, the cellular and sub-cellular expression patterns of the various sub-classes of K_v was systemically mapped as follows:

Immunolocalisation of the K_v1 family

Immunoreactivity for $K_v1.1$ presented as individual clusters that encircled but did not overlap with DARPP-32 immunopositive cell bodies (Fig 3.6 A). This indicates that $K_v1.1$ is not expressed by MSNs themselves and as such immunoreactivity most likely represents signal in axon terminals. This is in agreement with previously published reports of its expression profile (Trimmer,

2015). As shown earlier, since GABAergic axons preferentially innervate this sub-cellular region of MSNs, I compared the K_v1.1 immunoreactivity to that of VGAT (Fig 3.6 B) and confirmed a close association between these signals (Fig 3.6 C). I did not detect any association between K_v1.1 and glutamatergic markers or markers of any other inputs. This suggests that in the striatum, K_v1.1 regulate the activity of inhibitory inputs onto MSNs and therefore the mechanism that will influence the degree to which these projection cells can influence their targets in other brain regions.

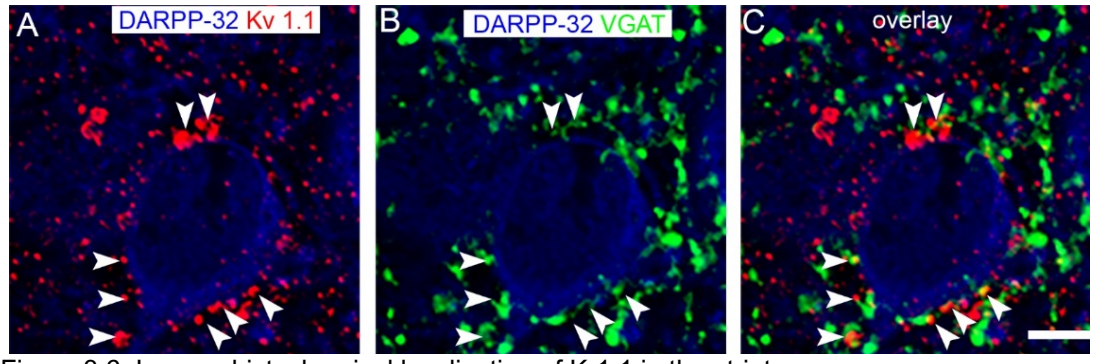

Figure 3.6. Immunohistochemical localisation of K_v1.1 in the striatum.
(A) shows immunoreactivity for K_v1.1 and how individual clusters of K_v1.1 encircled but did not overlap with MSN. (B) shows immunoreactivity for GABAergic axons, identified by VGAT expressed on MSN. (C) is an overlay of both (A and B) demonstrating a close association between GABAergic axons and K_v1.1 signal.
Scale bar: 5 µm.

In cortical brain regions, the predominant location for K_v1.2 expression is the axon initial segment (AIS). I therefore began by assessing whether this was also the case in the striatum. K_v1.2 immunoreactivity presented as individual clusters that were distributed throughout the DARPP-32 immunopositive cells, predominantly with dendrites, and to a lesser extent with cell bodies (Fig 3.7 A1). Again, there was no overlap between K_v1.2 and DARPP-32 indicating that within the striatum, MSNs did not express this ion channel. Using immunoreactivity for ankyrinG (Fig 3.7 A2), I detected only minimal association of K_v1.2 signal with that of ankyrinG (Fig 3.7 A3). This absence of K_v1.2 in MSNs AISs is a striking difference to cortical neurons, which have this sub-

domain enriched with this ion channel (A. Lorincz and Nusser, 2008). This suggest that this ion channel has a limited contribution to regulating the membrane potential of MSNs within this region of their axons. Since a large proportion of K_v1.2 clusters were associated with DARPP-32 immunopositive dendrites (Fig 3.7 B1), I next examined their association with the dendritic spine marker spinophilin (Fig 3.7 B2). The majority of K_v1.2 immunopositive clusters were located directly adjacent to clusters immunoreactive for spinophilin (Fig 3.7 B3). Since spinophilin is located in dendritic spines, which themselves are the postsynaptic domains of excitatory synapses, this suggests that K_v1.2 is associated with excitatory synapses. To confirm the association of K_v1.2 with synapses, I examined its expression alongside that of the generic presynaptic protein piccolo and confirmed that the majority of K_v1.2 clusters overlapped with those immunopositive for piccolo (Fig 3.7 C). To confirm that K_v1.2 was indeed expressed with glutamatergic axons, I verified the immunoreactivity for this on channel overlapped with signal for VGLUT1 (Fig 3.7 D) and VGLUT2 (Fig 3.7 E). This indicates that K_v1.2 contributes to the activity of axons that primarily determine the excitation of MSNs.

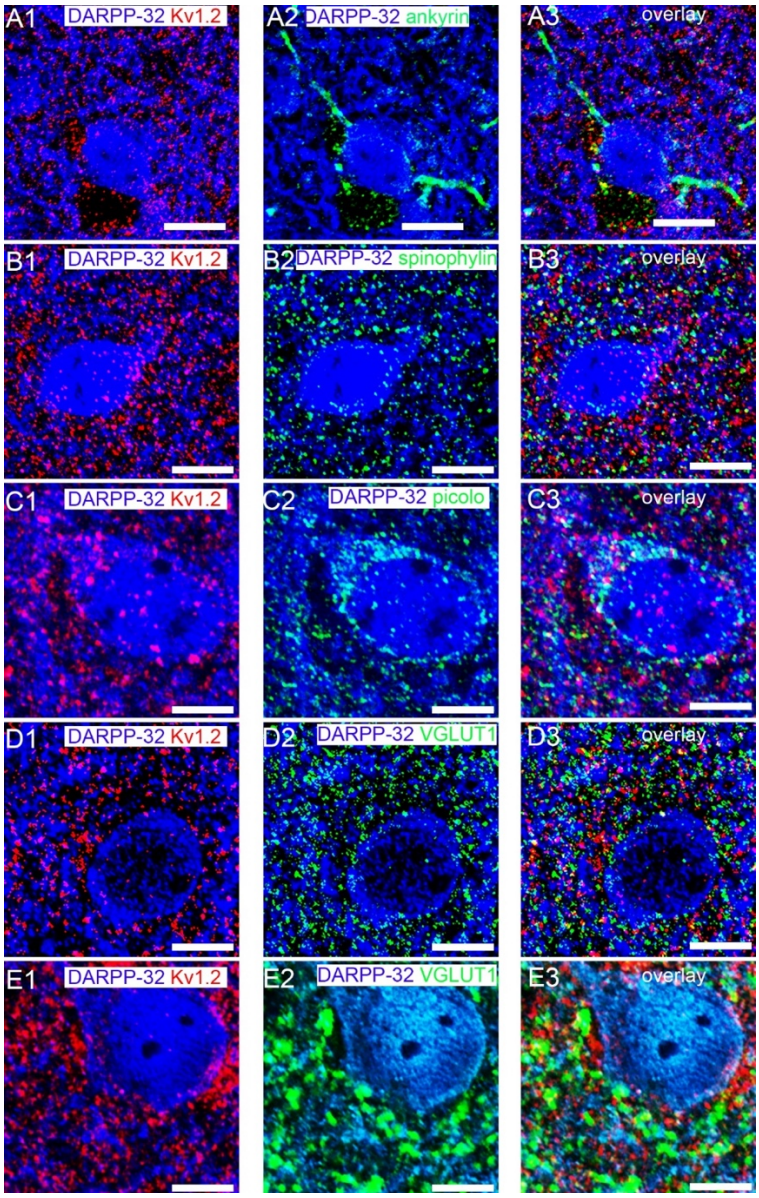

Figure 3.7. Immunohistochemical localisation of $K_v1.2$ in the striatum.
(A1) shows immunoreactivity for $K_v1.2$ and how it is expressed on DARPP-32 immunopositive cells (MSN). Individual clusters of $K_v1.2$ are distributed predominantly with dendrites, and to a lesser extent with cell bodies. (A2) shows immunoreactivity for ankyrinG used to identify the axon initial segment (AIS) of DARPP-32 cells. (A3) is an overlay of both (A1 and A2) in the same field of view demonstrating minimal association between ankyrinG and $K_v1.2$ signal. As with (A1), (B1) shows immunoreactivity for $K_v1.2$ expressed predominantly with dendrites. (B2) shows immunoreactivity for spinophilin used to identify dendritic spines of MSN. Dendritic spines are the postsynaptic domains of excitatory synapses (B3) is an overlay of both (B1 and B2) in the same field of view demonstrating association between spinophilin and $K_v1.2$ signal. This suggests that $K_v1.2$ is associated with excitatory synapses. As with (B1-3), (C1, D1 and E1) shows the association of $K_v1.2$ with MSN to compare association with synapses in the same field of view. Generic presynaptic protein identified by picolo (C2) was used as well as glutamatergic axons identified by VGLUT1 (D2) and VGLUT2 (E2). (C3) is an overlay of both (C1 and C2) in the same field of view demonstrating association between picolo and $K_v1.2$ signal. (D3) is an overlay of both (D1 and D2) in the same field of view demonstrating association between VGLUT1 and $K_v1.2$ signal. (E3) is an overlay of both (E1 and E2) in the same field of view demonstrating association between VGLUT2 and $K_v1.2$ signal. (C-E) demonstrates that $K_v1.2$ contributes to the activity of axons that primarily determine the excitation of MSNs.
Scale bars: (A) 20 µm; (B) 10 µm; (C-E) 5 µm.

Immunoreactivity for $K_v1.3$ was wholly restricted to DARPP-32 immunopositive cell bodies, located within the cytoplasm and most likely associated with specific cell organelles (Fig 3.8). In light of its lack of association with the plasma membrane, it is reasonable to conclude that this ion channel does not contribute to the regulating of the passage of K ions between intra and extracellular compartments and thus will have a minimal contribution to the membrane potential. It could, however, regulate K ions across the membranes of organelles.

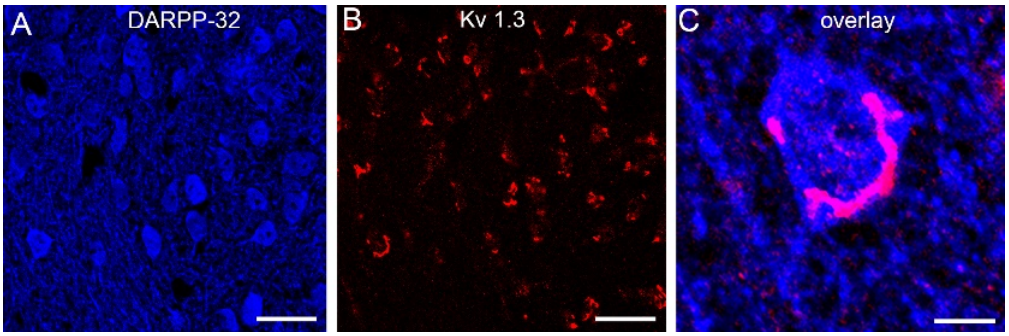

Figure 3.8. Immunohistochemical localisation of $K_v1.3$ in the striatum.
(A) shows immunoreactivity for DARPP-32. (B) shows immunoreactivity for $K_v1.3$ in the same field of view. (C) is an enlarged overlay of both (A and B) showing $K_v1.3$ expression restricted to DARPP-32 immunopositive cell bodies, located within the cytoplasm.
Scale bars: (A-B) 50 µm; (C) 5 µm.

Immunoreactivity for $K_v1.4$ also presented as individual clusters, representative of axon terminals, and were enriched in the regions surrounding DARPP-32 immunopositive cell bodies and proximal dendrites (Fig 3.9 A). The majority of these clusters were closely associated with clusters immunopositive for VGLUT2 (Fig 3.9 B, C). This suggest that in the striatum, $K_v1.4$ regulates the membrane potential of glutamatergic axons originating from the thalamus and thus impacts on how this brain region modulates the excitability of MSNs.

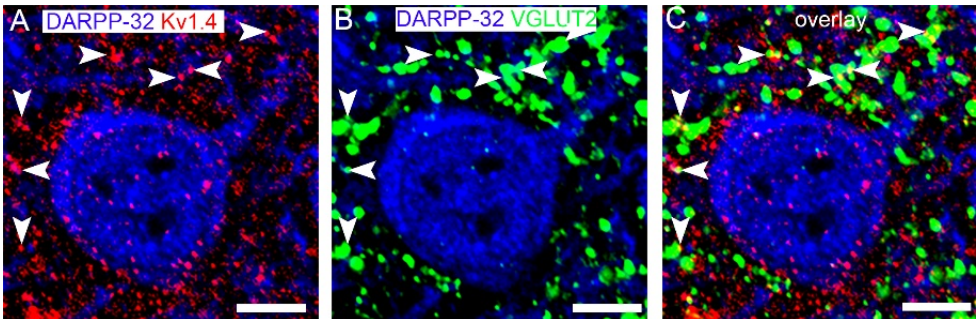

Figure 3.9. Immunohistochemical localisation of K_v1.4 in the striatum.
(A) shows immunoreactivity for K_v1.4 and how it is richly clustered in regions surrounding DARPP-32 immunopositive cell bodies and proximal dendrites. (B) shows immunoreactivity for glutamatergic axons, identified by VGLUT2. Glutamatergic axons originate from the thalamus. (C) is an overlay of both (A and B) in the same field of view demonstrating a close association between glutamatergic axons and K_v1.4 signal.
Scale bar: 5 µm.

K_v1.5 was distinctive in that it was associated with both DARPP-32 immunopositive and immunonegative cells (Fig 3.10 A). In terms of expression on MSNs, K_v1.5 signal was located on the plasma membrane of cell bodies as well as dendrites, suggesting a postsynaptic localisation. Thus, this is the only K_v1 subtype that is actually expressed on plasma membranes of MSNs, and therefore the only channel from this family to contribute to the regulation of MSN membrane potential. K_v1.5 clusters were located in close proximity to synapses, as demonstrated by their proximity to the synaptic protein piccolo (Fig 3.10 B). Apart from expression in MSNs, the strongest K_v1.5 signal was located with GABAergic interneurons that I confirmed with immunopositivity for the calcium binding protein parvalbumin (Fig 3.10 C). Thus, K_v1.5 also regulate the activity of cells that in turn control the activity of MSNs. Finally, K_v1.5 immunopositive clusters were also associated with cells that were immunoreactive for the protein neuron-glial antigen 2 (NG2), a chondroitin sulfate proteoglycan that is expressed in oligodendrocyte precursor cells (OPC). OPCs serve as a reservoir for the generation of new oligodendrocytes, the glial that produce myelin within the central nervous system. OPCs are highly dynamic and changes in response to brain activity and are also

associated with a range of disorders. I believe this to be the first demonstration of the expression of a K_v in NG2 cells and opens the possibility of a unique target for disorders associated with OPCs or myelin production.

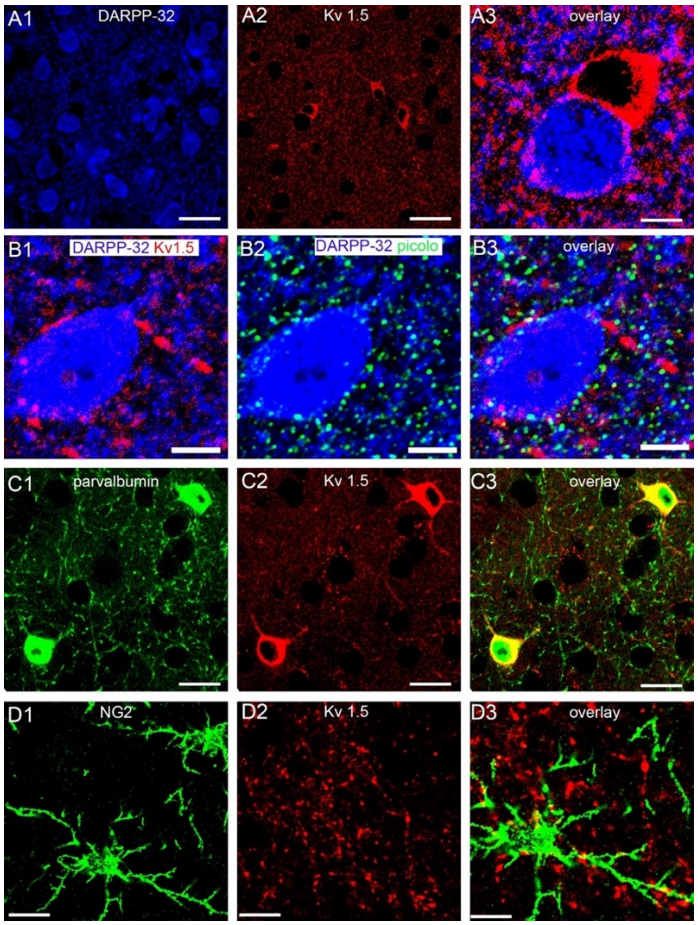

Figure 3.10. Immunohistochemical localisation of $K_v1.5$ in the striatum.
(A1) shows immunoreactivity for DARPP-32. (A2) shows immunoreactivity for $K_v1.5$ in the same field of view. (A3) is an enlarged overlay of both (A1 and A2) showing $K_v1.5$ to be associated with both DARPP-32 immunopositive and immunonegative cells. $K_v1.5$ signal was located on the plasma membrane of MSN cell bodies as well as dendrites suggesting a post synaptic localisation of $K_v1.5$. (B1) shows the association between clusters immunoreactive for $K_v1.5$ with DARPP-32 cell bodies and dendrites. (B2) shows immunoreactivity for presynaptic protein identified by picolo with DARPP-32 cell bodies. (B3) is an overlay of both (B1 and B2) in the same field of view demonstrating a close proximity between $K_v1.5$ and picolo. This suggest a presynaptic localisation of $K_v1.5$. (C1) shows immunoreactivity for GABAergic interneurons identified by immunoreactivity for parvalbumin. (C2) shows immunoreactivity for $K_v1.5$ in the same field of view. (C3) is an overlay of (C1 and C2) in the same field of view showing the strongest signal of $K_v1.5$ to be around GABAergic interneurons immunopositive for parvalbumin. (D1) shows immunoreactivity for neuron-glial antigen 2 (NG2), a protein used to identify oligodendrocyte precursor cells (OPC). (D2) shows immunoreactivity for $K_v1.5$ in the same field of view. (A3) is an overlay of both (D1 and D2) in the same field of view showing $K_v1.5$ clusters to be associated with OPC cells.
Scale bars: (A1-2) 30 µm; (A3) 5 µm; (B) 5 µm; (C-D) 10 µm.

In cortical brain regions, $K_v1.6$ is almost exclusively expressed in the AIS of neurons (A. Lorincz and Nusser, 2008). However, in the striatum, $K_v1.6$

immunoreactivity was expressed in cells that did not resemble neurons (Fig 3.11 A), and were confirmed to be microglia, identified by immunoreactivity for IBA1 (3.11 B). Microglia are the resident immune cells of the brain and are activated during neuroinflammation, a process associated with a range of brain disorders. While $K_v1.3$ (Nguyen *et al.*, 2017) and $K_v1.5$ (Kotecha and Schlichter, 1999) have been shown to be expressed in cortical microglia, this is the first demonstration that microglia expresses $K_v1.6$. This could represent a unique profile of these immune modulatory cells within the striatum and thus novel avenue for addressing neuroinflammation within this brain region.

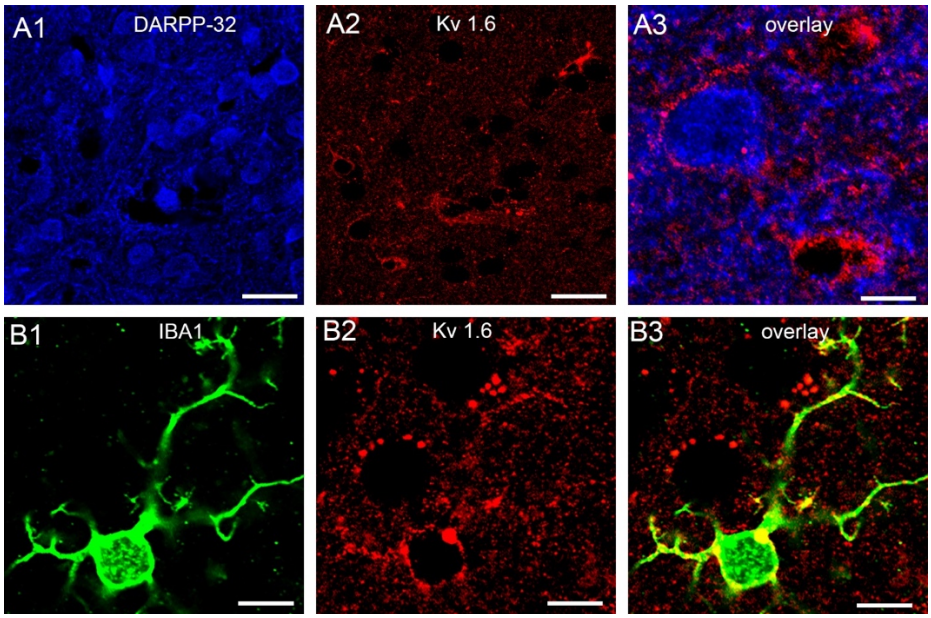

Figure 3.11. Immunohistochemical localisation of $K_v1.6$ in the striatum.
(A1) shows immunoreactivity for DARPP-32. (A2) shows immunoreactivity for $K_v1.6$ in the same field of view. (A3) is an enlarged overlay of both (A1 and A2) showing $K_v1.6$ to be expressed on DARPP-32 immunonegative cells. (B1) shows immunoreactivity for IBA1 used to identify microglia cells. (B2) shows immunoreactivity for $K_v1.6$ in the same field of view. (B3) is an overlay of both (A and B) in the same field of view confirming the DARPP-32 immunonegative cell which $K_v1.6$ is expressed on to be microglia cells.
Scale bars: (A1-2) 30 µm; (A3) 5 µm; (B) 10 µm.

Immunolocalisation of K_v2 family

Immunoreactivity for $K_v2.1$ was striking in that signal was enriched on the plasma membranes of cell bodies and proximal dendrites of MSNs (Fig 3.12 A). It was noticeable that distal dendrites were devoid of signal (Fig 3.12 B), in

a similar manner to cortical neurons (Trimmer, 2015). This indicates that an individual MSN will produce $K_v2.1$ but target its membrane insertion selectively to specific sub-cellular compartments. This suggests that different mechanisms control the membrane potential of different compartments of an individual cell. $K_v2.1$ signal was closely associated with GABAergic axon terminals, identified by immunoreactivity for VGAT (Fig 3.12 C). Thus, $K_v2.1$ could regulate the changes in membrane potential arising from inhibitory synaptic transmission.

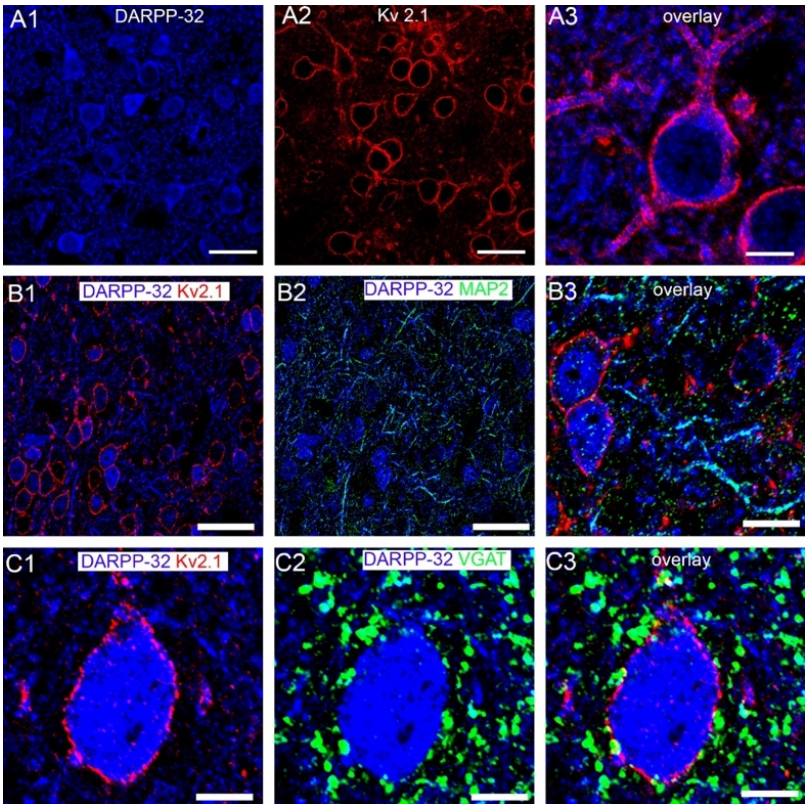

Figure 3.12. Immunohistochemical localisation of $K_v2.1$ in the striatum.
(A1) shows immunoreactivity for DARPP-32 immunopositive cells (MSN). (A2) shows immunoreactivity for $K_v2.1$ in the same field of view. (A3) is an enlarged overlay of both (A1 and A2) showing $K_v2.1$ to be expressed on the plasma membranes of MSN cell bodies and proximal dendrites. As in (A3), (B1) shows the association between $K_v2.1$ with MSN cell bodies. (B2) shows immunoreactivity for dendrites, identified by Map-2, to compare association of $K_v2.1$ to distal dendrites. (B3) is an enlarged overlay of both (B1 and B2) showing that there is no association between $K_v2.1$ and MAP-2 signals. As in (A3), (C1) shows the association between $K_v2.1$ with MSN cell bodies. (C2) shows immunoreactivity for GABAergic axon terminals, identified by immunoreactivity for VGAT in the same field of view to compare association of $K_v2.1$. (C3) is an overlay of both (B1 and B2) in the same field of view showing a strong association between GABAergic axon terminals and $K_v2.1$ signal. Thus, $K_v2.1$ could regulate the changes in membrane potential arising from inhibitory synaptic transmission.
Scale bars: (A-B1-2) 30 µm; (A3) 5 µm; (B3) 10 µm; (C) 5 µm.

Immunolocalisation of K_v3 family

$K_v3.1$ was not associated with MSNs and entirely expressed in parvalbumin immunopositive inhibitory interneurons (Fig 3.13 A), in agreement with other brain regions (Trimmer, 2015). In stark contrast, clusters immunoreactive for $K_v3.4$ richly decorated DARPP-32 immunopositive cell bodies and dendrites, in close association with the synaptic protein picolo (Fig 3.13 B). This indicates that different members of the K_v3 family regulate pre and postsynaptic signalling in the striatum.

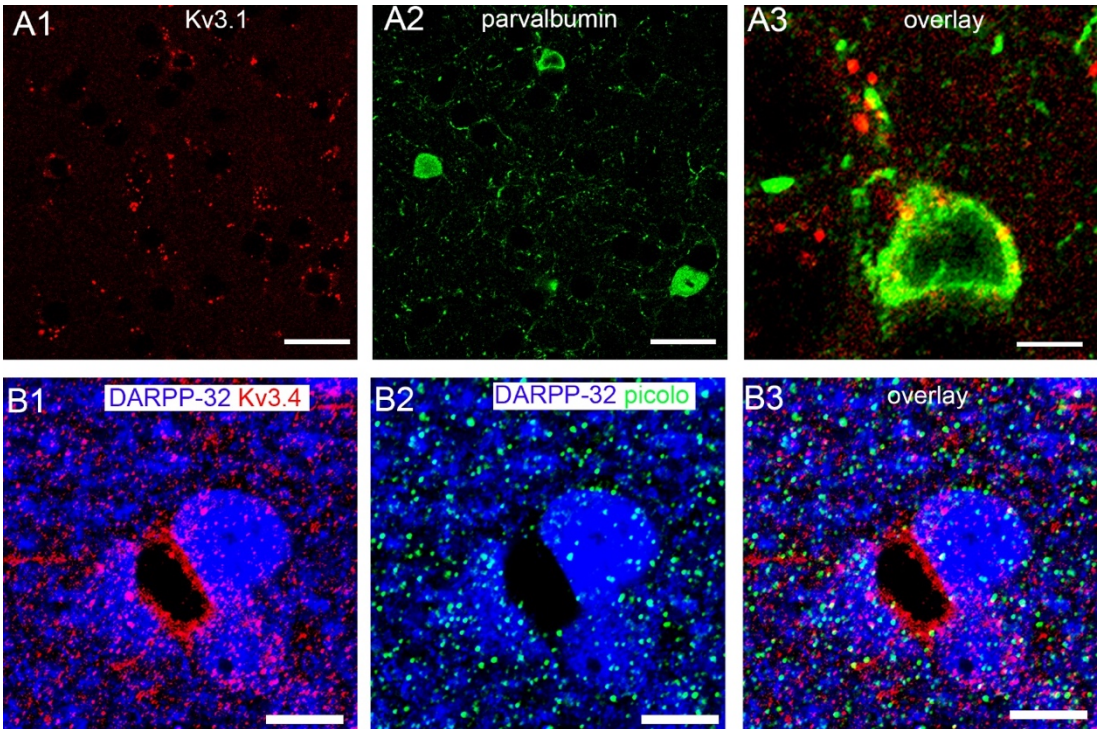

Figure 3.13. Immunohistochemical localisation of K_v3 family in the striatum.
(A1) shows immunoreactivity for $K_v3.1$. (A2) shows immunoreactivity for GABAergic interneurons containing parvalbumin in the same field of view. (A3) is an enlarged overlay of both (A1 and A2) showing the expression of $K_v3.1$ in parvalbumin immunopositive GABAergic interneuron. (B1) shows the association between clusters immunoreactive for $K_v3.4$ with DARPP-32 cell bodies and dendrites. (B2) shows immunoreactivity for presynaptic protein identified by picolo with DARPP-32 cell bodies. (B3) is an overlay of both (B1 and B2) in the same field of view demonstrating a close proximity between $K_v3.4$ and piccolo.
Scale bars: (A1-2) 30 µm; (A3) 5 µm; (B) 10 µm.

Immunolocalisation of K_v4 family

$K_v4.2$ immunoreactivity was almost the mirror image of signal for $K_v2.1$, in that it was restricted entirely to the distal dendritic compartments, with limited signal on MSN cell bodies and proximal dendrites (Fig 3.14 A). Collectively, this suggest that for an individual MSN, $K_v2.1$ regulates the membrane potential on the cell body and proximal dendrites, while $K_v4.2$ regulates it on the distal dendrites.

$K_v4.3$ was wholly enriched in parvalbumin expressing inhibitory interneurons (Fig 3.14 B). Again, this demonstrates that different members of the same family of K_v regulate the pre and postsynaptic elements within striatal neuronal circuitry.

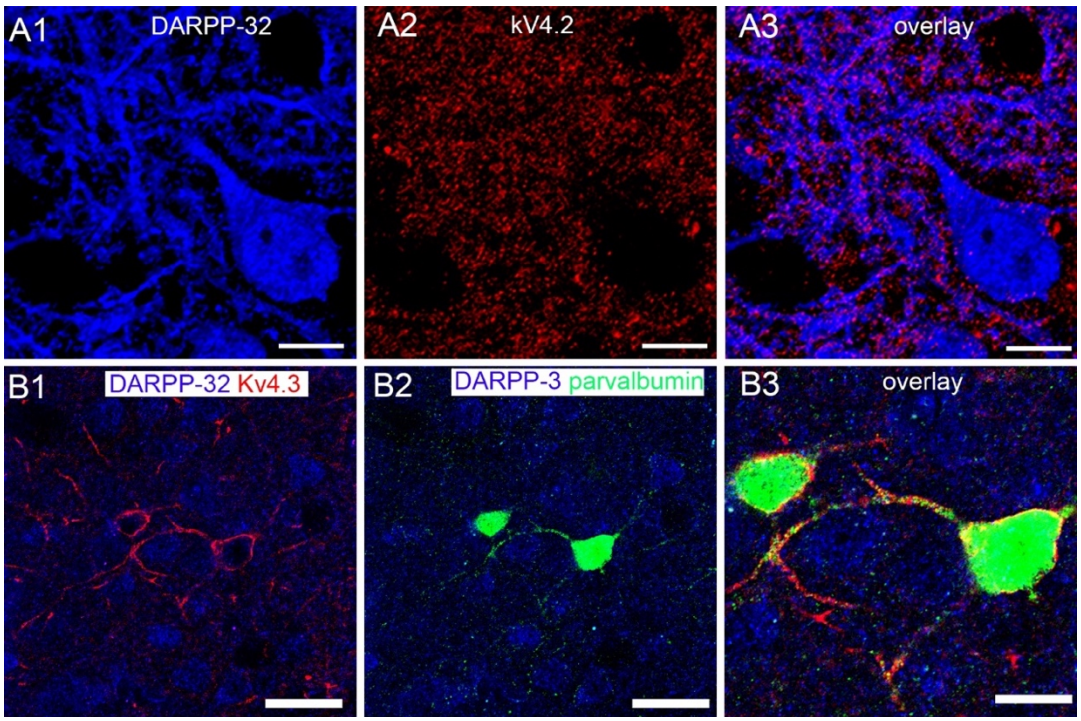

Figure 3.14. Immunohistochemical localisation of K_v4 family in the striatum.
(A1) shows immunoreactivity for MSN identified by DARPP-32 immunopositivity. (A2) shows immunoreactivity for $K_v4.2$ in the same field of view. (A3) is an overlay of both (A1 and A2) in the same field of view showing $K_v4.2$ to be expressed on distal dendritic compartments. (B1) shows expression of clusters immunoreactive for $K_v4.3$ on DARPP-32 immunonegative cells. (B2) shows immunoreactivity for GABAergic interneuron expressing parvalbumin. (B3) is an enlarged overlay of (B1 and B2) confirming the DARPP-32 immunonegative cell which $K_v4.3$ is expressed on to be parvalbumin containing GABAergic interneuron.
Scale bars: (A) 10 µm; (B1-2) 20 µm; (B3) 10 µm

3.4. Effect of early life stress on the native expression of K_v in the striatum

We live complex lives, enduring many experiences. In order to assess how stable the above K_v expression profiles are across a lifetime, I assessed the potential changes in K_v expression in response to something we all experience in our lifetime, namely stress. I opted for a model of chronic, rather than acute stress. This is because the more severe forms are associated with maladaptive responses and various diseases. Importantly, a novel stress pathway has recently been discovered in the striatum (Lemos *et al.*, 2012). To induce a chronic stress phenotype, I employed an animal model of early life stress (ELS) that our lab has shown to induce an enduring hyper-stress phenotype throughout adulthood as well as depressive like behaviour in mice (Gunn *et al.*, 2013). Our lab has furthermore shown that animals exposed to this form of ELS have profound changes in the activity of striatal neurons (Mitchell *et al.*, 2018), suggesting changes in the expression of protein that regulate such activity. The central role that K_v play is regulating neuronal activity. I next explored whether ELS impacts on K_v expression levels, using semi-quantitative immunohistochemistry and confocal microscopy. I restricted this analysis to the K_v2.1 and 4.2 subtypes since they were the only ones that were exclusively located on MSNs.

I detected a significant decrease in the mean fluorescence intensity of K_v2.1 in the ventral striatum ($P = 0.0489$, unpaired Student's t test, N = 5 mice for control and ELS), but not in the dorsal striatum ($P = 0.4656$, unpaired Student's t test, N = 5 mice for control and ELS) (Fig 3.15). There was also a significant decrease in the mean fluorescence intensity of K_v4.2 in both ventral (P =

0.0036, unpaired Student's t test, N = 5 mice for control and ELS) and dorsal striatum (P = 0.0098, unpaired Student's t test, N = 5 mice for control and ELS) of ELS mice (Fig 3.16).

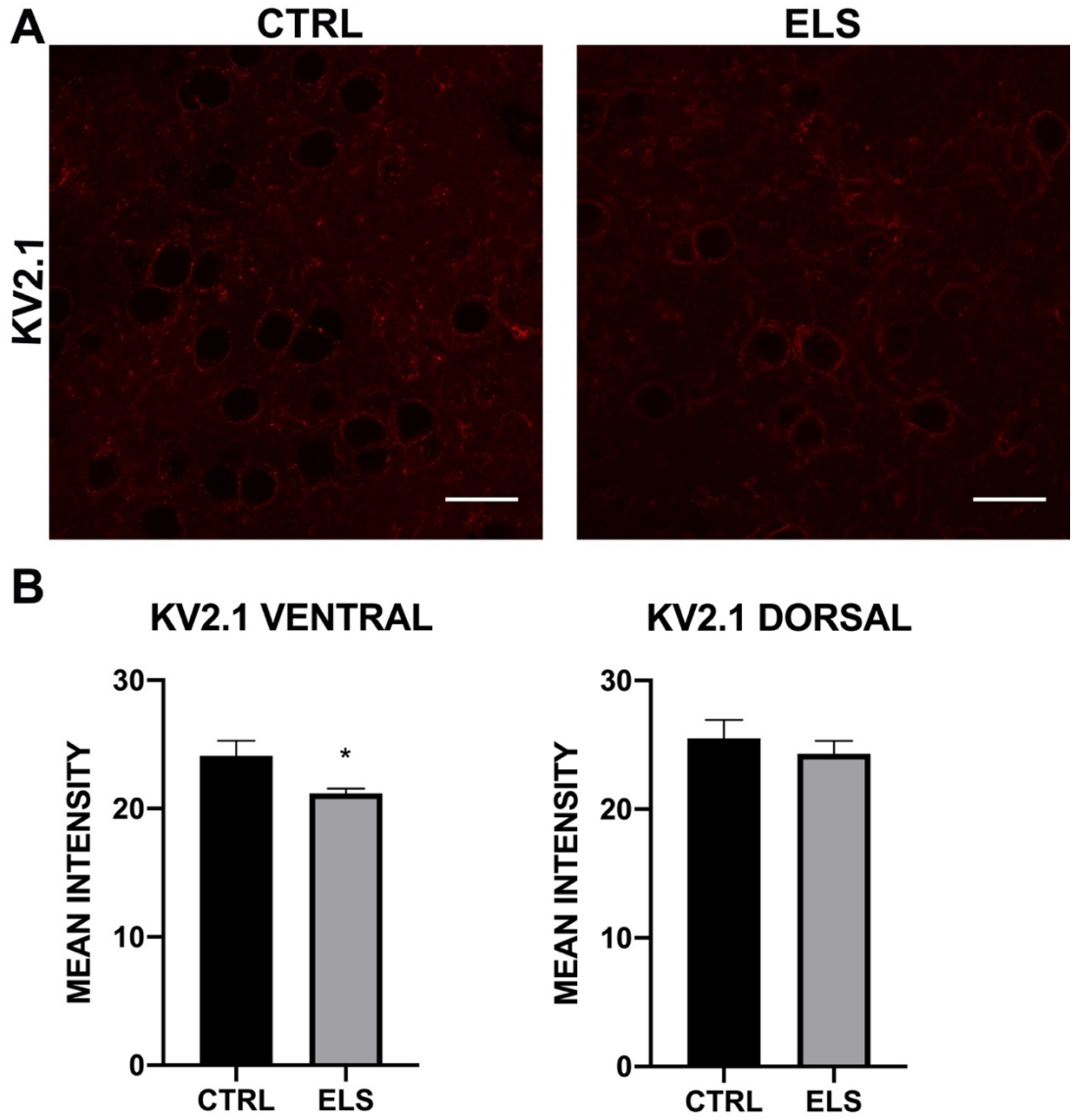

Figure 3.15. Quantification of $K_v2.1$ immunoreactivity in the striatum.
(A) shows representative image of $K_v2.1$ immunoreactivity in the striatum of CTRL and ELS mouse. (B) shows the fluorescence intensity of $K_v2.1$ in the ventral and dorsal striatum of CTRL and ELS mice. Bars represent the mean and error bars the SEM; * $P < 0.05$, Unpaired student's t-test N = $K_v2.1$ ventral striatum: Ctrl: 5, ELS: 5; $K_v2.1$ dorsal striatum: Ctrl: 5, ELS: 5 animals.
Scale bar: 20µm.

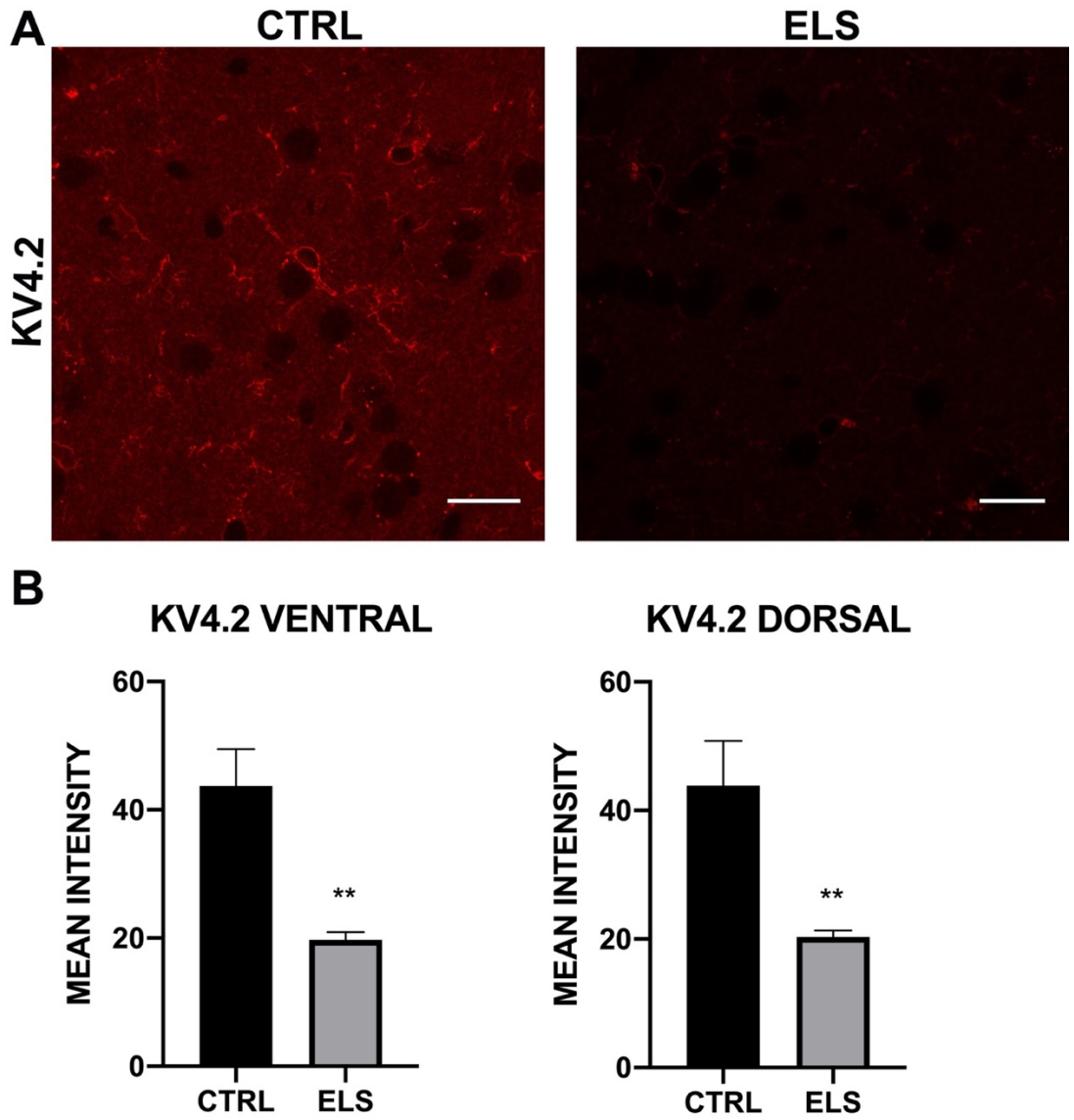

Figure 3.16. Quantification of $K_v4.2$ immunoreactivity in the striatum.
(A) shows representative image of $K_v4.2$ immunoreactivity in the striatum of CTRL and ELS mouse. (B) shows the fluorescence intensity of $K_v4.2$ in the ventral and dorsal striatum of CTRL and ELS mice. Bars represent the mean and error bars the SEM; ** $P < 0.01$, Unpaired student's t-test N = $K_v4.2$ ventral striatum: Ctrl: 5, ELS: 5; $K_v4.2$ dorsal striatum: Ctrl: 5, ELS: 5 animals.
Scale bar: 20µm.

Given the expression of $K_v1.6$ on microglia, which are the immune cells of the brain, and the strong association between stress and neuroinflammation (Wood *et al.*, 2015), I next investigated whether ELS altered the local immune system in the striatum, using immunoreactivity for Ionized calcium binding adaptor molecule 1 (IBA1), a marker of activated microglia. Intriguingly, I detected a significant decrease in the fluorescence intensity of IBA1 in both

the dorsal (P = 0.0033, unpaired Student's t test, N = 5 mice for control and ELS) and ventral (P = 0.0036, unpaired Student's t test, N = 5 mice for control and ELS) striatum.

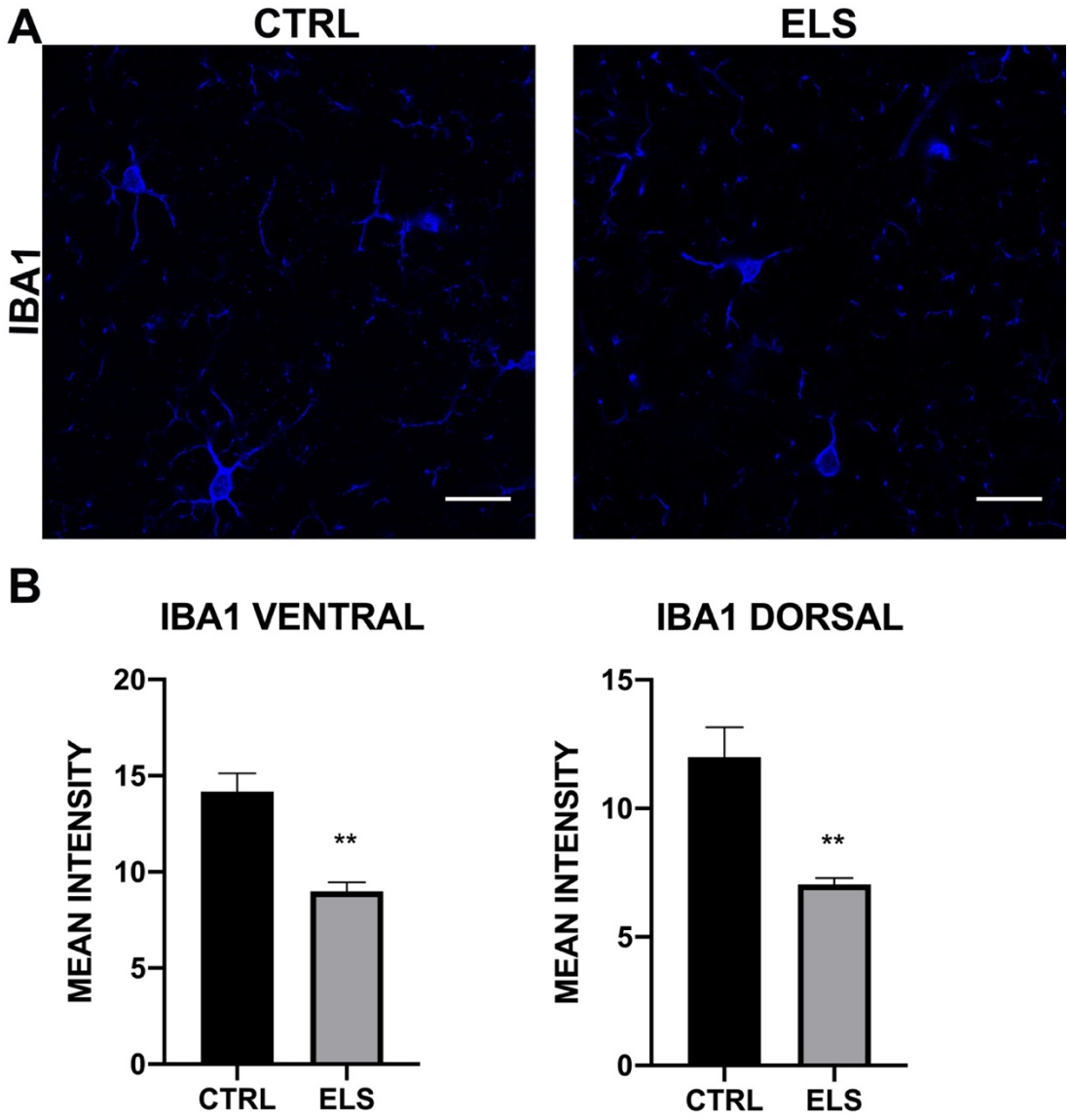

Figure 3.17. Quantification of IBA1 immunoreactivity in the striatum.
(A) shows representative image of IBA1 immunoreactivity in the striatum of CTRL and ELS mouse. (B) shows the fluorescence intensity of IBA1 in the ventral and dorsal striatum of CTRL and ELS mice. Bars represent the mean and error bars the SEM; ** $P < 0.01$, Unpaired student's t-test N = IBA1 ventral striatum: Ctrl: 5, ELS: 5; IBA1 dorsal striatum: Ctrl: 5, ELS: 5 animals.
Scale bar: 20µm.

The results of this chapter have been summarised in Table 3.1.

Table 3.1. Summary table of native K_v expression and plasticity following ELS. ND, not detected. NA, not assessed.

K_v subtype	**Specific signal detected in the striatum**	**Cellular localisation**	**Sub-cellular localisation**	**Changes with ELS**
K_v1.1	Yes	no	Axon terminals	NA
K_v1.2	Yes	no	Axon terminals	NA
K_v1.3	Yes	yes	MSN cytoplasm	NA
K_v1.4	Yes	no	Axon terminals	NA
K_v1.5	Yes	Parvalbumin cells and NG2 cells	PV cell body and axons NG2 cell processes	NA
K_v1.6	Yes	IBA1 microglia	Cell body and processes	NA
K_v2.1	Yes	MSN	Cell body and proximal dendrites	↓ in ventral but not dorsal striatum.
K_v2.2	ND			NA
K_v3.1	Yes	Parvalbumin cells		NA
K_v3.4	Yes	no	Axon terminals	NA
K_v4.2	Yes	MSN	distal dendrites	↓ in both the ventral and dorsal striatum.
K_v4.3	Yes	Parvalbumin cells	Cell body and dendrites	NA

Discussion

Data in this chapter reveal the rich diversity of K_v subtypes expressed in the striatum and also the manner in which they are expressed. The principal cells appear to predominantly rely on K_v2.1 and 4.2. However, MSNs target these different K_v to distinct compartments with K_v2.1 expression restricted to somatic and proximal dendritic compartments, whilst K_v4.2 is exclusively expressed in distal dendrites; all of these regions are postsynaptic domains suggesting a role for these K_v in regulating MSN membrane potential in response to synaptic activity. In contrast to this expression in the principal cells, K_v1.5, 3.1 and 4.3 were exclusively expressed in interneurons, suggesting role for these K_vs in the activity of cells that govern local neuronal control of MSN activity. Furthermore, a range of K_v (1.1, 1.2, 1.4, 3.4) were restricted to axon terminals that most likely originated from other brain regions, thereby suggesting a role for these K_v in regulating compartments associated with neurotransmitter release from distant brain regions. Intriguingly, some K_v were expressed on non-neuronal cells, namely microglia (K_v1.6) and OPCs (K_v1.5), suggesting that some K_v contribute to the regulation of the local immune system as well as ongoing myelination of striatal neurons. Finally, my data show for the first time that the expression of the K_v are highly plastic in response to life experience, with significant changes occurring as a result of life experience stress. Collectively, these data provide novel insights into the native K_v system within the striatum.

Segregation of K_v2.1 and 4.2 to distinct sub-cellular compartments

It is intriguing why a neuron would synthesise two different protein responsible essentially for the same function, namely passing K ions from the cytoplasm to the extracellular fluid and target these different proteins to different compartments of the same cell. This highly orchestrated trafficking of different K_v are most likely due to two inextricably linked phenomena: 1) the unique functional properties of the two classes of K_v and 2) the synaptic inputs that target these different compartments of the MSN. The primary role of K_v, in neurons, is to repolarise the plasma membrane following the depolarisation that results from an action potential. Different classes of K_v contribute differently to the process due to their biophysical properties. K_v4 as a class, are known as transient currents because they activate at subthreshold membrane potentials, inactivate rapidly, and recover from inactivation quickly compared with other K_v channels (Birnbaum *et al.*, 2004). As such, during action potential generation, they have the ability to react early, and repeatedly, during the depolarising phase. They are thus ideally suited to regions of the cell that likely to be exposed to significant membrane potential depolarisations due to significant excitatory synaptic transmission. In contrast, K_v2 are known as the delayed rectifiers (Misonou, Mohapatra and Trimmer, 2005). Their biophysical properties result in them being activated much later in the phase of the action potential. They are therefore not suited for regions of the cell in which rapid fluctuations in membrane potential occur as a result of significant excitatory input. As demonstrated with my immunohistochemistry, the distal dendrites that selectively express K_v4.2, also selectively receive all the glutamatergic axons that innervate MSNs. Such inputs have an immense

potential to depolarise the MSNs because they are extremely numerous, from a vast array of different brain regions, and glutamate as a neurotransmitter elicits an extremely powerful excitatory drive. Thus, in order to ensure that such inputs do not result in over activity of MSNs, it is essential that effective counter measures are in place to repolarise the postsynaptic membranes in a timely manner. Thus, the rapidly acting K_v4.2 channels are ideally located to integrate such rapidly changing membrane potentials. In contrast, the slower acting K_v2.1 is located in regions that receive limited glutamate input. Instead, these somatic and proximal dendritic regions are generally innervated by monoaminergic inputs such as noradrenaline or dopamine. The nature of such diffuse modulatory neurotransmission is significantly slower, compared to glutamatergic transmission. Thus, the slower acting K_v2.1 are ideally placed to respond to these slower changes in membrane potential. Thus, striatal principal cells exploit different K_v to integrate the complex network of functionally diverse synaptic inputs they receive, thereby ensuring coordinated neuronal excitability.

K_v expression in non-neuronal cells

An intriguing finding from my data was expression of specific K_v in non-neuronal cells within the brain. I found the expression of the K_v1.6 in microglia particularly interesting. The brain has its own unique immune system in order to protect it from the immensity of the rest of the body's immune system. Microglia are the principal immune cells utilised by the brain. They are highly motile and are capable of rapid proliferation as part of the neuroinflammatory processes (Cianciulli *et al.*, 2020), that we are now beginning to understand

are part of a host of brain disorders (de Araújo Boleti *et al.*, 2020). As such, identifying the molecules expressed by such important neuromodulators, will be instrumental in developing effective therapies for associated disorders. Targeting ion channels in microglia, with a view to developing therapies for various brain disorders is gaining rapid traction, with both voltage gated calcium (Hopp, 2020) and sodium (Hossain *et al.*, 2018) ion channels being considered. To date, only the K_v7 family has been associated with neuroinflammation, which was due to neuronal hyperexcitability, rather than an intrinsic K_v-mediated microglia pathway (Tzour *et al.*, 2017). Thus, future studies in which $K_v1.6$ could be selectively deleted from microglia, and changes in brain immune status assessed, will be instrumental taking this work forward.

Stress and K_v expression

A striking discovery was that ELS resulted in decreased expression of both $K_v2.1$ and 4.2. As mentioned above, both channels are likely to be instrumental in dampening MSN activity. Therefore, the stress-induced decrease in their expression is likely to result in enhanced activity of MSNs. Altered activity of striatal MSNs are associated with a range of diseases that affect this region. Motor deficits associated with Parkinson's arise from the altered activity of dorsal striatal MSNs due to the absence of dopamine input to this sub-region. Various psychiatric disorders related to the brain's reward system, such as drug addiction or apathy are also related to altered excitability of MSNs in the ventral striatum. Importantly, such changes in the reward pathways are also a component of certain neurodegenerative diseases such as Alzheimer's and

Parkinson's, resulting in apathy in such patients. This symptom significantly magnifies the disease burden for both Alzheimer's and Parkinson's patients, and is currently poorly treated. As such, identifying the underlying mechanisms for such symptoms could be instrumental in developing targeted therapies. It should be noted that there are intricate links between these stress data and the native expression data. Stress is known to have a profound effect on the brain's immune system, resulting in neuroinflammation. Furthermore, neuroinflammation is a central component of these neurodegenerative diseases. Since stress altered both striatal K_v and immune status, I therefore speculate whether the pathology associated with Alzheimer's and Parkinson's alters native K_v expression in this brain region. I explore this hypothesis in the following chapters.

Chapter Four

Effect of Parkinson's disease pathology on the expression of K_v in the striatum

Summary and importance

Background

In the previous chapter, the first high resolution demonstration of the native expression of various K_v subtypes throughout the cellular networks of the striatum was provided. such expression profile was also shown to be plastic and influenced by life experience, such as psychosocial stress. This suggests that their expression, and by extension their function, could be altered in various brain disorders and therefore represent potential therapeutic targets. One category of brain disorders in which K_v function is poorly explored is neurodegenerative diseases, in particular Parkinson's and Alzheimer's diseases (PD, AD). This could represent a missed opportunity to directly target associated changes in neuronal activity in such disorders. Therefore, in the following chapters, I will explore whether core pathology associated with these diseases impacts on K_v expression in the striatum, beginning with Parkinson's in this chapter.

Methods

To model PD, a transgenic mouse line that over-expresses the key protein associated with PD, namely α-synuclein (α-syn) was used and is termed the OVX mouse. Wildtype (WT) littermates were used as controls. Young mice,

aged 3 months were deliberately used, thus prior to the onset of PD motor pathology which occurs at 14 months, because I was interested in assessing the early, prodromal changes that occur. Immunohistochemistry with confocal microscopy was used to determine the expression of α-syn and to determine the changes in expression levels of various neurochemicals in the striatum of OVX mice. I used qRT-PCR to quantify relative levels of the mRNA of various neurochemicals in the striatum of the WT and OVX mice.

Results

In OVX mice, immunohistochemistry revealed a more intense expression of α-syn in the striatum when compared to the expression observed in WT mice. This indicates that that PD pathology affects the native α-syn in the mice striatum by increasing the expression level. Immunoreactivity for α-syn was enriched in axon terminals immunoreactive for VGLUT1, but not VGLUT2, indicating that glutamatergic axon terminals from the cortex are likely impacted by such pathology. Increased α-syn signal in OVX samples was also contained in axon terminals immunopositive for VGAT and TH, suggesting an association with GABAergic and monoaminergic inputs respectively. Intriguingly, IBA1, a marker of neuroinflammation, was significantly decreased in OVX samples, suggesting an altered immune state. Finally, protein expression levels for K_v2.1, 4.2 and 4.3 was significantly decreased, while K_v4.3 mRNA levels were increased in OVX samples.

Importance

The data reveal novel changes in a host of neurochemical pathways within the striatum, during the earliest stages of the condition, significantly prior to the onset of the cardinal motor features of the condition. The changes in K_v most likely point to compensatory changes as a result of altered levels of activity of striatal neurons. If so, this suggests profound changes in striatal function, which could help us to understand some of the prodromal changes in emotion that precede the onset of motor symptoms, including apathy, agitation and anxiety.

Results

4.1. Characterisation of PD-like pathology in the striatum of OVX mouse

Increased expression of α-syn is a pathological hallmark of PD (Polymeropoulos *et al.*, 1997). Thus, a mouse model that overexpresses α-syn (OVX) at disease relevant levels was used. This mouse model results in the core features of PD, namely degeneration of dopaminergic neurons and decreased striatal dopamine input, in old age (Janezic *et al.*, 2013). However, neurochemical changes in the striatum, prior to the onset of such dopaminergic degeneration have not been investigated. Therefore, PD-associated pathology, and associated changes in striatal neurochemistry in OVX mice and WT littermates aged 3 months were first characterised. In the striatum, α-syn presented as individual clusters that did not overlap with DARPP-32 immunoreactivity. This indicates that α-syn was not expressed by MSNs within the striatum. However, MSN could express α-syn in their axons that innervate other brain regions. Furthermore, the level of expression of α-syn was confirmed to be significantly increased in OVX, compared to WT, thereby confirming the model used (Fig 4.1).

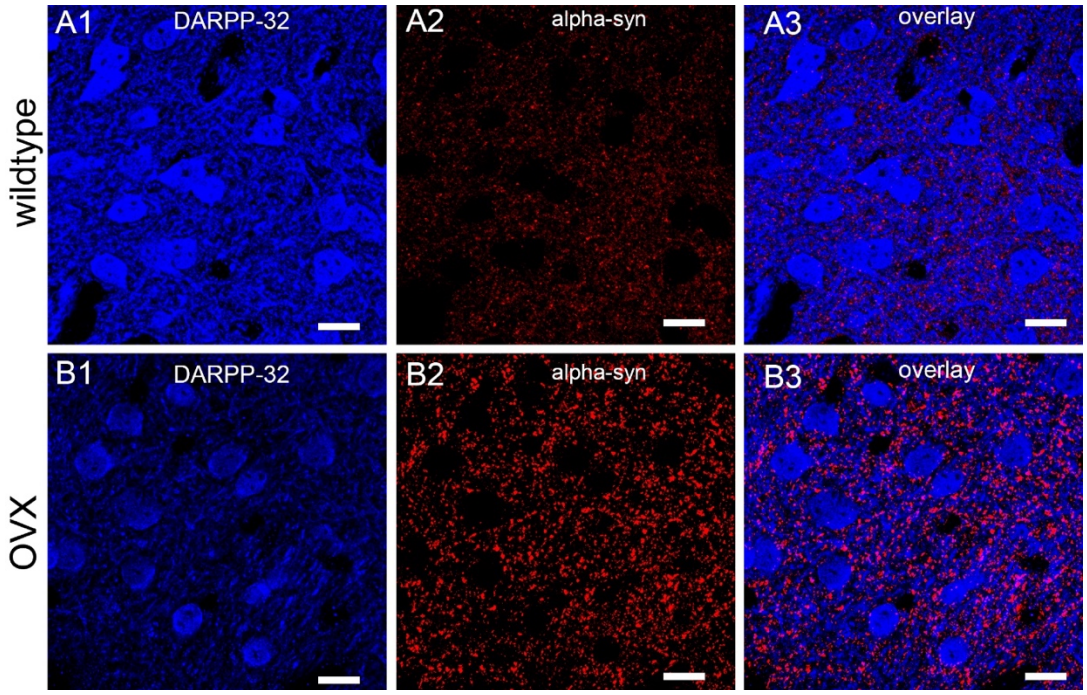

Figure 4.1. Immunoreactivity for α-syn in the striatum of WT and OVX mice.
(A1) shows immunoreactivity for DARPP-32 immunopositive cells (MSN) in the striatum of WT mice. (A2) shows immunoreactivity for α-syn in the same field of view. As with (A1-A2), (B1-B2) shows immunoreactivity for MSN and α-syn in the striatum of OVX mice. (A2) shows less intensity of α-syn expression while (B2) shows a more intense expression of α-syn. This indicates that PD pathology affects native α-syn in the mice striatum by increasing the expression level. (A3, B3) is an overlay of (A1-2, B1-2) in the same field of view demonstrating that α-syn is presented as individual clusters that did not overlap with MSN. This suggests that MSN expresses α-syn in their axons.
Scale bars: 10 μm.

The presentation of the α-syn immunoreactivity pattern, as individual clusters, rather than cell bodies, is representative of axon terminal profiles. I therefore assessed which striatal axonal inputs contained α-syn in OVX mice. Immunoreactivity for α-syn showed significant co-localisation with signal for VGLUT1 (Fig 4.2 A). This indicated that such PD-related pathology is enriched in glutamatergic axons originating from the cortex. In contrast, there was limited association between immunoreactivity for α-syn and VGLUT2 (Fig 4.2 B). This suggest that PD-related pathology is not contained in glutamatergic inputs from the thalamus.

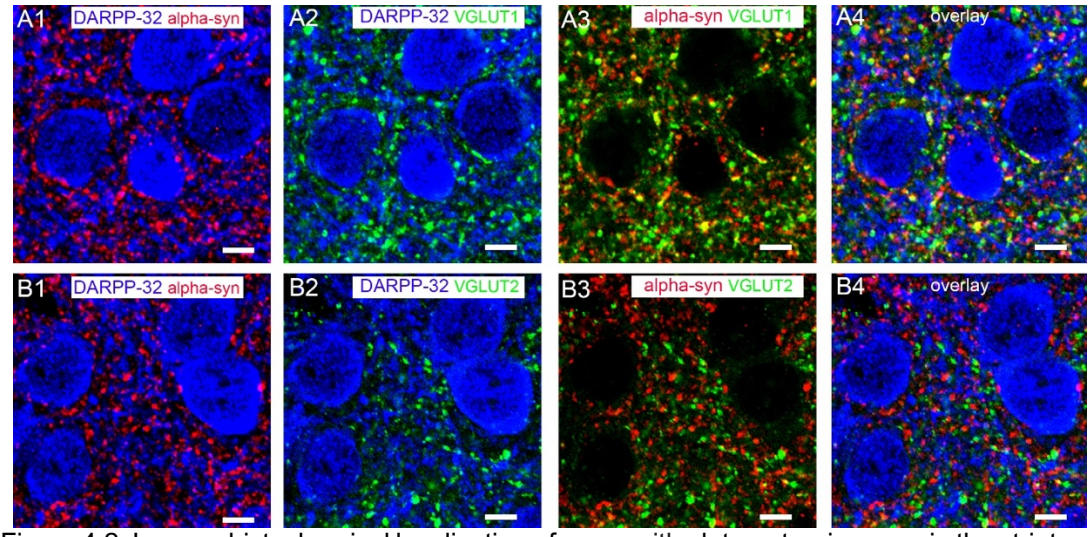

Figure 4.2. Immunohistochemical localisation of α-syn with glutamatergic axons in the striatum of OVX mouse.
(A1) shows the immunoreactivity for α-syn and how it is expressed on DARPP-32 immunopositive cells (MSN). (A2) shows the immunoreactivity for VGLUT1 and how it is expressed on MSN. VGLUT1 is expressed as individual clusters representative of axon terminal profiles originating from the cortex. (A3-4) is an overlay of both (A1 and A2) in the same field of view demonstrating α-syn co-localisation with VGLUT1 signal. This suggests that α-syn is enriched in glutamatergic axons originating from the cortex. As with (A1-4), (B1-4) demonstrates the association between α-syn and VGLUT2 signal. There was limited association between immunoreactivity for α-syn and VGLUT2. This suggest that PD-related pathology is not contained in glutamatergic inputs originating from the thalamus.
Scale bars: 5 μm.

Immunoreactivity for VGAT, and thus axon terminals from local GABAergic interneurons were also strongly associated with α-syn immunoreactive clusters (Fig 4.3 A). This suggests that PD-associated pathology could impact on synaptic transmission between GABAergic neurons and MSNs. Finally, α-syn immunoreactive clusters also overlapped with varicosities immunopositive for TH, the enzyme responsible for synthesising noradrenaline and dopamine (Fig 4.3 B). This confirms that such PD pathology is likely to impact on mono-aminergic modulation of striatal function.

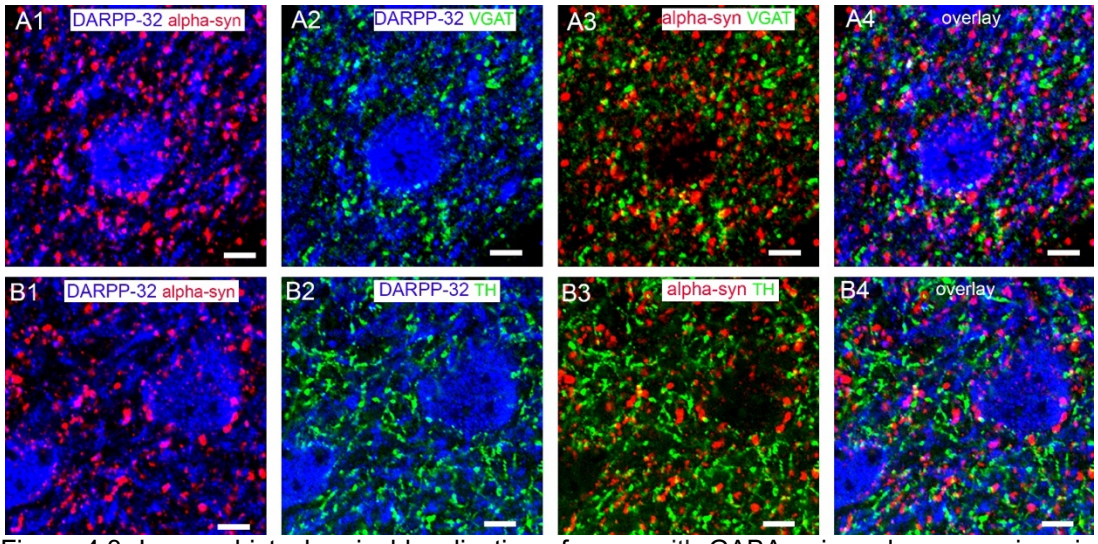

Figure 4.3. Immunohistochemical localisation of α-syn with GABAergic and mono-aminergic axon terminals in the striatum of OVX mouse.
(A1) shows the immunoreactivity for α-syn and how it is expressed on DARPP-32 immunopositive cells (MSN). (A2) shows the immunoreactivity for VGAT and how it is expressed on MSN. (A3-4) is an overlay of both (A1 and A2) in the same field of view demonstrating α-syn association with VGAT signal. This suggests that PD-associated pathology could impact on synaptic transmission between GABAergic neurons and MSNs. As with (A1-4), (B1-4) demonstrates the association between α-syn and TH signal. α-syn immunoreactive clusters overlapped with varicosities immunopositive for TH, an enzyme responsible for synthesising noradrenaline and dopamine. This suggests that PD pathology is likely to impact on mono-aminergic modulation of striatal function.
Scale bars: 5 μm.

4.2. Effect of PD pathology on striatal neurochemical expression

As mentioned above, while changes in dopamine brain centres of OVX have been investigated in aged OVX, changes in native striatal neurochemistry in young mice have not. I therefore used a combination of qPCR and quantitative immunohistochemistry to probe for such changes. A pivotal finding revealed that mRNA levels of tyrosine hydroxylase gene (TH) was statistically significantly increased in OVX mice ($P < 0.0257$, unpaired Student's t test, N = 5 animals). In contrast, I found a statistically significant decrease in the mRNA levels for tryptophan hydroxylase 1 gene (TPH1) in OVX mice ($P < 0.0452$, unpaired Student's t test, N = 4 animals). However, there were no statistically significant differences in the expression levels for serotonin transporter gene (slc6a4) (Fig 4.4).

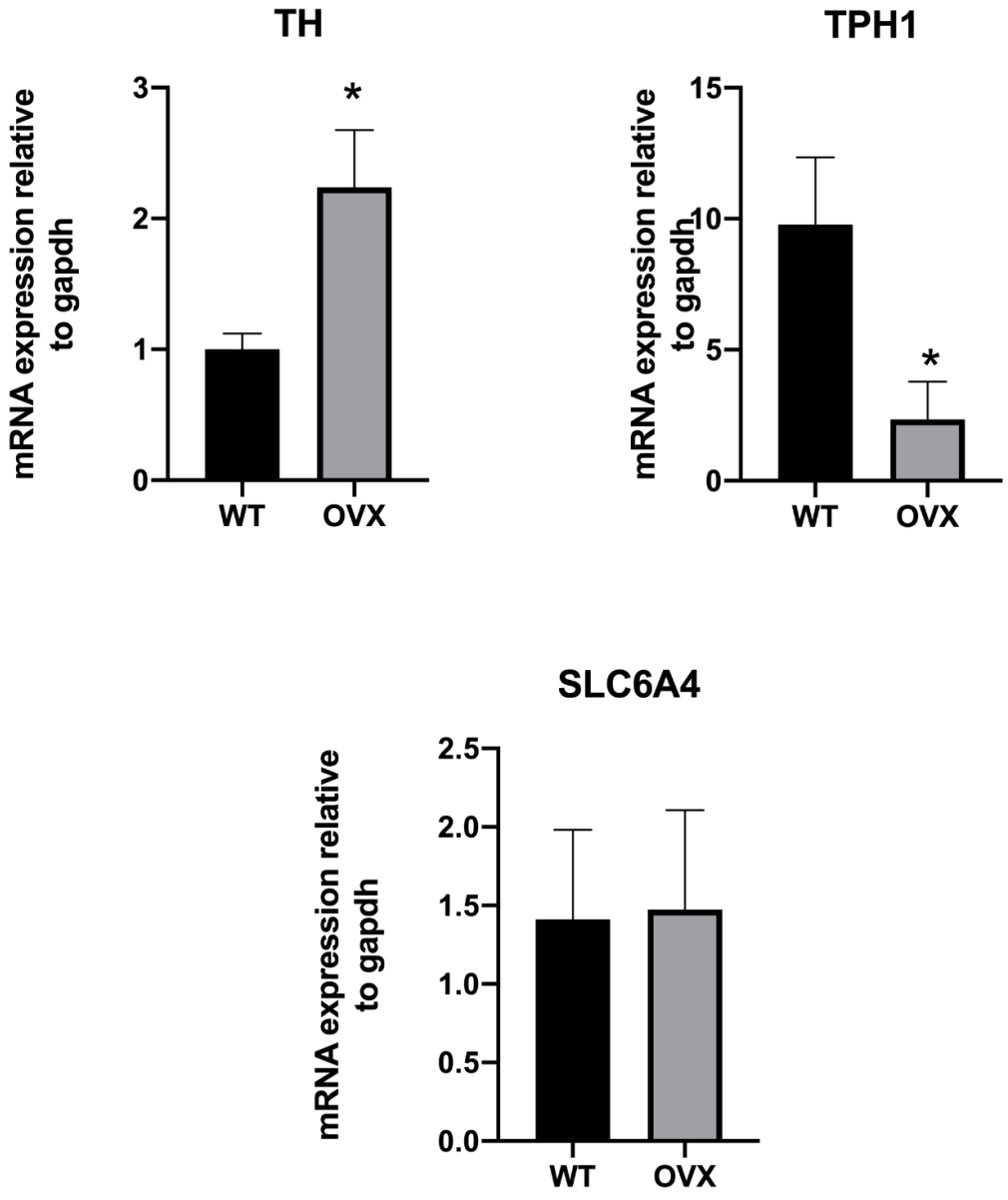

Figure 4.4. Quantification of neurochemical-encoding mRNAs in the striatum shows the levels of TH, TPH1, and SERT encoding mRNAs in isolated samples from WT and OVX mice. Bars represent the mean and error bars the SEM; * $P < 0.05$, Unpaired student's t-test N = TH: WT: 5, OVX: 5; TPH1: WT: 4, OVX: 4; Slc6a4: WT: 6, OVX: 6 animals.

Since PD pathology have an effect on TH in which the mRNA level of TH was significantly increased in OVX mice, I then assess any changes in TH immunoreactivity at the protein level. To this end, immunohistochemistry with confocal microscopy was performed to assess the effect of PD pathology on the fluorescence intensity of TH in the ventral and dorsal striatum of OVX mice

in comparison to WT littermates as control. While there was a trend towards lower levels of TH immunoreactivity in the dorsal striatum, these changes were not statistically significant (Fig 4.5 B).

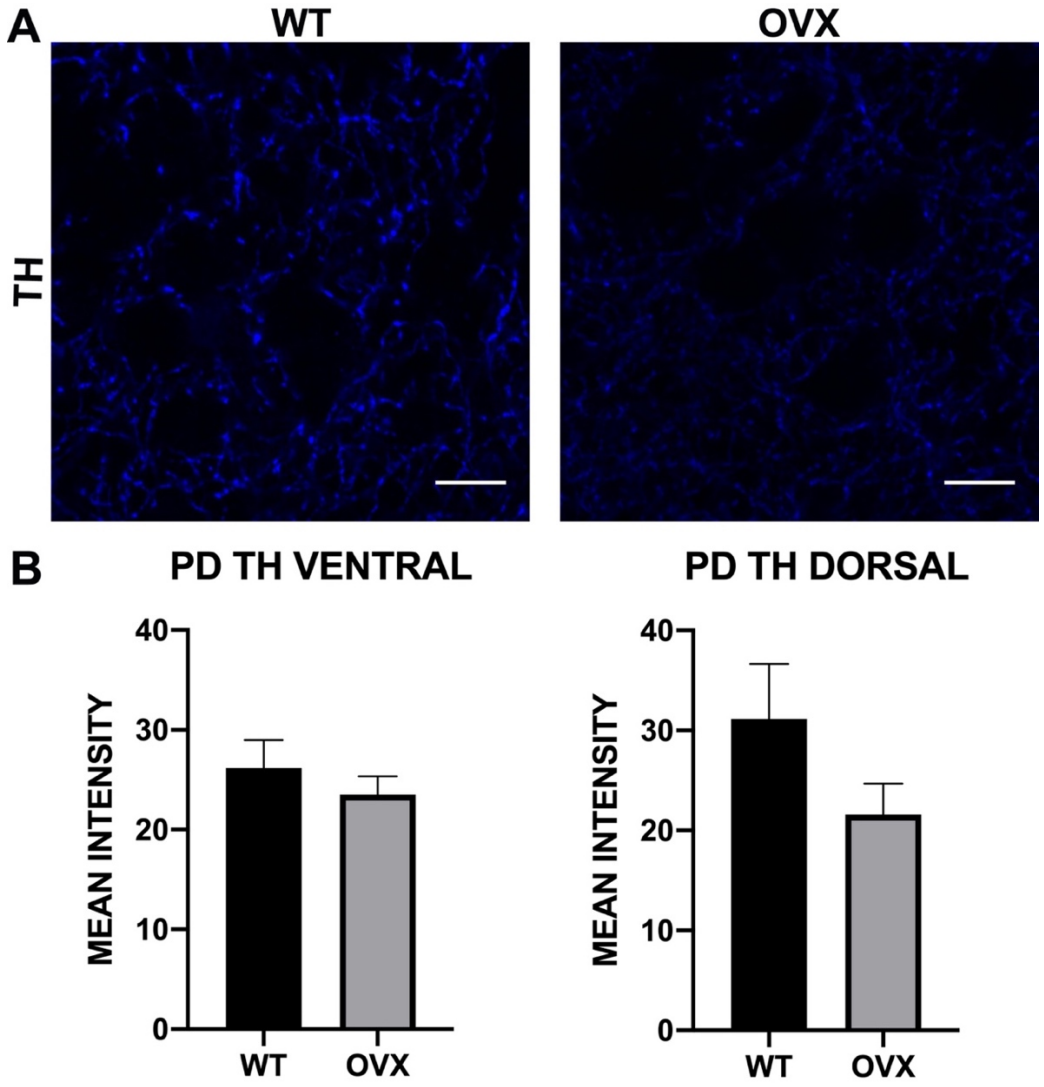

Figure 4.5. Quantification of TH immunoreactivity in the striatum of WT and OVX mice.
(A) shows representative image of TH immunoreactivity in the striatum of WT and OVX mouse. (B) shows the fluorescence intensity of TH in the ventral and dorsal striatum of WT and OVX mice. Bars represent the mean and error bars the SEM; Unpaired student's t-test *N* = TH ventral striatum: WT: 4, OVX: 4; TH dorsal striatum: WT: 4, OVX: 4 animals.
Scale bars: 10μm.

Since a key aspect of PD is the impairment of dopaminergic neurons which innervate the striatum and release dopamine to activate dopamine receptors on MSNs, I next explored whether the expression of the protein responsible for regulating dopamine receptors, namely DARPP-32 is altered in OVX. I

detected a significant decrease in DARPP-32 fluorescence intensity in the ventral striatum (P = 0.0429, unpaired Student's t test, N = 4 animals), but not in the dorsal region (Fig 4.6 B).

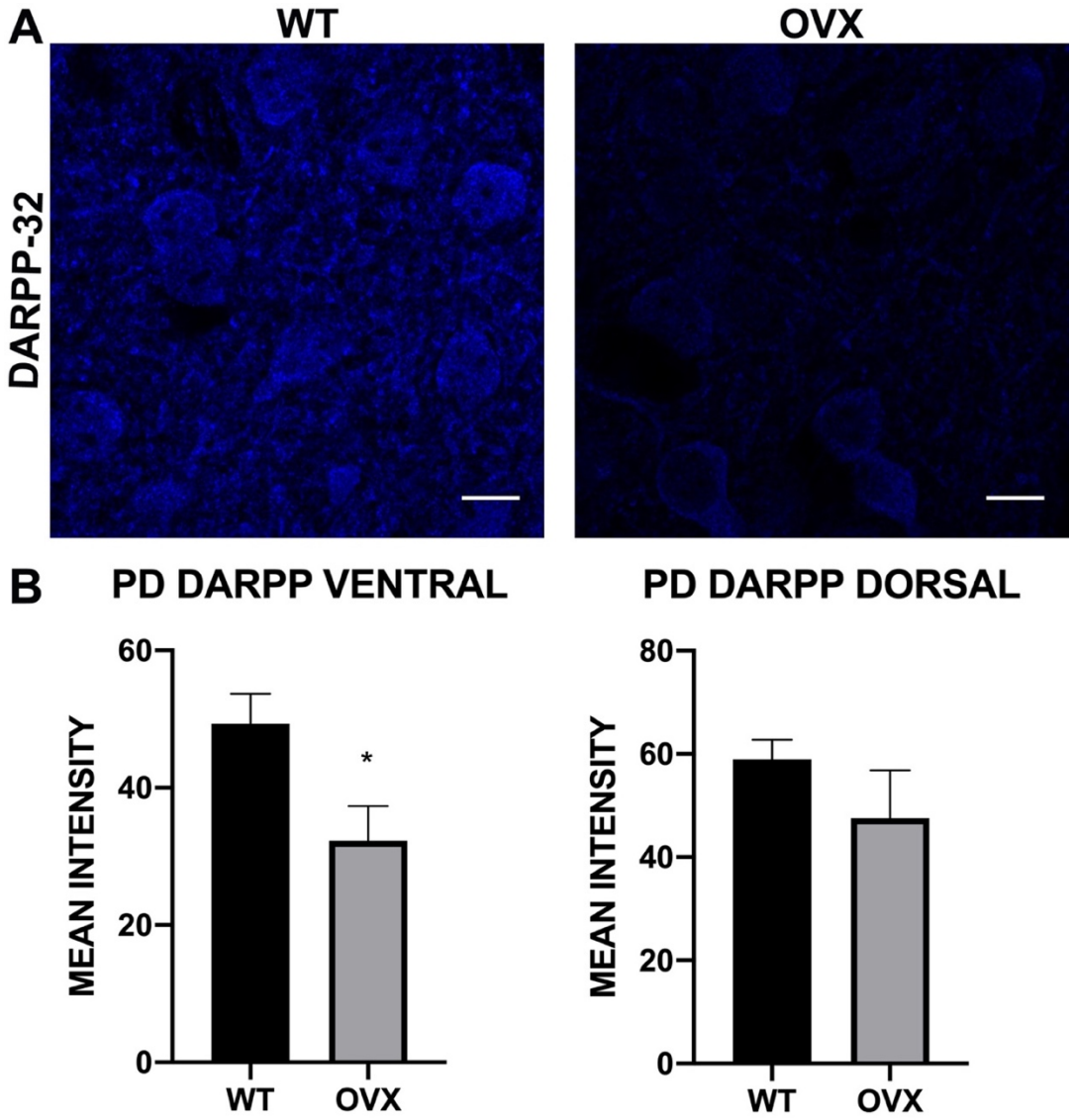

Figure 4.6. Quantification of DARPP-32 immunoreactivity in the striatum of WT and OVX mice. (A) shows representative image of DARPP-32 immunoreactivity in the striatum of WT and OVX mouse. (B) shows the fluorescence intensity of DARPP-32 in the ventral and dorsal striatum of WT and OVX mice. Bars represent the mean and error bars the SEM; * $P < 0.05$, Unpaired student's t-test *N* = DARPP-32 ventral striatum: WT: 4, OVX: 4; DARPP-32 dorsal striatum: WT: 4, OVX: 4 animals.
Scale bars: 10μm.

Since in the OVX, α-syn colocalised with clusters immunoreactive for VGAT, I next assessed whether there were any changes in the expression of markers associated with local interneurons. While there was a trend for mRNA levels

for ChAT to increase, and for PV to decrease, in OVX samples, these changes were not statistically significant (Fig 4.7).

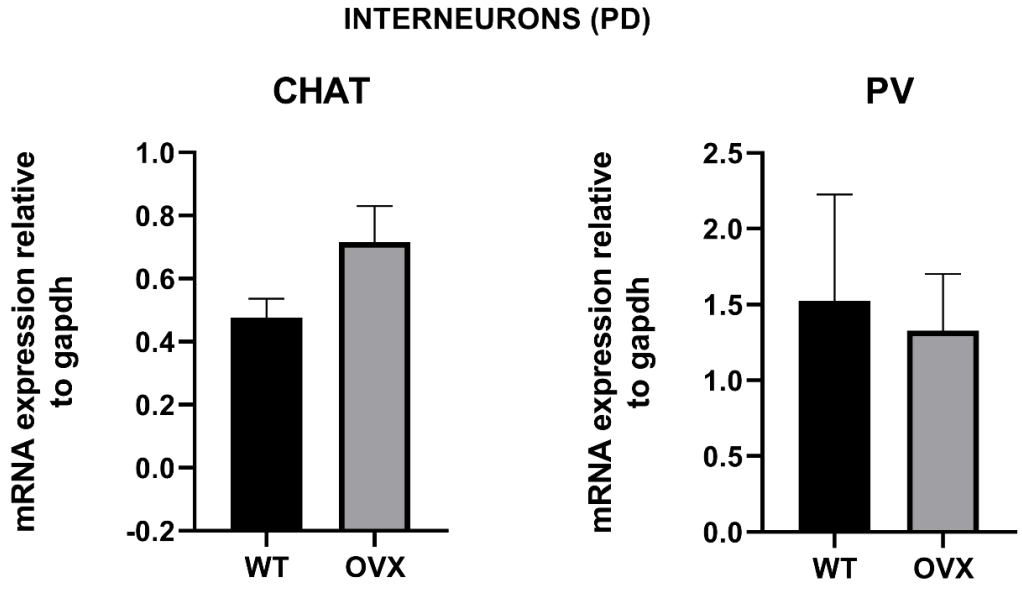

Figure 4.7 Quantification of interneuron-encoding mRNAs in the striatum shows the levels of ChAT and PV-encoding mRNAs in isolated samples from WT and OVX mice. Bars represent the mean and error bars the SEM; Unpaired student's t-test *N* = ChAT: WT: 6, OVX: 6; PV: WT: 6, OVX: 6 animals.

There were also no significant changes in the fluorescence intensity for parvalbumin in OVX samples although there was a trend for the intensity level to reduce in the ventral and dorsal striatum of OVX samples (Fig 4.8 B).

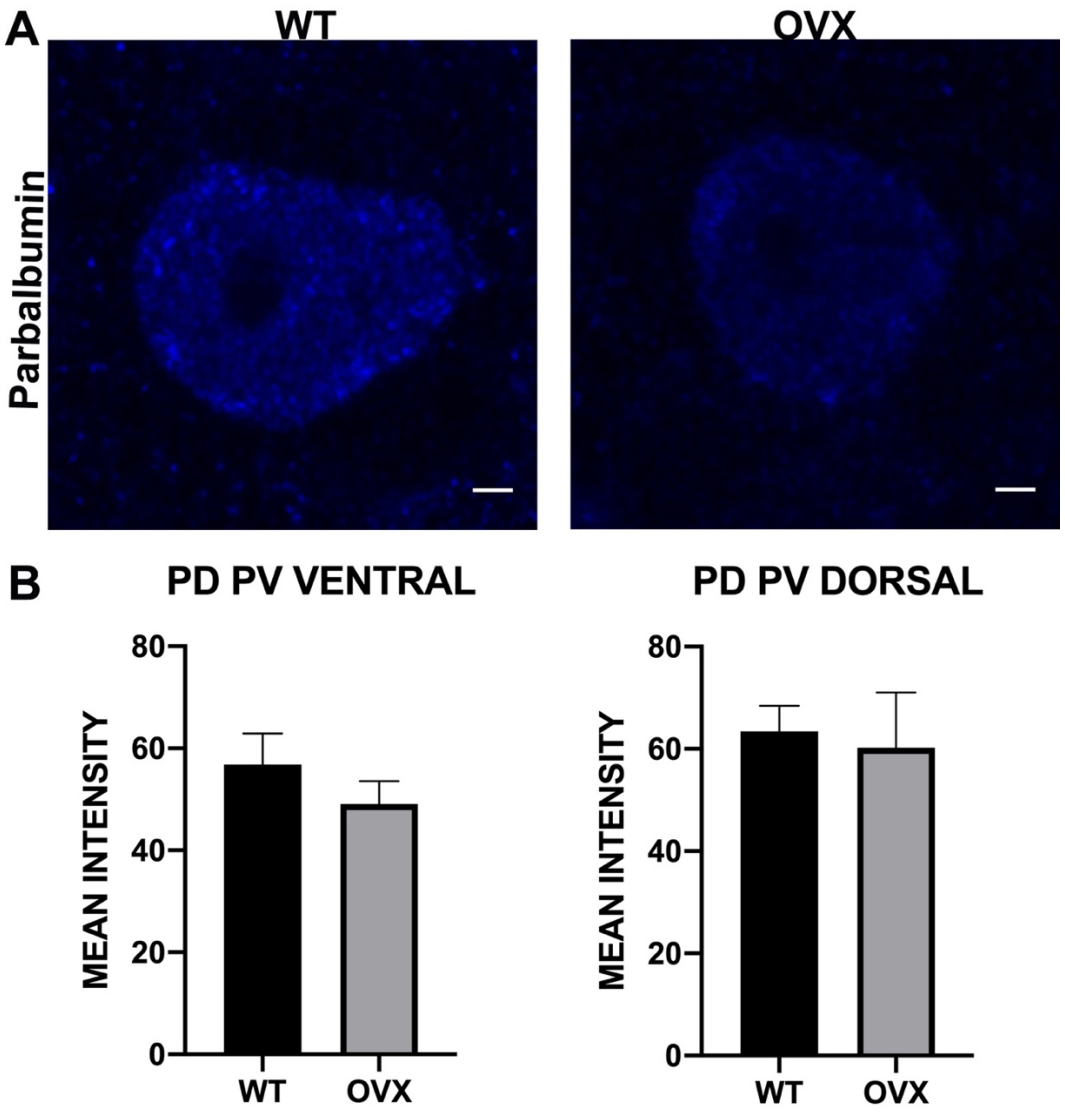

Figure 4.8. Quantification of parvalbumin immunoreactivity in the striatum of WT and OVX mice.
(A) shows representative image of Parvalbumin (PV) immunoreactivity in the striatum of WT and OVX mouse. (B) shows the fluorescence intensity of PV cells in the ventral and dorsal striatum of WT and OVX mice. Bars represent the mean and error bars the SEM; Unpaired student's t-test *N* = PV ventral striatum: WT: 4, OVX: 4; PV dorsal striatum: WT: 4, OVX: 4 animals.
Scale bars: 2μm.

Finally, neuroinflammation is a key component of PD pathology (Joers *et al.*, 2017)(de Araújo Boleti *et al.*, 2020). I investigated whether there were signs of inflammation in the striatum as a result of PD using IBA1, the standard cellular marker of neuroinflammation. However, surprisingly I detected a significant decrease in the fluorescence intensity of IBA1 in the ventral (P = 0.0009,

unpaired Student's t test, N = 4 animals) and dorsal striatum of OVX mice (P = 0.0162, unpaired Student's t test, N = 4 animals) (Fig 4.9 B).

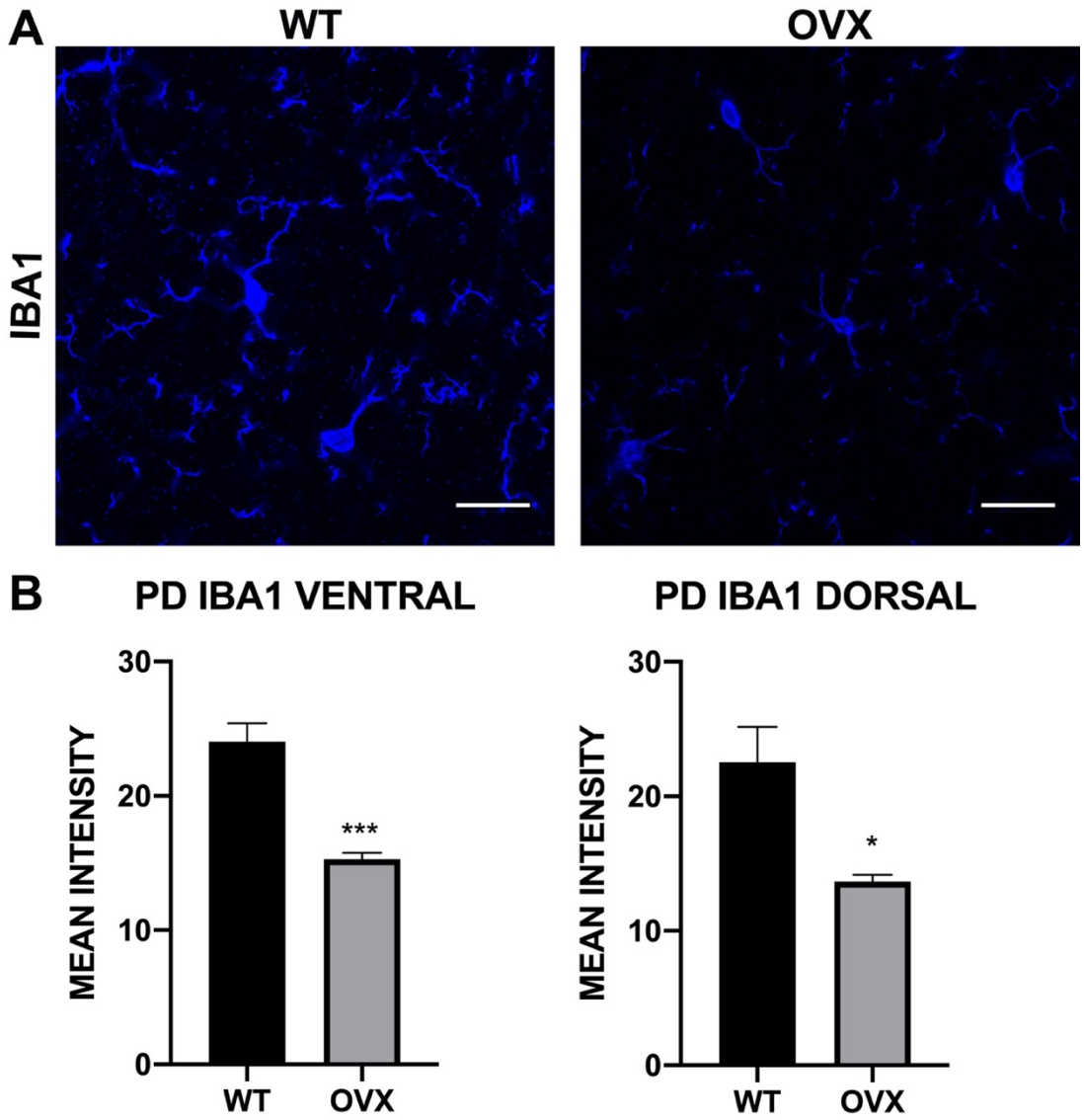

Figure 4.9. Quantification of IBA1 immunoreactivity in the striatum of WT and OVX mice.
(A) shows representative image of IBA1 immunoreactivity in the striatum of WT and OVX mouse. (B) shows the fluorescence intensity of IBA1 in the ventral and dorsal striatum of WT and OVX mice. Bars represent the mean and error bars the SEM; * $P < 0.05$, *** $P < 0.001$, Unpaired student's t-test N = IBA1 ventral striatum: WT: 4, OVX: 4; IBA1 dorsal striatum: WT: 4, OVX: 4 animals.
Scale bars: 20µm.

4.3. Quantification of K_v-encoding mRNAs in the striatum of PD mice

I next assessed whether PD pathology affects the expression of K_v in the striatum, beginning at the mRNA level. I focussed only on K_v that I have shown from my previous immunohistochemistry to be expressed in striatal neurons. To this end, I performed qPCR on K_v1.2, K_v2.1, K_v4.2 and K_v4.3 to assess K_v changes at the mRNA level of OVX mice in comparison to WT littermates as control. A pivotal finding revealed that K_v4.3 mRNA levels was significantly increased in OVX mice ($P = 0.0037$, unpaired Student's t test, $N = 6$ animals). However, there were no significant differences in the mRNA levels for K_v1.2, K_v2.1 and K_v4.2 in OVX mice (Fig 4.10).

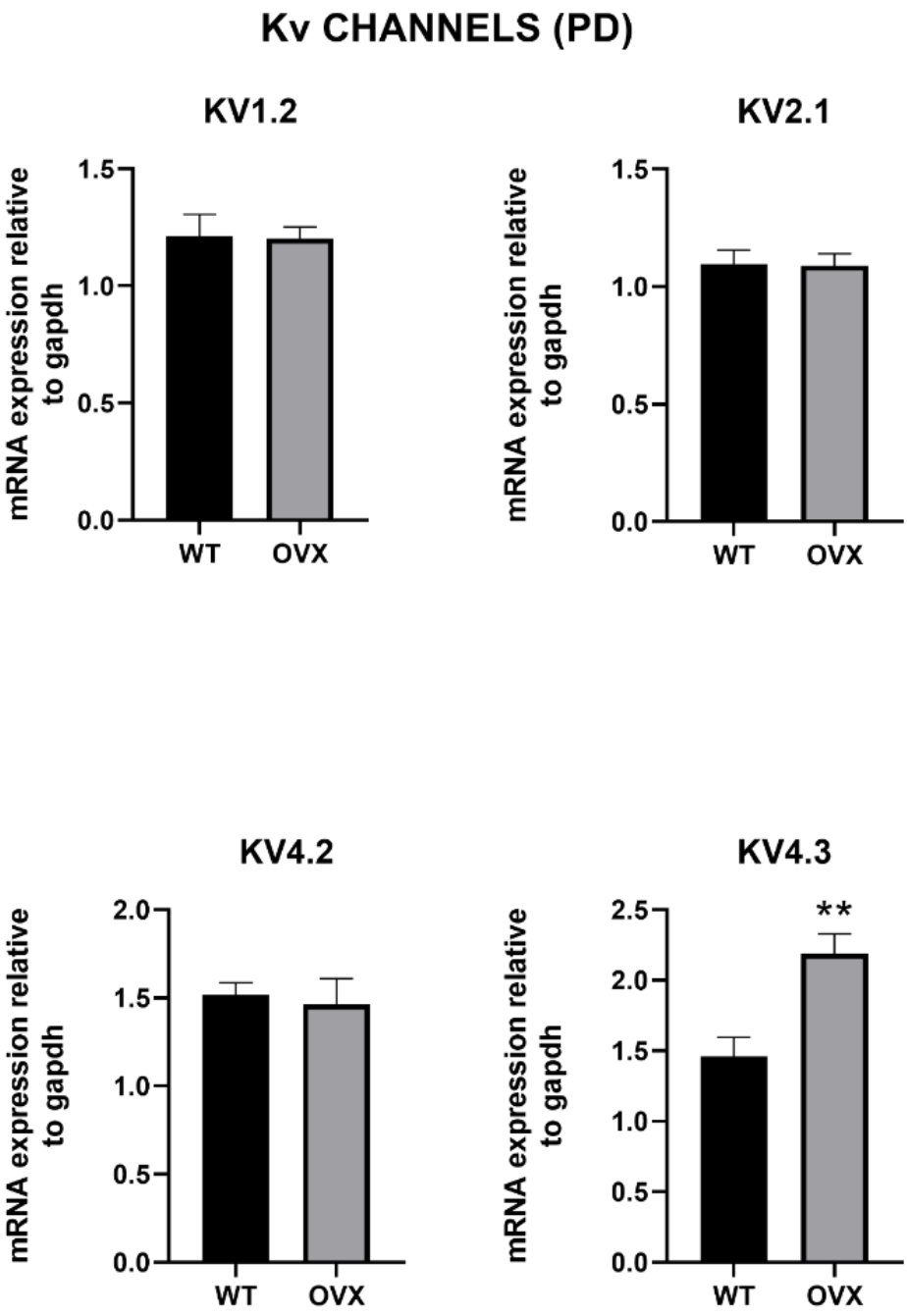

Figure 4.10. Quantification of K_v-encoding mRNAs in the striatum shows the levels of K_v-encoding mRNAs in isolated samples from WT and OVX mice. Bars represent the mean and error bars the SEM; ** $P < 0.01$, unpaired student's t-test N = K_v1.2: WT: 6, OVX: 6; K_v2.1: WT: 6, OVX: 6; K_v4.2: WT: 6, OVX: 6; K_v4.3: WT: 6, OVX: 6 animals.

4.4. Quantification of K_v protein in the striatum of PD mice

I then assess whether these changes in mRNA were translated at the protein levels as well. I detected robust decreases in the fluorescence intensity for:

K_v2.1 in ventral striatum (P = 0.0105, unpaired Student's t test, N = 8 animals) and dorsal striatum (P = 0.0279, unpaired Student's t test, N = 8 animals) (Fig 4.11 B); K_v4.2 in ventral striatum (P = 0.0067, unpaired Student's t test, N = 8 animals) and dorsal striatum (P = 0.0035, unpaired Student's t test, N = 8 animals) (Fig 4.12 B); and K_v4.3 in ventral striatum (P = 0.0025, unpaired Student's t test, N = 4 animals) and dorsal striatum (P = 0.0058, unpaired Student's t test, N = 8 animals) (Fig 4.13 B).

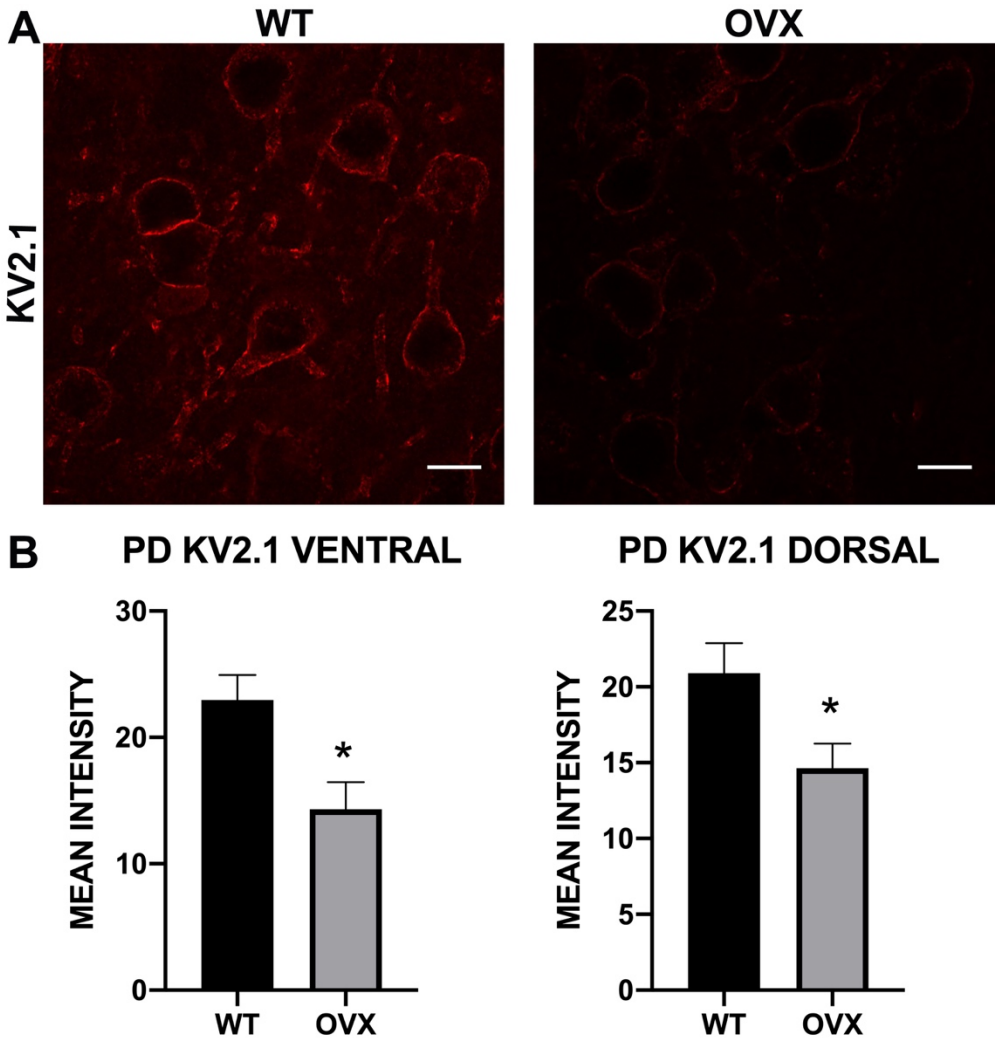

Figure 4.11. Quantification of K_v2.1 immunoreactivity in the striatum of WT and OVX mice. (A) shows representative image of K_v2.1 immunoreactivity in the striatum of WT and OVX mouse. (B) shows the fluorescence intensity of K_v2.1 in the ventral and dorsal striatum of WT and OVX mice. Bars represent the mean and error bars the SEM; * $P < 0.05$, Unpaired student's t-test N = K_v2.1 ventral striatum: WT: 8, OVX: 8; K_v2.1 dorsal striatum: WT: 8, OVX: 8 animals.
Scale bars: 10µm.

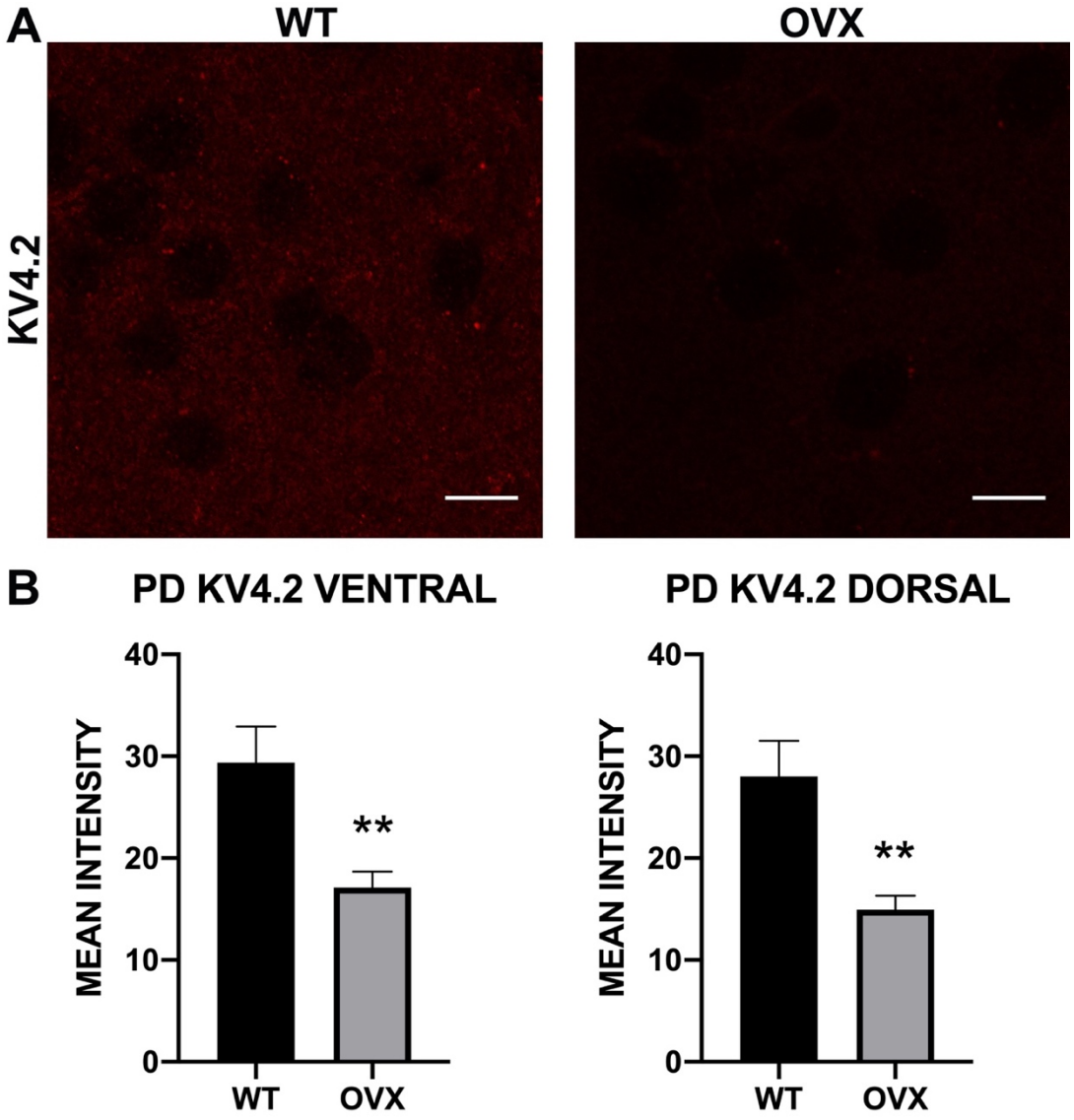

Figure 4.12. Quantification of $K_v4.2$ immunoreactivity in the striatum of WT and OVX mice. (A) shows representative image of $K_v4.2$ immunoreactivity in the striatum of WT and OVX mouse. (B) shows the fluorescence intensity of $K_v4.2$ in the ventral and dorsal striatum of WT and OVX mice. Bars represent the mean and error bars the SEM; ** $P < 0.01$, Unpaired student's t-test N = $K_v4.2$ ventral striatum: WT: 8, OVX: 8; $K_v4.2$ dorsal striatum: WT: 8, OVX: 8 animals.
Scale bars: 10µm.

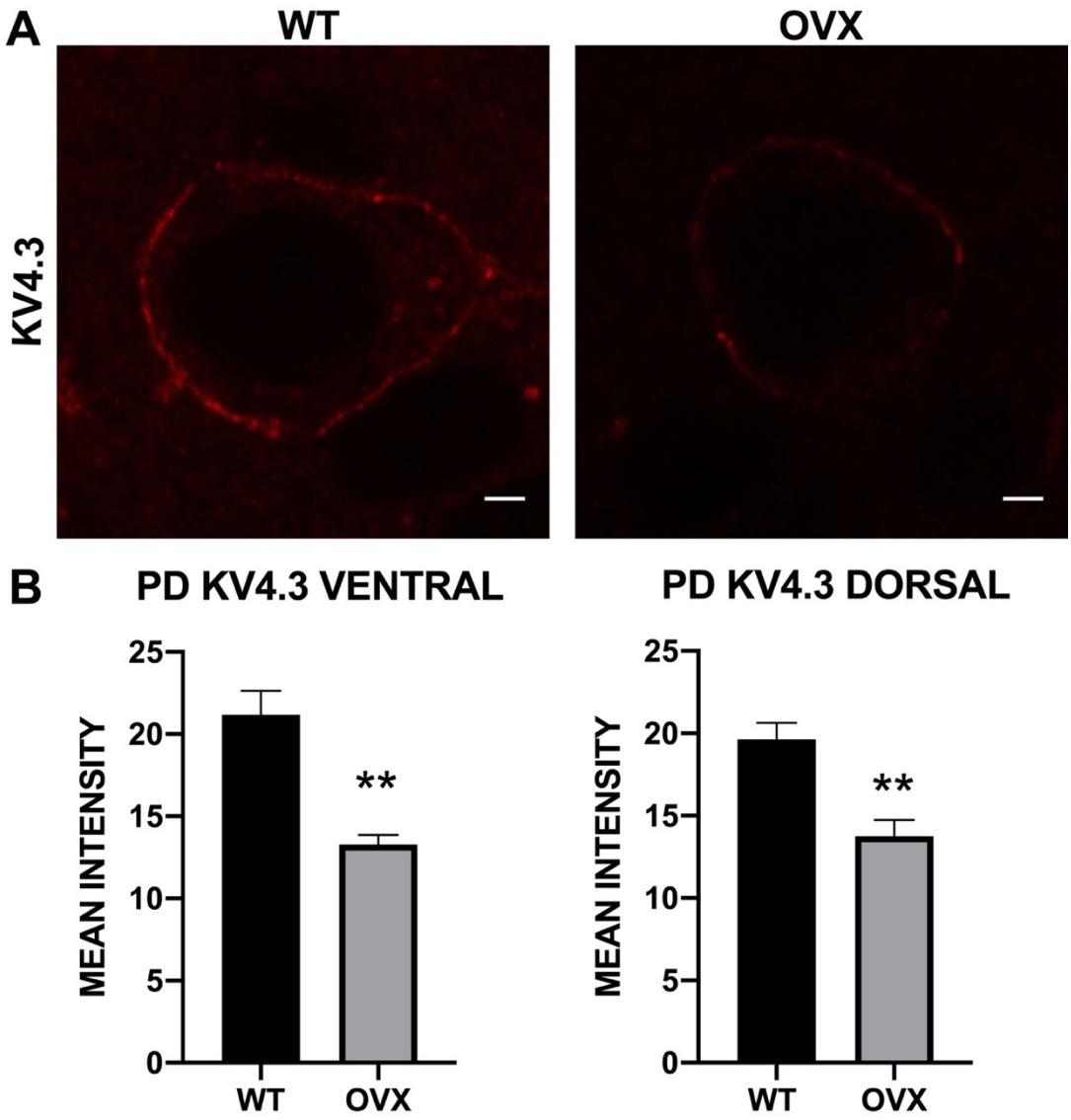

Figure 4.13. Quantification of $K_v4.3$ immunoreactivity in the striatum of WT and OVX mice. (A) shows representative image of $K_v4.3$ immunoreactivity in the striatum of WT and OVX mouse. (B) shows the fluorescence intensity of $K_v4.3$ in the ventral and dorsal striatum of WT and OVX mice. Bars represent the mean and error bars the SEM; ** $P < 0.01$, Unpaired student's t-test N = $K_v4.3$ ventral striatum: WT: 4, OVX: 4; $K_v4.3$ dorsal striatum: WT: 4, OVX: 4 animals.
Scale bars: 2µm.

Discussion

In the current chapter, I demonstrate that in the prodromal phase of PD, there are significant changes in the expression of a range of key neurochemical pathways within the striatum. Key amongst these changes were the altered levels of expression for specific K_v subtypes. Such changes are likely to significantly impact on the activity of striatal neurons and thus the overall functioning of the striatum. Given the widespread connectivity of the striatum with the rest of the brain, such altered functioning of the striatum could add to the overall disease spectrum of PD and thus the myriad of symptoms associated with this condition which extend beyond the classical motor deficits, such as apathy, altered levels of stress and anxiety.

PD-dependent neurochemical plasticity in early stages of the condition

PD is a progressive condition with its pathology thought to initiate many decades before the onset of the cardinal motor deficits of bradykinesia, rigour, tremor (Williams and Litvan, 2013). When such symptoms present, irreversible neurodegeneration has already occurred. The result is a purely symptomatic approach to enhancing patient care. Therefore, a fervent area of research is the identification of early stage symptoms that may be predictive of the condition, thereby allowing for interventions at a time when the trajectory of the disease can still be modified. The data arising from this chapter are therefore important because they could be instrumental in providing a platform for the further understanding of some of the early stage changes that occur

throughout different brain regions, and thus the earliest symptoms to arise in such patients.

It is unsurprising that some of the changes occurring in the OVX mice relate to neurotransmitter system. α-syn functions primarily as a protein within axon terminals to regulate the release of neurotransmitters (Jessika C. Bridi and Hirth, 2018). Although it is thought to be ubiquitously expressed in most axon terminals, its associated pathology appears to preferentially impact on only specific subset of neurotransmitter pathways. Indeed, in PD patients, the pathological form of α-syn, namely Lewy bodies, is concentrated in catecholamine centres, although these may spread to other regions with advancing age. Furthermore, in α-syn knockout mice, the synaptic release of dopamine is preferentially impaired (Lotharius and Brundin, 2002) (Nemani *et al.*, 2010). Since the striatum is one of the brain regions to receive the highest levels of dopamine innervation, evidenced by the intense expression of DARPP-32 (see Figure 3.1), it is predictable that the increased expression of α-syn that occurs in OVX mice will impact on this brain region. What is unclear, and needs to be followed up in the future, is whether this increased α-syn expression results in the altered release of dopamine in the striatum, at this early age. In OVX mice, I detected a decreased expression of DARPP-32. Since DARPP-32 is a substrate of cAMP-dependent protein kinase (PKA) and is also involved in the phosphorylation of dopamine receptors (Hemmings and Greengard, 1986), its altered expression could indicate changes in dopamine receptor activation, which most likely occurs from changes in dopamine synaptic release. Altered levels of dopamine release are closely related with psychiatric disorders of the striatum, such as

motivation, anxiety and aggression (Calabresi *et al.*, 2000). Changes in emotion related to such disorders are known to be part of the early spectrum of symptoms prior to PD motor deficits. Therefore, future studies to fully characterise such changes in dopamine signalling during this early stage of the disease could be valuable in addressing this aspect of the condition.

I found it intriguing that expression of the inflammatory marker, IBA1, was decreased in OVX mice. This is because neuroinflammation is known to be a key component of the PD pathology (de Araújo Boleti *et al.*, 2020). Since increased expression of IBA1 is generally considered to be representative of neuroinflammation, this diminished expression, logically, would suggest a dampened immune response. If so, it is unclear whether this is representative of a persistent suppressed immune state, or merely a compensatory decrease, during these early stages, to counteract any ongoing pathology. I predict it could be latter because the age-related onset of PD pathology. Perhaps, ongoing PD pathology induces a range of compensatory changes in various brain pathways allowing patients in early to mid-life to contain the disease. However, such counteractive measures could be exhausted if one lives to old age, precipitating the onset of symptoms. It would therefore be useful in future studies to compare the levels of IBA1 expression in young and old animals to assess whether there is a temporal profile to the immune status in OVX mice. Such studies of IBA1 should also be accompanied by assessing other markers of neuroinflammation.

Changes in K_v expression in OVX mice

My data show that the increased expression of α-syn has a profound effect on various K_v subtypes, at both the gene and protein levels. It is unclear whether such changes are due to a direct interaction between α-syn and K_v, or merely compensatory changes due to alterations in neuronal activity as a result of α-syn dependent neurotransmitter release. Future studies focussed on protein-protein interaction analyses for α-syn and various K_v will be instrumental in addressing this important question. However, since K_v functions to dampen action potential activity, their decreased expression at the protein levels could be indicative of underactivity of the neurons on which they are expressed, in order to maintain basal levels of activity. Given the changes in DARPP-32 expression, another surrogate marker of dopamine receptor activation. Collectively, such changes in K_v expression could infer altered levels of activity for striatal neurons, and thus striatal function, at this early age. Therefore, future electrophysiological studies focussed on assessing changes in MSN excitability at various ages of OVX mice could provide unique insights into the earliest functional changes to occur in the striatum, during the PD process, and thus inform on the understanding and treatment of the earliest symptoms to emerge.

In the next chapter, I investigate whether pathology related to Alzheimer's, impacts on native K_v expression.

Chapter Five

Effect of Alzheimer's disease pathology on the expression of K_v in the striatum

Summary and importance

Background

In chapter 4, I demonstrated that in an age-related neurodegenerative disease that primarily impacts on a very select groups of brain regions including the striatum, namely PD, such pathology has a significant impact on the native expression patterns of K_v within this brain region. This suggest that some of the changes in striatal neuronal activity, and therefore striatal-related brain functions, could be due to this altered level of K_v expression, therefore revealing potential therapeutic targets. The question therefore arises whether the pathology of other age-related neurodegenerative diseases that affect the brain more broadly, in particular dementias such as AD, also impact on striatal K_v, and therefore underlie some of the striatal-related symptoms of AD, such as apathy or emotional disturbances. Therefore, in this chapter, I aim to explore whether pathology associated with AD alters striatal K_v expression.

Methods

I used the APP-PS1 transgenic (TG) mouse model of AD which results in accelerated production of amyloid beta (Aβ), which is a pathological hallmark of AD. As controls, I used wild-type (WT) littermates. All animals were males, aged 6 months. I used immunohistochemistry with confocal microscopy to

determine the expression of Aβ peptides as well as changes in the expression levels of various striatal neurochemicals in the TG mouse. Quantitative PCR (qPCR) and immunohistochemistry was used to assess changes in the expression of various K_v subtypes.

Results

A surprising discovery was that Aβ was expressed in only a subset of DARPP-32 immunopositive cells. This indicates that only a subset of MSNs are impacted by AD pathology. Furthermore, Aβ was expressed in cholinergic and parvalbumin interneurons, indicating that AD pathology also affects local circuit interneurons. I did not detect any changes in the expression levels of other striatal neurochemicals, including markers of their inputs or inflammation. qPCR revealed that mRNA for the $K_v4.3$ was significantly decreased in TG mice compared to WT. There were no other differences in expression for other K_v examined. At the protein level, I did not detect any changes in the expression for various K_v.

Importance

The data revealed that classic AD pathology presents selectively in specific cell types of the striatum. Furthermore, the striatum overall is remarkably resilient to the presence of AD pathology, with minimal changes in expression for various neural markers detected. Finally, the decreased mRNA expression for $K_v4.3$, which is expressed on the GABAergic parvalbumin interneurons that provide key inhibitory modulation, could with age result in increased activity of such cells, resulting in changes in overall striatal activity.

Results

5.1. Characterisation of AD-like pathology in the striatum of TG mouse

The TG AD mouse model I utilised has been widely used (Borchelt *et al.*, 1997). However, most investigators focus on cortical brain regions. As a result, the disease phenotype in the striatum has yet to be reported on. Therefore, as a start, I sought to characterise the type of AD-associated pathology that is expected in this model. The TG model has two transgenes for human amyloid precursor protein and presenilin 1 that results in the over-expression of the amyloid beta 1-42 peptide, a key pathological hallmark of AD (Tanzi *et al.*, 1987). The production of Aβ increases with age, resulting in the development of Aβ plaques in cortical regions, in advanced age (Fig 5.1).

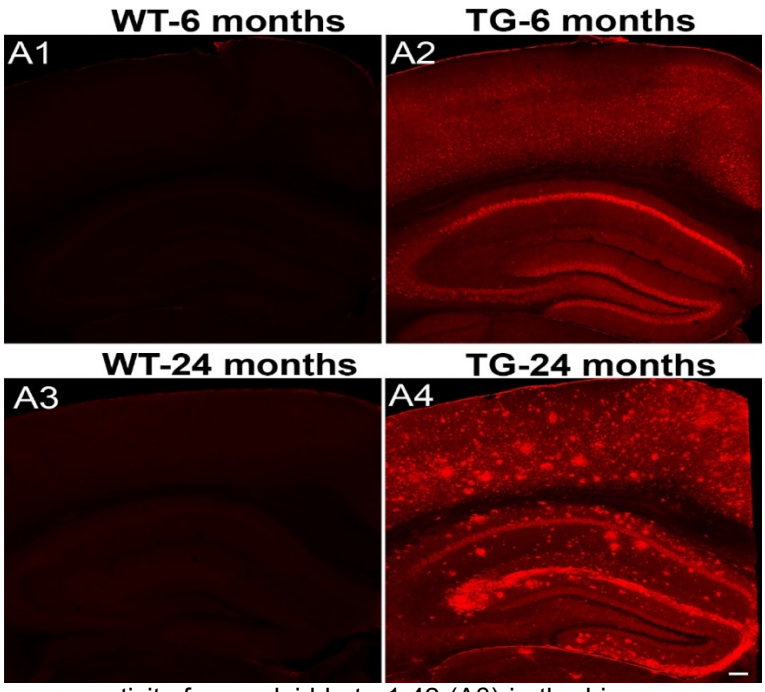

Figure 5.1. Immunoreactivity for amyloid beta 1-42 (Aβ) in the hippocampus of WT and TG mice.
(A1-2) shows immunoreactivity for Aβ in the hippocampus of 6 months old WT and TG mice in the same field of view. (A3-4) shows immunoreactivity for Aβ in the hippocampus of 24 months old WT and TG mice in the same field of view. (A2) shows an intense expression of Aβ which is even more intense resulting in the expression of Aβ plaques in (A4). This indicates that AD pathology results in accelerated production of Aβ which increases with age.
Scale bar 500 μm.

However, in the striatum of TG mice, Aβ immunoreactivity was widespread throughout this brain region and presented as cytoplasmic signal in DARPP-32 immunopositive neurons, indicating that the principal MSN neurons contained this AD-like pathology (Fig 5.2 B). It was noticeable that not all DARPP-32 were immunopositive for Aβ. (Fig 5.2 B3). No specific signal was detected in wildtype mice (Fig 5.2 A).

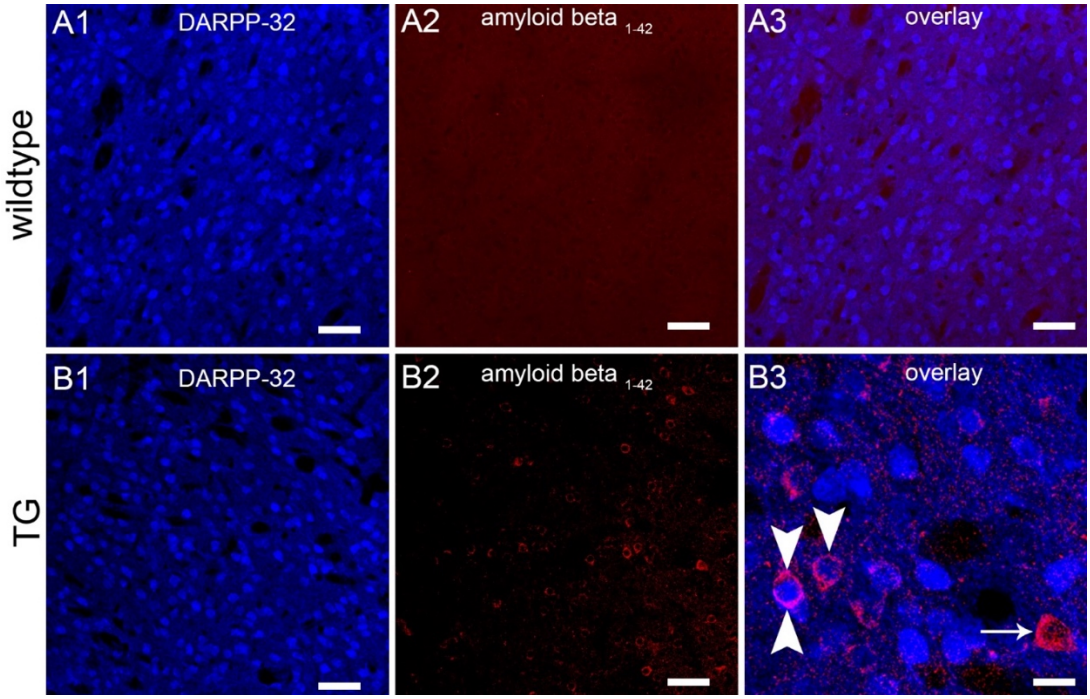

Figure 5.2. Immunoreactivity for Aβ in the striatum of WT and TG mice.
(A1) shows immunoreactivity for DARPP-32 immunopositive cells (MSN) in the striatum of WT mice. (A2) shows immunoreactivity for Aβ in the same field of view. (A3) is an overlay of (A1, A2) in the same field of view suggesting that no specific signal was detected in the striatum of WT mice. As with (A1-A2), (B1-B2) shows immunoreactivity for MSN and Aβ in the striatum of TG mice. (B3) is an enlarged overlay of (B1, B2) showing the expression of Aβ presented as cytoplasmic signal in DARPP-32 immunopositive neurons. Not all DARPP-32 were immunopositive for Aβ.
Scale bar (A; B1-2) 50 μm; (B3) 10 μm.

Intrigued by the presentation of Aβ signal in only I subpopulation of MSNs, I hypothesised that this could be based on their dopamine receptor (DR) profiles since some express D1R and other D2R, never both. I therefore evaluated Aβ immunoreactivity in conjunction with that for D1R. There was no clear correlation between DR and Aβ expression in DARPP-32 neurons, with some D1R-DARPP-32 positive neurons containing signal for Aβ, whilst others did

not (Fig 5.3). It is therefore unclear whether the expression of the transgenes, and thus the development of the pathology, is random in terms of MSNs, or related to a more refined, and yet to be discovered molecular profile.

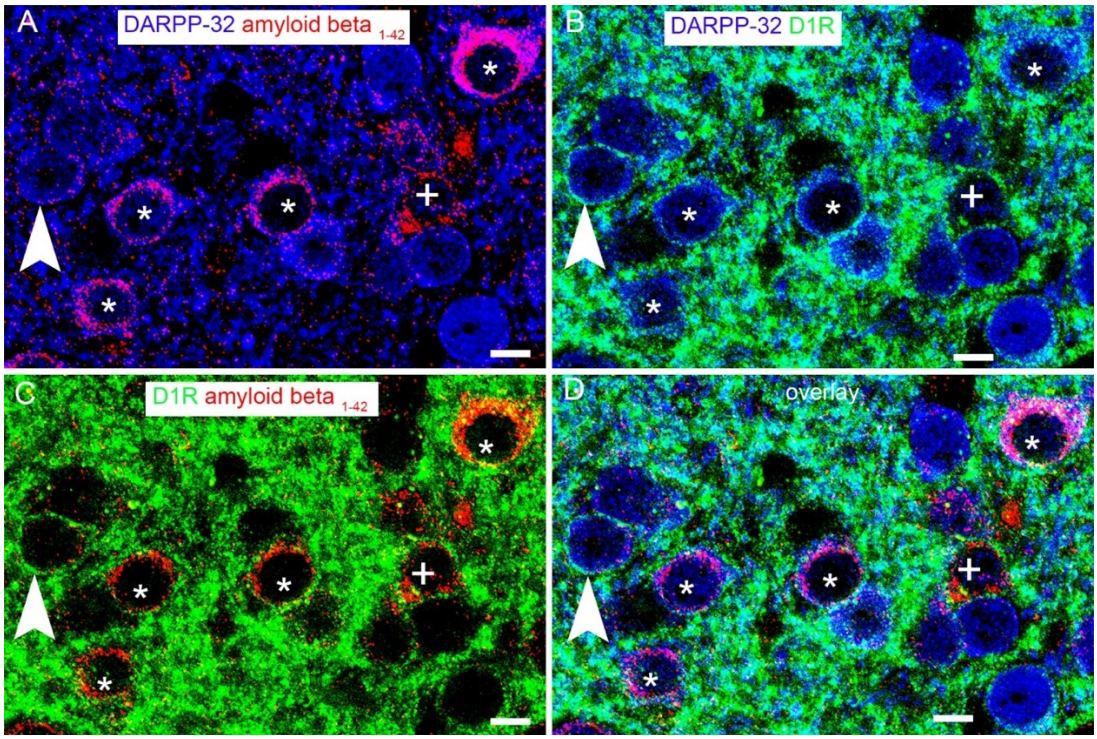

Figure 5.3. Immunohistochemical localisation of Aβ with dopamine 1 receptor (D1R) in the striatum of TG mice.
(A) shows the immunoreactivity for Aβ and how it is expressed on DARPP-32 immunopositive cells (MSN). Aβ signal is expressed on subpopulation of MSNs (*) and DARPP-32 immunonegative neurons (+). (B) shows the immunoreactivity for D1R and how it is expressed on MSN. (C, D) is an overlay of both (A and B) in the same field of view demonstrating the association between Aβ and D1R. There is no clear correlation between D1R and Aβ expression in DARPP-32 neurons, with some D1R-DARPP-32 positive neurons containing signal for Aβ, whilst others did not.
Scale bars 10 μm.

It was noticeable that some DARPP-32 immunonegative neurons also expressed Aβ signal, indicating that some interneurons contained this AD-like pathology. I therefore sought to determine the neurochemical identity of these Aβ immunopositive interneurons. A systematic analysis revealed that cholinergic (Fig 5.4 A) and parvalbumin (Fig 5.4 B) interneurons expressed Aβ.

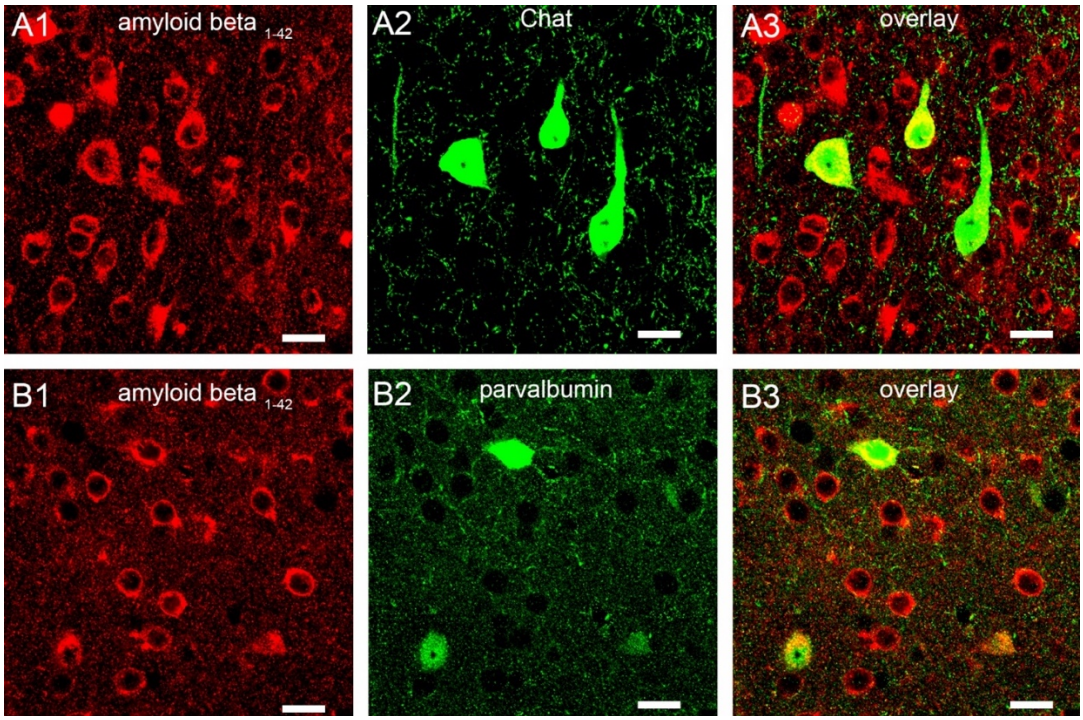

Figure 5.4. Immunohistochemical localisation of Aβ with interneurons in the striatum of TG mice.
(A1) shows the immunoreactivity for Aβ. (A2) shows the immunoreactivity for ChAt expressed on cholinergic interneurons. (A3) is an overlay of both (A1 and A2) showing the expression of Aβ in cholinergic interneurons. As with (A1-3), (B1-3) shows the expression of Aβ in parvalbumin containing GABAergic interneurons.
Scale bars 10 μm.

Apart from the Aβ 1-42 peptide that results in insoluble plaques, newly synthesised Aβ can also exist as soluble oligomers (AβO) which are purported to actually drive Aβ pathology in AD (Cline *et al.*, 2018). I therefore used two different antibodies that recognises different sizes of AβO, termed NU1 and NU2, to assess whether AβO expression occurs in the striatum. Immunoreactivity for NU1 was found in both DARPP-32 immunopositive and immunonegative neurons (Fig 5.5 A). However, NU2 was exclusively expressed in DARPP-32 immunonegative neurons. Since NU1 and NU2 recognise different sized AβO, the above suggests that different facets of AD-associated pathology target the different cell types of the striatum.

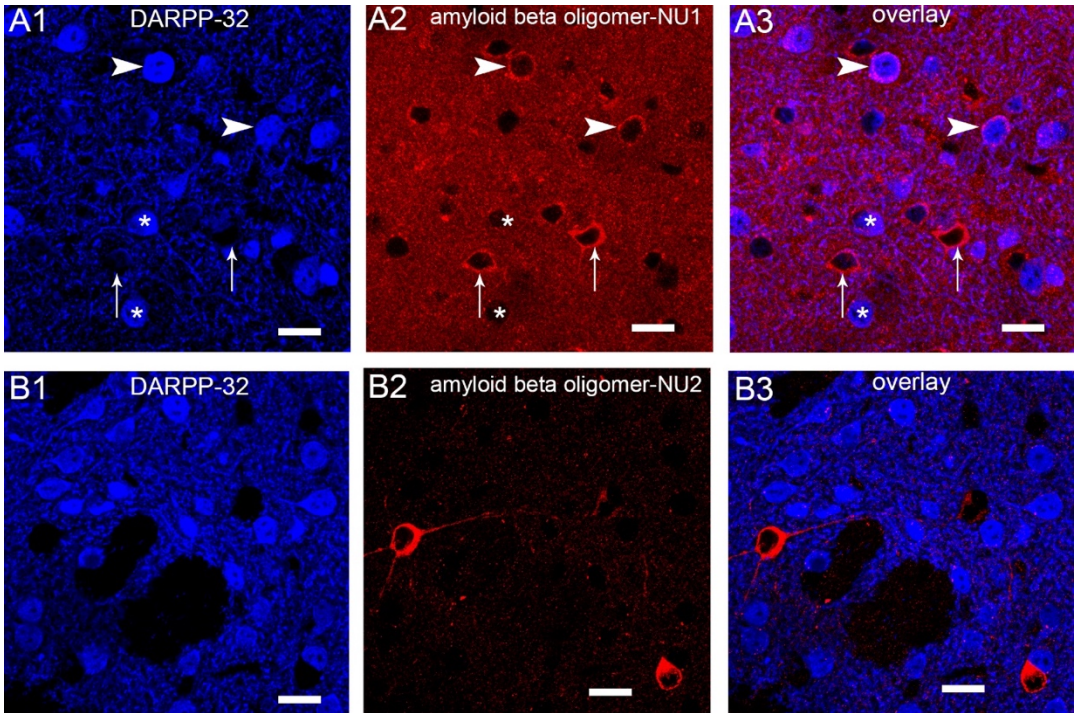

Figure 5.5. Immunoreactivity for amyloid beta oligomer (AβO) in the striatum of TG mice. (A1) shows immunoreactivity for DARPP-32 immunopositive cells (MSN). (A2) shows immunoreactivity for the AβO- NU1. (A3) is an overlay of both (A1 and A2) in the same field of view showing the expression of NU1 in DARPP-32 immunopositive and immunonegative cells. As with (A1-2), (B1-2) shows immunoreactivity for MSN and the AβO- NU2. (B3) is an overlay of both (B1 and B2) in the same field of view showing the expression of NU2 exclusively in DARPP-32 immunonegative cells. This suggests that different facets of AD-associated pathology target the different cell types of the striatum.
Scale bar 20 μm.

5.2. Impact of AD pathology on striatal neurochemical expression

Any AD-related changes to striatal function could be due to consequences of such pathology on the native neurochemicals within this brain region. I therefore began by assessing whether there were any changes in the mRNA levels for afferent pathways that drive striatal function. To this end, I performed qPCR to measure changes in the mRNA levels for the following genes: tyrosine hydroxylase gene (TH), serotonin transporter gene (Slc6a4), tryptophan hydroxylase 1 gene (TPH1), tryptophan hydroxylase 2 gene (TPH2) and dopamine β-hydroxylase gene (DBH). mRNA levels of TH, Slc6a4, TPH2 and DBH were decreased in TG mice and levels of TPH1 was

increased in TG mice. However, these changes were not statistically significant (Fig 5.6).

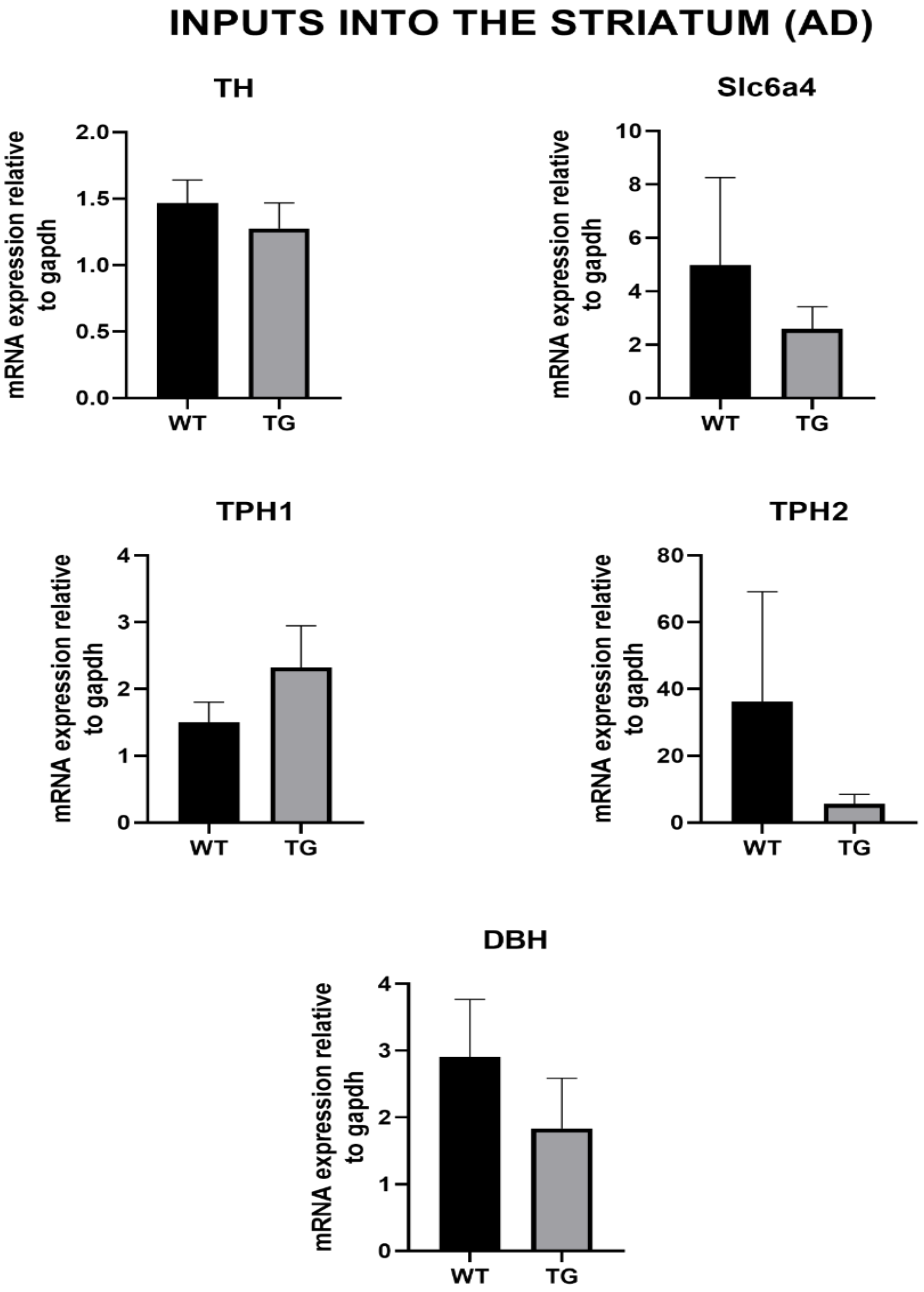

Figure 5.6. Quantification of neurochemical-encoding mRNAs in the striatum shows the levels of TH, slc6a4, TPH1, TPH2 and DBH-encoding mRNAs in isolated samples from WT and TG mice. Bars represent the mean and error bars the SEM; Unpaired student's t-test *N* = TH: WT: 15, TG: 15; Slc6a4: WT: 11, TG: 11; TPH1: WT: 15, TG: 15; TPH2: WT: 11, TG: 11; DBH : WT: 6, TG: 6 animals.

Since a core feature of AD is neurodegeneration, I next assessed whether such AD-like pathology has an impact on the density of MSN neurons. I used the levels of DARPP-32 immunoreactivity as a surrogate marker of MSN

numbers. The mean intensity of DARPP-32 was lower in both the ventral striatum (P > 0.3252, unpaired Student's t test, N = 5 animals), and dorsal striatum (P > 0.3408, unpaired Student's t test, N = 5 animals) of TG mice. However, these changes were not statistically significant (Fig 5.7).

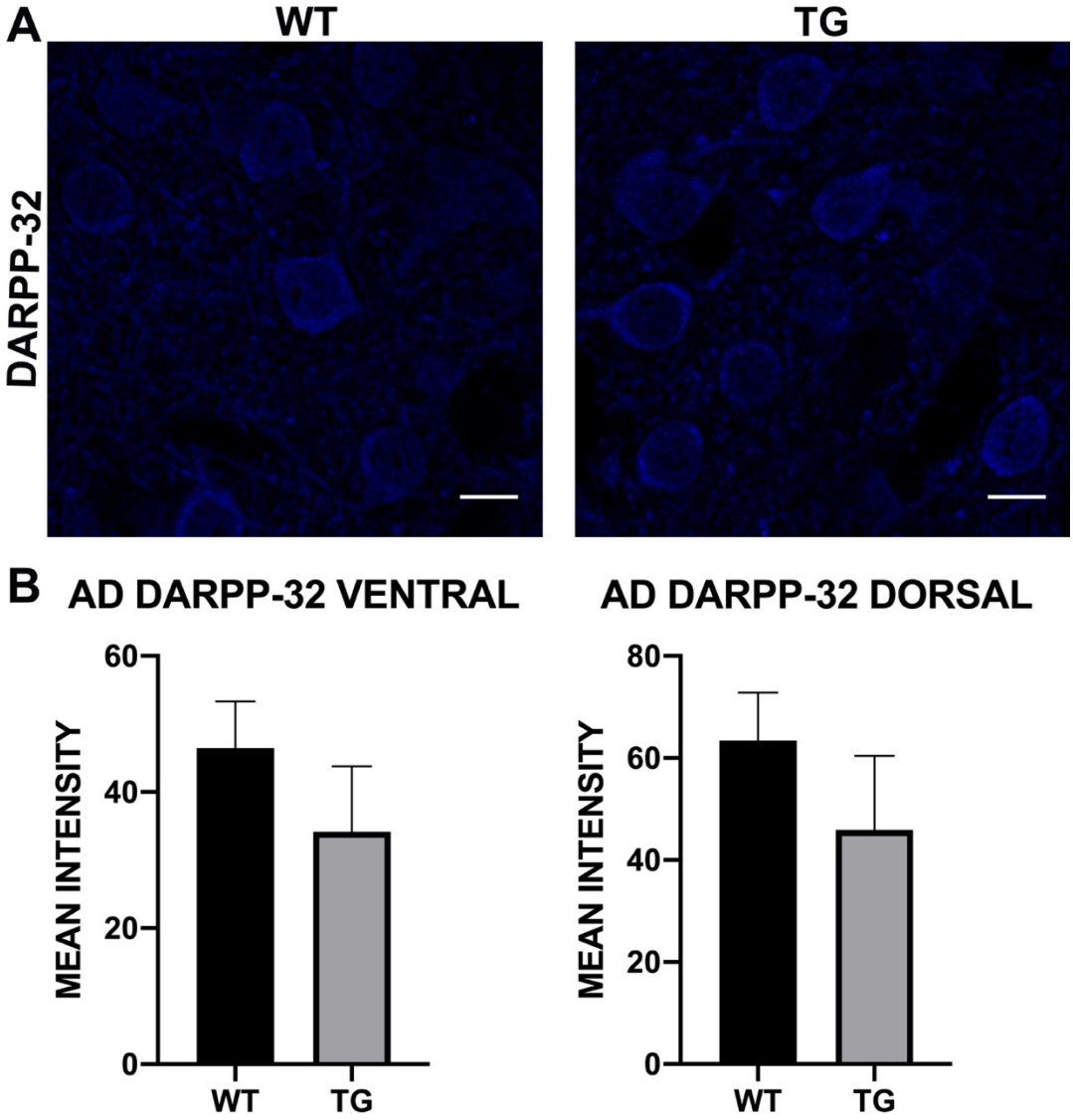

Figure 5.7. Quantification of DARPP-32 immunoreactivity in the striatum of WT and TG mice. (A) shows representative image of DARPP-32 immunoreactivity in the striatum of WT and TG mouse. (B) shows the fluorescence intensity of DARPP-32 in the ventral and dorsal striatum of WT and TG mice. Bars represent the mean and error bars the SEM; Unpaired student's t-test *N* = DARPP-32 ventral striatum: WT: 5, TG: 5; DARPP-32 dorsal striatum: WT: 5, TG: 5 animals.
Scale bars: 10μm.

Given the central roles that inhibitory interneurons play in regulating the activity of MSNs, I next explored whether AD-like pathology has any impact on such

cell types. To this end, I performed qRT-PCR to assess changes in the mRNA levels for ChAt and parvalbumin in the striatum of WT and TG mice. ChAt and PV mRNA levels were increased in TG mice. However, the changes were not statistically significant (Fig 5.8).

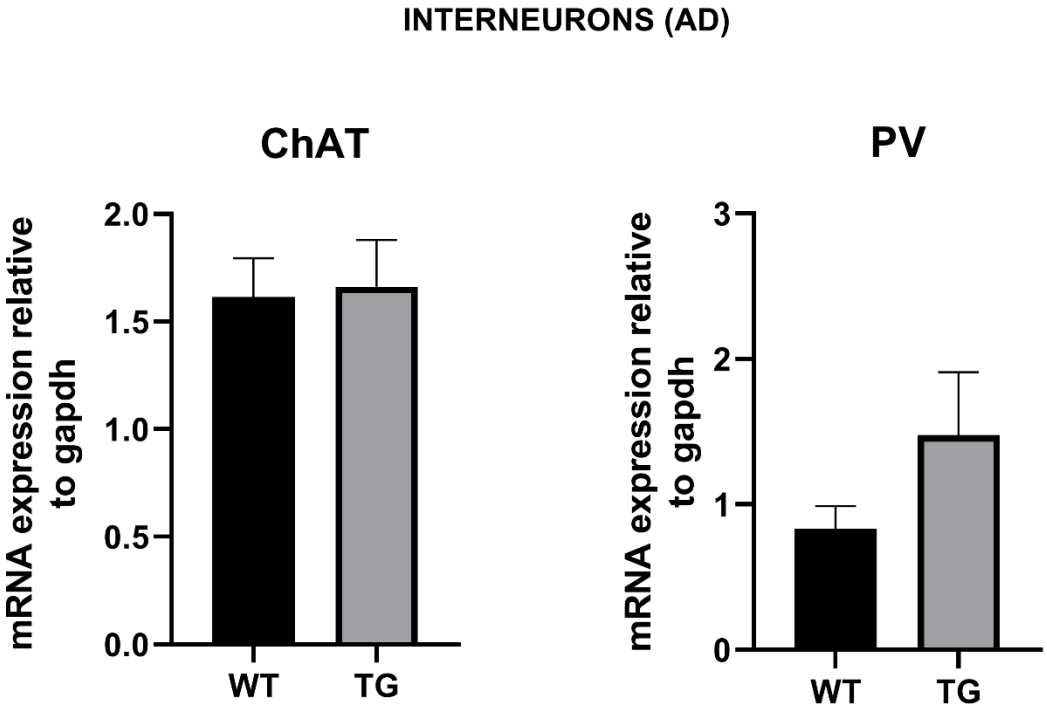

Figure 5.8. Quantification of interneuron-encoding mRNAs in the striatum shows the levels of ChAt and PV-encoding mRNAs in isolated samples from WT and TG mice. Bars represent the mean and error bars the SEM; Unpaired student's t-test *N* = ChAt: WT: 6, TG: 6; PV: WT: 18, TG: 18 animals.

I then assessed whether there may be changes at the protein level, focussing on parvalbumin expressing interneurons since they are the most numerous and were also the only ones to express any K_v. To this end, I performed immunohistochemistry with confocal microscopy to assess the effect of AD pathology on the fluorescence intensity of PV cells in the ventral and dorsal striatum of TG mice in comparison to WT littermates as control. The mean intensity of PV cell was lower in the ventral striatum of TG mice ($P > 0.3068$, unpaired Student's t test, N = 5 animals), but slightly higher in the dorsal

striatum (P > 0.9383, unpaired Student's t test, N = 5 animals). However, the changes were not statistically significant (Fig 5.9).

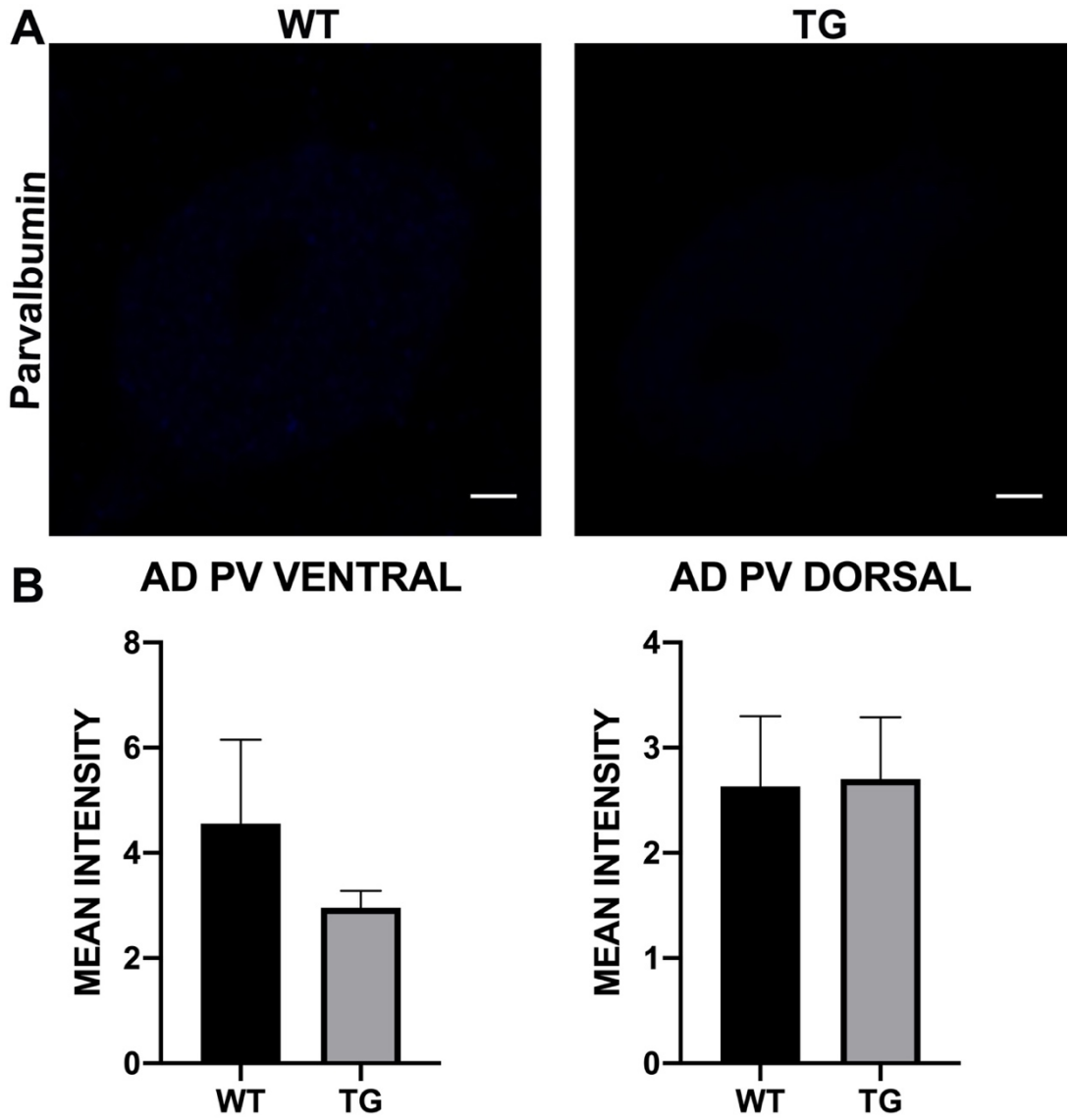

Figure 5.9. Quantification of parvalbumin immunoreactivity in the striatum of WT and TG mice. (A) shows representative image of parvalbumin (PV) immunoreactivity in the striatum of WT and TG mouse. (B) shows the fluorescence intensity of PV cells in the ventral and dorsal striatum of WT and TG mice. Bars represent the mean and error bars the SEM; Unpaired student's t-test *N* = PV ventral striatum: WT: 4, TG: 5; PV dorsal striatum: WT: 4, TG: 5 animals.
Scale bars: 2μm.

Inflammation is a hallmark of AD pathology and has been documented in cortical brain regions in our AD mouse model. I investigated whether there were any signs of inflammation in the striatum, using the standard cellular marker of neuroinflammation, namely the microglia protein IBA1. The mean

intensity of IBA1 was slightly higher in the ventral (P > 0.7053, unpaired Student's t test, N = 5 animals), and dorsal striatum (P > 0.5021, unpaired Student's t test, N = 5 animals) of TG mice. However, the changes were not statistically significant (Fig 5.10).

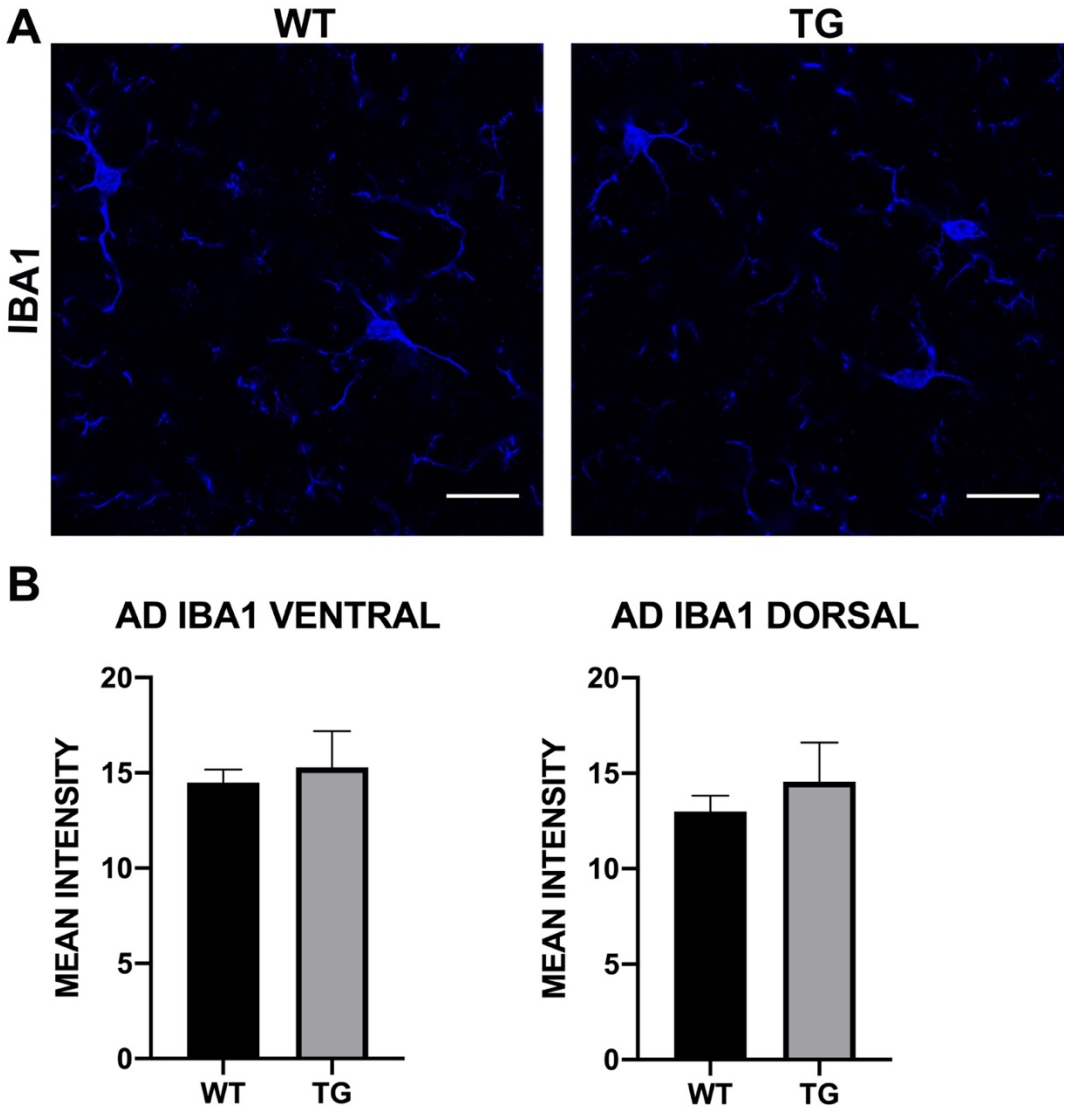

Figure 5.10. Quantification of IBA1 immunoreactivity in the striatum of WT and TG mice.
(A) shows representative image of IBA1 immunoreactivity in the striatum of WT and TG mouse. (B) shows the fluorescence intensity of IBA1 in the ventral and dorsal striatum of WT and TG mice. Bars represent the mean and error bars the SEM; Unpaired student's t-test *N* = ventral striatum: WT: 5, TG: 5; dorsal striatum: WT: 5, TG: 5 animals.
Scale bars: 20μm.

5.3. Quantification of K_v-encoding mRNAs in the striatum of AD mice

I next assessed whether such AD-associated pathology in striatal neurons has an impact on the expression of K_v in this brain region, beginning at the mRNA level, using qRT-PCR. Since mRNA is primarily located in cell bodies, I focussed only on those K_v which my previous immunohistochemistry revealed to be expressed in striatal neurons. These include the K_v1.2, 2.1, 4.2 and 4.3. I detected a significant decrease in the mRNA levels of the K_v4.3 in TG mice compared to WT littermates ($P < 0.0066$, unpaired Student's t test, N = 11 WT and TG mice) (Fig 5.11). Also, there was a trend towards a decrease in the mRNA levels for K_v1.2 and 2.1, and an increase for K_v4.2, but these did not reach statistical significance (Fig 5.11).

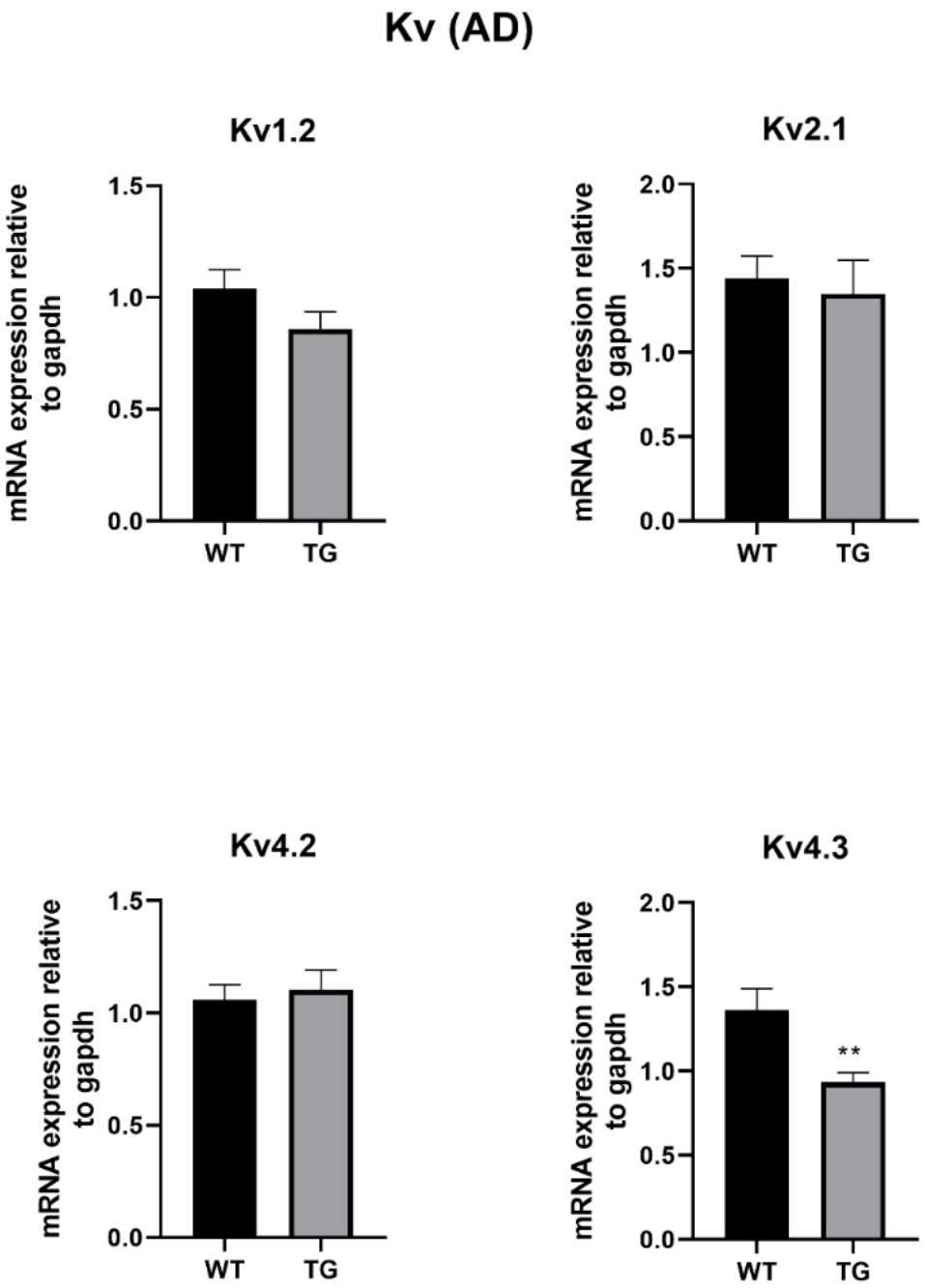

Figure 5.11. Quantification of K_v-encoding mRNAs in the striatum shows the levels of K_v-encoding mRNAs in isolated samples from WT and TG mice. Bars represent the mean and error bars the SEM; ** $P < 0.01$, unpaired student's t-test N = K_v1.2: WT: 15, TG: 15; K_v2.1: WT: 19, TG: 19; K_v4.2: WT: 6, TG: 6; K_v4.3: WT: 11, TG: 11 animals.

5.4. Quantification of K_v protein in the striatum of AD mice

The impact of AD pathology on K_V expression could be either at the mRNA or protein levels, or both. I therefore assessed whether the minimal effect that AD pathology had on K_v mRNA expression, persisted at the protein level. To

this end, I performed immunohistochemistry with confocal microscopy to assess the effect of AD pathology on the fluorescence intensity of $K_v2.1$, $K_v4.2$ and $K_v4.3$ in the ventral and dorsal striatum of TG mice in comparison to WT littermates as control. I detected a decrease in the mean intensity of $K_v2.1$ in ventral striatum (P = 0.5895, unpaired Student's t test, N = 5 animals) and no change in the mean intensity in dorsal striatum (P = 0.9959, unpaired Student's t test, N = 5 animals) of TG mice (Fig 5.12 B). The mean intensity of $K_v4.2$ in ventral striatum (P = 0.2128, unpaired Student's t test, N = 5 animals) and dorsal striatum (P = 0.2884, unpaired Student's t test, N = 5 animals) was decreased in TG mice (Fig 5.13 B). Also, the mean intensity of $K_v4.3$ in ventral striatum (P = 0.0738, unpaired Student's t test, N = 5 animals) and dorsal striatum (P = 0.1871, unpaired Student's t test, N = 5 animals) was decreased in TG mice (Fig 5.14 B). There was a trend towards a decrease in the protein levels of $K_v2.1$ (Fig 5.12 B), $K_v4.2$ (Fig 5.13 B) and $K_v4.3$ (Fig 5.14 B). However, these changes were not statistically significant.

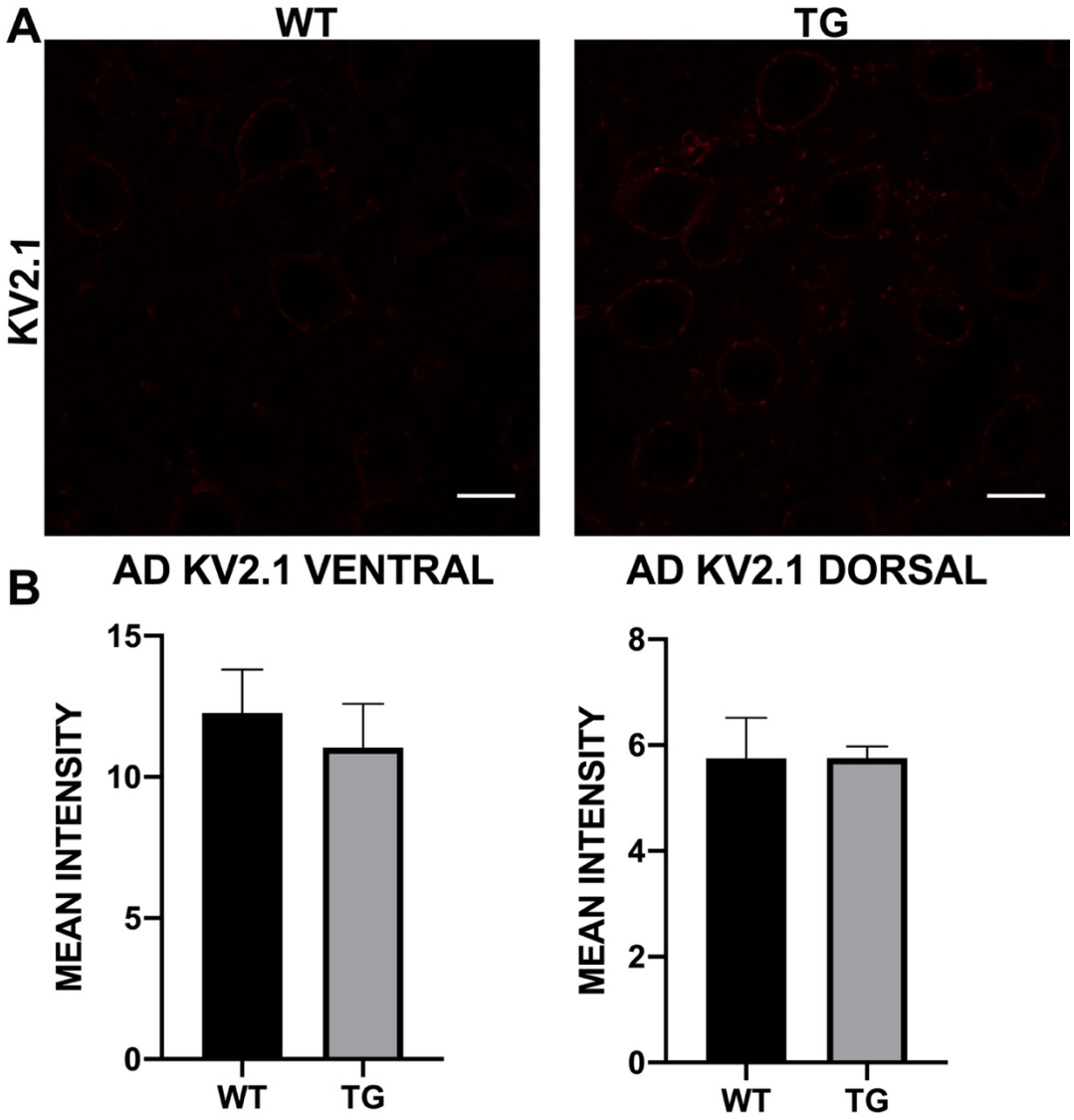

Figure 5.12. Quantification of $K_v2.1$ immunoreactivity in the striatum of WT and TG mice. (A) shows representative image of $K_v2.1$ immunoreactivity in the striatum of WT and TG mouse. (B) shows the fluorescence intensity of $K_v2.1$ in the ventral and dorsal striatum of WT and TG mice. Bars represent the mean and error bars the SEM; Unpaired student's t-test *N* = $K_v2.1$ ventral striatum: WT: 5, TG: 5; $K_v2.1$ dorsal striatum: WT: 5, TG: 5 animals.
Scale bars: 10µm.

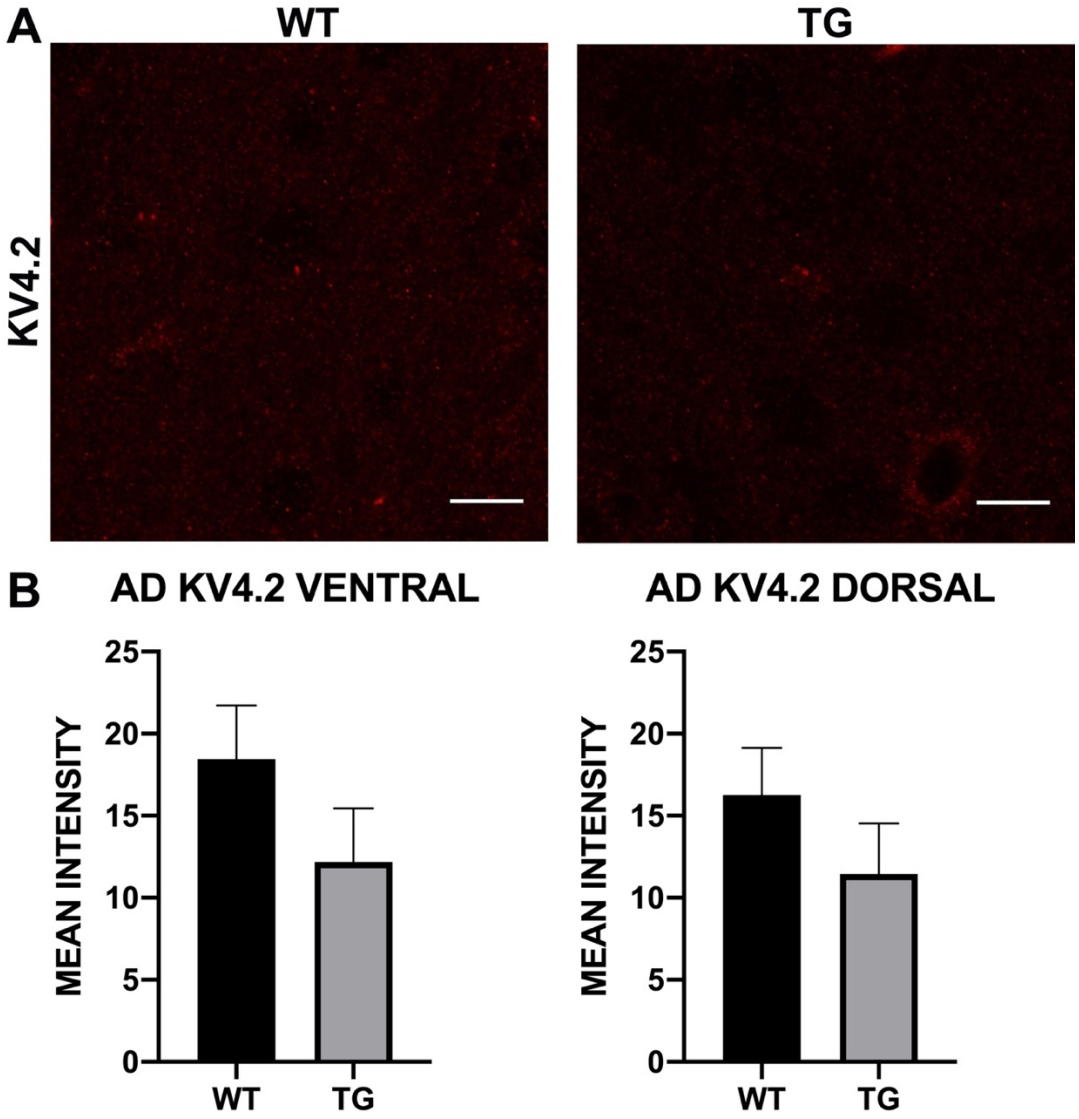

Figure 5.13. Quantification of $K_v4.2$ immunoreactivity in the striatum of WT and TG mice. (A) shows representative image of $K_v4.2$ immunoreactivity in the striatum of WT and TG mouse. (B) shows the fluorescence intensity of $K_v4.2$ in the ventral and dorsal striatum of WT and TG mice. Bars represent the mean and error bars the SEM; Unpaired student's t-test *N* = $K_v4.2$ ventral striatum: WT: 5, TG: 5; $K_v4.2$ dorsal striatum: WT: 5, TG: 5 animals.
Scale bars: 10µm.

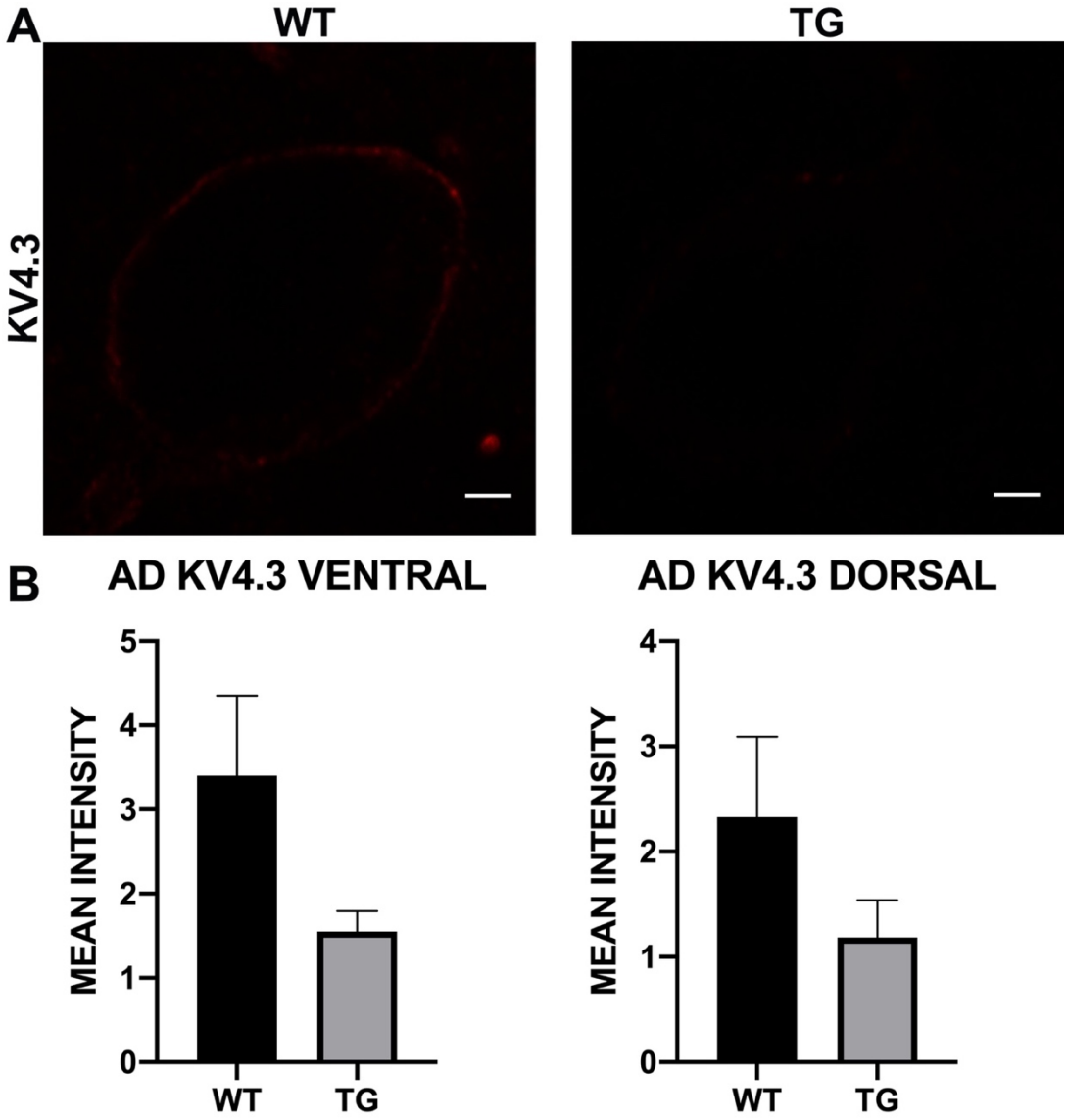

Figure 5.14. Quantification of $K_v4.3$ immunoreactivity in the striatum of WT and TG mice. (A) shows representative image of $K_v4.3$ immunoreactivity in the striatum of WT and TG mouse. (B) shows the fluorescence intensity of $K_v4.3$ in the ventral and dorsal striatum of WT and TG mice. Bars represent the mean and error bars the SEM; Unpaired student's t-test *N* = $K_v4.3$ ventral striatum: WT: 4, TG: 5; $K_v4.3$ dorsal striatum: WT: 4, TG: 5 animals.
Scale bars: 2μm.

Discussion

In this chapter, I provide the first demonstration of the expression of AD-associated pathology in the striatum of a widely used AD mouse model. Different forms of Aβ were expressed within sub-populations of principal cells as well as interneurons. Despite the expression of what is supposedly a neurotoxic protein, I did not detect any changes in striatal neurochemistry, including K_V. This suggests that the striatum is remarkably resilient to core AD processes and possibly explains why there is limited impact on this brain region in terms of the core feature of AD, namely neurodegeneration.

AD pathology in striatal neural circuits

An interesting finding was that only a sub-population of MSNs express Aβ. This could be due to the age of the animals used (6 months), and it could be possible that with age, all MSNs express Aβ. Unfortunately, due to time constraints, I was unable to undertake and ageing component to this analysis. However, I would argue against the possibility of this age profile changing with age, because in other brain regions, it's only the onset of Aβ insoluble plaques that emerge with ageing, not the number of cells that express Aβ (Borchelt *et al.*, 1997). I therefore posit that this represents a constant pattern of expression of Aβ in this brain region. The question therefore arises as to why only some cells express Aβ. It could be a manifestation of the transgenic technology for this mouse model. The transgenes are expected to be constitutively expressed throughout the body. However, it could be possible that not all cells express the transgenes, although this is unlikely, based on the genotyping experiments we perform on all mice used. This divergent expression of Aβ could therefore

uncover an added layer of diversity to striatal cell categorisation. Historically, MSNs have been divided into two classes, based on their expression of either D1R or D2R, and their projection patterns to other brain regions, termed direct or indirect pathways respectively (Gerfen *et al.*, 1990). Such nomenclature has remained in place with limited consideration of the possibility of more refined sub-classes of MSNs. With the advent of cutting-edge single cell transcriptomic and proteomics, it would be intriguing to assess whether the Aβ-expression MSNs are aligned with specific gene or protein profiles.

Resilience of striatal neurochemistry to AD pathology

I find it remarkable that the presence of a transgene, and the product of the transgene, had limited impact on the expression levels of various neurochemicals within the striatum, including K_V. This is at odds with brain regions in which various neurotransmitters systems have been altered (O'Neil *et al.*, 2007). This therefore raises the question whether some brain regions may have a higher pathology burden in this mouse model, or the striatum somehow is able to better compensate for such pathology. Generally, in human AD, although the condition begins in sub-cortical brain regions, the most significant damage, in the form of neurodegeneration, occurs in cortical brain regions (Braak *et al.*, 2011). I expect that the high level of glutamate-containing neurons in cortical regions, and the known contribution of glutamate excitotoxicity in AD may be a factor, in contrast, the striatum is largely a GABAergic centre since MSNs utilise GABA as the primary neurotransmitter. Therefore, any dysregulation of the activity, is unlikely to lead to the massive glutamate release that occurs in the cortex and contributes to AD pathology. I

did not detect any striking changes in K_v expression in the stratum, as a result of the AD pathology. That is surprising since these ion channels have been implicated in AD-related pathology (Shah and Aizenman, 2014). I expect that this is related to the limited impact overall that Aβ expression had on striatal neurochemistry.

In summary, Pathology associated with a major neurodegenerative disease, Alzheimer's had limited impact on the native expression patterns of K_v in the striatum.

Chapter Six

General discussion

At the outset of my PhD research, my broad aims were to provide the first high resolution characterisation of the native K_v expression patterns within the striatum, and whether such expression profiles are subject to change as a result of different life experiences or diseases. The ensuing data provide unique insights into the cellular and subcellular localisation of K_v subtypes in the striatum and the extent to which they evolve in response to early life stress or pathology associated with PD and AD. Below, I provide a summary of the findings of my research and the implications they pose in the wider neuroscience research.

Technical considerations

All scientific experiments took place within the context of certain technical parameters which I address below.

Early life stress (ELS) mouse model

Animal model of ELS based on fragmented maternal care within the first week of life has been shown to reliably result in a hyper-stress phenotype throughout adulthood (Rice *et al.*, 2008). This early-life experiences of abnormal maternal care program and abnormal stress response in the brain, also affects the expression and function of brain proteins, such as neurotransmitter receptors (Gunn *et al.*, 2013). As such, I am confident that the ELS paradigm was an

appropriate model for stress as I am working on a region of the brain that receive various neurochemical inputs from other brain regions.

Alpha-synuclein (α-syn) mouse model of PD

α-syn is the main component of Lewy bodies (LB) which has been shown to play a central role in PD (Osterhaus *et al.*, 1997). A mutation in α-syn (A53T), encoded by the *SNCA/PARK1* gene (Polymeropoulos *et al.*, 1997) as well as missense point mutations in the N-terminal of α-syn (Osterhaus *et al.*, 1997) has been shown to be the step for the formation of insoluble inclusions or LBs which plays a role in PD pathology (Miraglia *et al.*, 1997). The pathological state of PD was replicated in mouse models by generating bacterial artificial chromosome transgenic mice (OVX) that display a transgene expression profile identical to endogenous α-syn and display age-dependent loss of nigrostriatal dopamine neurons and motor impairments (Janezic *et al.*, 2013). Since the OVX mouse model closely mirrors the human pathological profile of PD in the striatum, it was therefore an appropriate model for my PhD. My findings in chapter four confirmed PD-associated pathology in the OVX models as the level of α-syn expression was significantly increased compared to WT mice.

Mo/HuAPP695swe and PS1-dE9 mouse model of AD

Over-expression of the amyloid beta 1-42 peptide (Aβ) displayed in Mo/HuAPP695swe transgenes for human amyloid precursor protein and presenilin 1 (TG) model (Tanzi *et al.*, 1987) has been shown to result in accelerated deposition of Aβ plaques and used as a pathological feature of

AD (Borchelt *et al.*, 1997). As such I made use of this model for my PhD but first of all characterise it for AD-associated pathology in the striatum as previous studies mostly focussed on cortical brain regions. My findings in chapter five confirmed AD-associated pathology in the TG models as Aβ was expressed in striatal principal neurons and interneurons. A major limitation of the data in chapter 5 is that the AD model used does not replicate the other pathological hallmark of AD, namely hyperphosphorylated Tau tangles (Mattson, 1997). This is important because Tau tangles are postulated to more closely correlate with AD pathology (Serrano-Pozo *et al.*, 2011) (Lane, Hardy and Schott, 2018). Therefore, future studies using AD models based on Tau pathology could yet reveal significant changes in K_v expression.

Immunohistochemistry and confocal microscopy

Immunohistochemistry with confocal microscopy is useful for determining the localisation and quantification of specific protein in the brain thus it is dependent on antibody specificity. All antibodies used in this thesis have had their specificity fully characterised prior to the collection of data either by myself or colleagues in my laboratory, or the lack of specific signal appropriate for gene-deleted mice, or through published reports in the literature referenced in **Table 2.1.** Immunohistochemistry with confocal microscopy is also useful for double- and -triple immunolabelling in determining the distribution of proteins in the brain within cellular and subcellular compartments, and associations existing between multiple proteins by comparing immunoreactivity of a protein with that of characterised markers. The achievable resolution of the final image is based on the microscope used. I

made use of confocal microscope which enabled me to determine the precise localisation of synaptic proteins in certain experiments. However, the sub-synaptic distribution of a protein cannot be defined. Determination of such requires the use of transmission electron microscopy in which samples are frozen at ultra-low temperature, coated with carbon and platinum, pressed between brass plates, and rapidly separated to provide an intact single representation of a single synapse which is then incubated with gold particle-conjugated antibodies and viewed under electron microscope. This technique would provide definitive localisation of proteins in sub-synaptic compartments useful in determining the exact location of neurochemical inputs. However, it is very expensive and rare.

I used immunohistochemistry with confocal microscopy to reveal the different subfamilies of K_v targeted to different striatal cell types, subcellular compartments and non-neuronal cells within the striatum, and to quantify K_v changes in response to ELS or pathology associated with PD and AD. For the purpose of my research, I opted for immunohistochemistry rather than protein immunoblot (western blot), which is also widely used for quantifying protein levels, because western blot has limitations in determining the association between multiple proteins and the precise distribution of proteins. In the case of the native expression of K_v in the striatum which was the aim of my research, investigation of the precise cellular and subcellular localisation of K_vs and determination of neurochemical inputs integrated by striatal neurons was possible through the use of immunohistochemistry with confocal microscopy and wouldn't have been achieved by western blot. However, difficulty in protein quantification which is a limitation in immunohistochemistry with

confocal microscopy was considered carefully and measures put in place to address the limitations. When comparing immunofluorescence intensity, exact processing of tissue samples was ensured at every stage. High-quality and consistent perfusion-fixation was ensured as variation in fixation can be caused by changes in chemical and molecular components of the fixative. Also, tissue samples in the same quantification study were processed with the same equipment, reagents and at the same time making sure there is consistency in the antibody incubation, washing and mounting of sections.

Quantitative reverse transcription-polymerase chain reaction (qRT-PCR) was useful throughout my study in quantifying the relative changes at the mRNA level. However, unlike in immunohistochemistry, I was limited in micro dissecting specific anatomical regions of interest within the striatum such as the ventral and dorsal striatum. As such, I used gross anatomical landmarks to dissect the striatal region of the brain. I made use of RT-PCR to enable me to have an overview of all the K_vs expressed in the striatum. Then I made use of qRT-PCR to reveal changes in native K_vs in the striatum in response to ELS, PD and AD pathology at the mRNA level. The RT-PCR and qRT-PCR data were supplemented by data from immunohistochemistry with confocal microscopy in determining the localisation of K_vs and quantifying changes in response to ELS, PD and AD pathology at the protein level.

Collectively, I have addressed the major technical considerations in this study, and my choice and application of technique was within the confines of the available resources, equipment, and technical expertise to answer the scientific questions set during my PhD research.

Localisation of K_v subfamilies in the striatum

The discovery of the rich diversity and manner of expression of native K_v subtypes in the striatum provided a bedrock for my PhD research and can be linked to an array of intra- and intercellular signalling events that underlie striatal function. K_v has been shown to sense and respond to local changes in levels of their activating stimuli (Trimmer, 2015), thus discovery of its rich diversity helps to further investigate changes that occur in response to stress and diseases. The overall picture from the localisation of K_v is that Individual K_v subtypes are present at precise locations with: K_v3.1 and 4.3 exclusively expressed in parvalbumin containing GABAergic interneurons; K_v1.1 expressed in axon terminals originating from local GABAergic axons that innervate the subcellular region of MSNs; K_v1.2 expressed in glutamatergic axons (originating from the cortex, amygdala, hippocampus, and cortex), and post-synaptic domains of excitatory axon terminals; K_v1.3 expressed in glutamatergic axons originating from the thalamus; and K_v1.4 expressed in presynaptic terminals of axons.

A very striking discovery is the expression of two different K_v subtypes exclusively located on MSNs with K_v2.1 expression restricted to somatic and proximal dendritic compartments of MSN, while K_v4.2 is exclusively expressed in distal dendrites. This localisation of K_v2.1 and K_v4.2 into distinct MSN subcellular compartments suggests the unique functional properties of the two K_v subtypes and uniqueness of the synaptic inputs that target these different compartments of the MSN. K_v2 have been shown to be distinguished by their restricted high-level expression in proximal dendrites (Trimmer, 2015) which is consistent with my data. K_v2 are delayed rectifiers (Misonou, Mohapatra and

Trimmer, 2005) and my data showed K_v2.1 to be located on proximal dendrites that are generally innervated by monoaminergic inputs such as noradrenaline or dopamine and receive limited glutamate input indicating that they are ideally placed to respond to slower changes in membrane potential. On the other hand, K_v4 are transient currents because they activate at subthreshold membrane potentials, inactivate rapidly, and recover from inactivation quickly (Birnbaum *et al.*, 2004) and my data showed K_v4.2 to be expressed on distal dendrites that selectively receive all the glutamatergic axons that innervate MSNs indicating that they are also ideally placed to integrate the rapidly changing membrane potentials from glutamate inputs. This is because glutamate as a neurotransmitter elicits an extremely powerful excitatory drive. Also, glutamatergic inputs are extremely numerous from a vast array of different brain regions.

K_v1.5 is expressed on the plasma cell membrane and dendrites of MSN. However, its expression is not exclusive to MSNs as it is also expressed on parvalbumin containing GABAergic neurons and oligodendrocyte precursor cells (OPC). OPC is a non-neuronal cell that serve as a reservoir for the generation of new oligodendrocytes. The expression of K_v1.5 on OPC opens the possibility of a unique target for disorders associated with OPC production. Overall, identification of the rich diversity of K_v in the striatum is a valuable contribution to knowledge as this is the first high resolution characterisation of the diverse cellular and subcellular localisation of K_v subtypes in the striatum, thus, providing a novel insight into the native K_v system in the striatum.

Inflammation and neurochemical plasticity in the striatum

An important discovery is the expression of $K_v1.6$ on microglia, a non-neuronal cell activated during neuroinflammation and regarded as the resident immune cells of the brain. Inflammatory process of the brain involved in triggering various neurological diseases such as AD and PD (de Araújo Boleti *et al.*, 2020) has been shown to be a major factor in susceptibility to stress-induced pathologies due to the several neurochemical adaptations associated with it (Wood *et al.*, 2015). Such neurochemical adaptation is what bring about K_v changes as revealed in the ELS data in which the mean fluorescence intensity of $K_v2.1$ in ventral striatum and $K_v4.2$ in ventral and dorsal striatum were significantly decreased. Since studies have shown that inflammation triggers stress-induced pathologies as well as neurological diseases due to neurochemical adaptation, I investigated whether there were signs of inflammation in the striatum as a result of ELS and neurological diseases pathology. My data revealed IBA1 immunoreactivity, used as marker for microglia to be significantly decreased in the ventral and dorsal striatum of ELS mice when compared to WT littermates as control. IBA1 was also significantly decreased in PD-associated pathology both in the ventral and dorsal striatum. This is intriguing since increased expression of IBA1 is generally considered to be representative of neuroinflammation. Logically, the diminished expression of IBA1 observed in ELS and PD suggests a dampened immune response which may be representative of a compensatory decrease to counteract any ongoing pathology. Such counteractive measures could be exhausted if one lives to old age, precipitating the onset of symptoms.

Overall, K_vs expressed in the striatum are highly plastic in response to life experience with significant changes occurring as a result of ELS. Furthermore, future studies in which the expression levels of IBA1 and other markers of neuroinflammation is compared in young and old animal models of stress and neurological diseases pathology will be instrumental in assessing changes in the brain immune status.

Neurotransmitter response to PD pathology

PD pathology is thought to be initiated long before the onset of the cardinal motor deficits of bradykinesia, rigour, tremor (Williams and Litvan, 2013). α-syn plays an important role in PD (Osterhaus *et al.*, 1997) and its overexpression at disease relevant levels, as exhibited in OVX mice model, results in the core features of PD displayed in old age (Janezic *et al.*, 2013). My data in chapter four revealed that α-syn is enriched in glutamatergic axon terminals originating from the cortex, axon terminals from local GABAergic interneurons, dopaminergic axons and noradrenergic axons. This is consistent with studies that shows that α-syn functions primarily as a protein within axon terminals to regulate the release of neurotransmitters (Jessika C. Bridi and Hirth, 2018). My data further revealed the changes in expression of neurotransmitters in which there was a significant increase in tyrosine hydroxylase (TH) while tryptophan hydroxylase 1 (TPH1) was decreased significantly in the striatum of OVX mice at the mRNA level. These changes in neurotransmitters which have been shown to be released at axon terminals associated with α-syn provide unique insights into the earliest functional changes in PD.

K_v response to PD pathology

Studies have shown that the onset of PD is as a result of neuronal deaths mainly in the substantia nigra pars compacta (SNc) where dopamine is normally synthesised and pumped into movement-regulating brain regions and that symptoms are seldom noticed because the striatum, immediately downstream of the SNc, can compensate to some extent. However, massive neurons in the striatum also start to die eventually (Zeng *et al.*, 2018). A good understanding of PD-associated changes in K_v in young mice is instrumental in understanding some of the early stage changes and thus the earliest symptoms to arise in PD patients before the onset of neuronal deaths. My data in chapter four revealed K_v2.1, 4.2 and 4.3 at the protein level to be decreased significantly in OVX mice. These significant decrease in protein levels can be due to a direct interaction between α-syn and K_vs, or compensatory changes due to alterations in neuronal activity as a result of α-syn dependent neurotransmitter release.

The changes in K_vs revealed by my data provide unique insights into the earliest functional changes to occur in the striatum before the onset of cardinal motor deficits. Further studies focussed on protein-protein interaction analyses for α-syn and various K_vs can inform more on the understanding and treatment of the earliest symptoms to emerge.

Resilience of the striatum to AD pathology

AD have been shown to disrupt synaptic function and contribute to cognitive impairment (Hsiao *et al.*, 1996) and central to this is the accelerated deposition of amyloid beta (Aβ) in the brain (Borchelt *et al.*, 1997). To model AD

pathology, I made use of TG mice model with two transgenes for human amyloid precursor protein and presenilin 1 that results in the over-expression of Aβ and my data revealed the expression of Aβ in some MSNs as well as cholinergic and parvalbumin interneurons. This indicates that AD pathology affects the principal neurons and local circuit interneurons of the striatum. This is an important finding as it is the first demonstration of the expression of AD-associated pathology in the striatum of a widely used AD mouse model. A comparison of the striatum of WT and TG mice did not show significant changes in the expression levels of striatal neurochemicals. There was no significant change in neurochemical markers such as ChAt and DARPP-32 that are expressed on neurons which studies have shown to be affected by AD pathology in other parts of the brain. For the K_vs, there was no significant change at the protein level while at the mRNA level, K_v4.3 was significantly decreased in TG mice. Also, inflammatory process of the brain has been shown to trigger neurological diseases such as PD and AD (de Araújo Boleti *et al.*, 2020). Whilst my data in chapter four showed that PD pathology results in reduced expression of inflammatory marker, IBA1, in the striatum, AD pathology did not result in significant change in IBA1 expression.

Overall, my data reveals that the striatum is resilient to AD pathology which could mean that the striatum has a higher pathology burden in TG mouse model, or the striatum somehow is able to compensate for AD pathology.

In summary, I have provided novel data to demonstrate high resolution characterisation of the expression patterns of different K_v subtypes and the

neurochemical inputs they integrate in the striatum. I have also shown K_v to be highly plastic in response to life experience, providing insights into the earliest functional changes in PD, and showing the resilience of striatal neurochemicals to AD pathology. I therefore believe that my research has provided valuable contributions to our understanding of K_v diversity in the striatum and the changes that occur in response to life experience, or pathology relating to specific neurodegenerative diseases, namely Parkinson's and Alzheimer's.

Bibliography

Aigelsreiter, A. *et al.* (2013) ‘Low expression of the putative tumour suppressor spinophilin is associated with higher proliferative activity and poor prognosis in patients with hepatocellular carcinoma’, *British Journal of Cancer*. Nature Publishing Group, 108(9), pp. 1830–1837. doi: 10.1038/bjc.2013.165.

Albin, R. L. *et al.* (1989) ‘<TRENDS in Neurosciences 1989 Albin-1.pdf>’, 12(10).

de Araújo Boleti, A. P. *et al.* (2020) ‘Neuroinflammation: An overview of neurodegenerative and metabolic diseases and of biotechnological studies’, *Neurochemistry International*. Elsevier, 136(November 2019), p. 104714. doi: 10.1016/j.neuint.2020.104714.

Arispe, N., Diaz, J. C. and Simakova, O. (2007) ‘A β ion channels . Prospects for treating Alzheimer ’ s disease with A β channel blockers’, 1768, pp. 1952–1965. doi: 10.1016/j.bbamem.2007.03.014.

Baimbridge, K. G., Celio, M. R. and Rogers, J. H. (1992) ‘Calcium-binding proteins in the nervous system’, *Trends in Neurosciences*, 15(8), pp. 303–308. doi: 10.1016/0166-2236(92)90081-I.

Bauer, C. K. and Schwarz, J. R. (2001) ‘Physiology of EAG K+ channels’, *Journal of Membrane Biology*, 182(1), pp. 1–15. doi: 10.1007/s00232-001-0031-3.

Bennett, B. D. and Bolam, J. P. (1993) ‘Characterization of calretinin-immunoreactive structures in the striatum of the rat’, *Brain Research*, 609(1–2), pp. 137–148. doi: 10.1016/0006-8993(93)90866-L.

Birnbaum, S. G. *et al.* (2004) ‘Structure and function of Kv4-family transient

potassium channels', *Physiological Reviews*, 84(3), pp. 803–833. doi: 10.1152/physrev.00039.2003.

Bloom, G. S. (2014) 'Amyloid-β and tau: The trigger and bullet in Alzheimer disease pathogenesis', *JAMA Neurology*, 71(4), pp. 505–508. doi: 10.1001/jamaneurol.2013.5847.

Borchelt, D. R. *et al.* (1997) 'Accelerated amyloid deposition in the brains of transgenic mice coexpressing mutant presenilin 1 and amyloid precursor proteins', *Neuron*, 19(4), pp. 939–945. doi: 10.1016/S0896-6273(00)80974-5.

Braak, H. *et al.* (2011) 'Stages of the pathologic process in alzheimer disease: Age categories from 1 to 100 years', *Journal of Neuropathology and Experimental Neurology*, 70(11), pp. 960–969. doi: 10.1097/NEN.0b013e318232a379.

Brice, A. (2000) 'Alpha-synuclein and Parkinson ' s disease', 57, pp. 1894–1908.

Bridi, Jessika C. and Hirth, F. (2018) 'Mechanisms of α-Synuclein induced synaptopathy in parkinson's disease', *Frontiers in Neuroscience*, 12(FEB), pp. 1–18. doi: 10.3389/fnins.2018.00080.

Bridi, Jessika C and Hirth, F. (2018) 'Mechanisms of α -Synuclein Induced Synaptopathy in Parkinson ' s Disease', 12(February), pp. 1–18. doi: 10.3389/fnins.2018.00080.

Britt, J. P. *et al.* (2012) 'Synaptic and Behavioral Profile of Multiple Glutamatergic Inputs to the Nucleus Accumbens', *Neuron*. Elsevier Inc., 76(4), pp. 790–803. doi: 10.1016/j.neuron.2012.09.040.

Brown, D. A. and Passmore, G. M. (2009) 'Neural KCNQ (Kv7) channels',

British Journal of Pharmacology, 156(8), pp. 1185–1195. doi: 10.1111/j.1476-5381.2009.00111.x.

Burg, E. D., Remillard, C. V. and Yuan, J. X. J. (2006) 'K+ channels in apoptosis', *Journal of Membrane Biology*, 209(1), pp. 3–20. doi: 10.1007/s00232-005-0838-4.

Calabresi, P. *et al.* (2000) *Synaptic transmission in the striatum: From plasticity to neurodegeneration*, *Progress in Neurobiology*. doi: 10.1016/S0301-0082(99)00030-1.

Castellani, R. J., Rolston, R. K. and Smith, M. A. (2011) 'Alzheimer Disease author manuscript', 56(9), pp. 1–60. doi: 10.1016/j.disamonth.2010.06.001.Alzheimer.

Catacuzzeno, L., Sforna, L. and Franciolini, F. (2020) 'Voltage-dependent gating in K channels: experimental results and quantitative models', *Pflugers Archiv European Journal of Physiology*, 472(1), pp. 27–47. doi: 10.1007/s00424-019-02336-6.

Cauli, B. *et al.* (2004) 'Cortical GABA interneurons in neurovascular coupling: Relays for subcortical vasoactive pathways', *Journal of Neuroscience*, 24(41), pp. 8940–8949. doi: 10.1523/JNEUROSCI.3065-04.2004.

Cianciulli, A. *et al.* (2020) 'Microglia mediated neuroinflammation: Focus on PI3K modulation', *Biomolecules*, 10(1), pp. 1–19. doi: 10.3390/biom10010137.

Cline, E. N. *et al.* (2018) 'The Amyloid-β Oligomer Hypothesis: Beginning of the Third Decade', *Journal of Alzheimer's Disease*, 64(s1), pp. S567–S610. doi: 10.3233/JAD-179941.

Cotella, D. *et al.* (2012) 'Toxic role of K + channel oxidation in mammalian

brain', *Journal of Neuroscience*, 32(12), pp. 4133–4144. doi: 10.1523/JNEUROSCI.6153-11.2012.

Cowan, R. L. *et al.* (1990) 'Parvalbumin-containing gabaergic interneurons in the rat neostriatum', *Journal of Comparative Neurology*, 302(2), pp. 197–205. doi: 10.1002/cne.903020202.

Danese, A. and J Lewis, S. (2017) 'Psychoneuroimmunology of Early-Life Stress: The Hidden Wounds of Childhood Trauma', *Neuropsychopharmacology*. Nature Publishing Group, 42(1), pp. 99–114. doi: 10.1038/npp.2016.198.

Dehmelt, L. and Halpain, S. (2005) 'The MAP2/Tau family of microtubule-associated proteins', *Genome Biology*, 6(1), pp. 1–10. doi: 10.1186/gb-2004-6-1-204.

Dijkstra, A. A. *et al.* (2015) 'Evidence for immune response, axonal dysfunction and reduced endocytosis in the substantia nigra in early stage Parkinson's disease', *PLoS ONE*, 10(6), pp. 1–21. doi: 10.1371/journal.pone.0128651.

Dimitrov, E. and Usdin, T. B. (2010) 'Tuberoinfundibular peptide of 39 residues modulates the mouse hypothalamic-pituitary-adrenal axis via paraventricular glutamatergic neurons', *Journal of Comparative Neurology*, 518(21), pp. 4375–4394. doi: 10.1002/cne.22462.

Du, J. *et al.* (1998) 'The K+ channel, Kv2.1, is apposed to astrocytic processes and is associated with inhibitory postsynaptic membranes in hippocampal and cortical principal neurons and inhibitory interneurons', *Neuroscience*, 84(1), pp. 37–48. doi: 10.1016/S0306-4522(97)00519-8.

Durán-González, J. *et al.* (2013) 'Amyloid β peptides modify the expression

of antioxidant repair enzymes and a potassium channel in the septohippocampal system', *Neurobiology of Aging*. doi: 10.1016/j.neurobiolaging.2013.02.005.

Ell, T. P. S. P. O. W. (1971) 'THE S T R U C T U R E OF THE C A U D A T E N U C L E U S OF TH E CAT : L IG H T AND E L E C T R O N M IC R O S C O P Y', 262(September), pp. 383–401.

Emson, P. C. *et al.* (1993) 'Chemical signalling and striatal interneurones', pp. 155–165.

Eyre, M. D. *et al.* (2012) 'Setting the time course of inhibitory synaptic currents by mixing multiple GABAA receptor α subunit isoforms', *Journal of Neuroscience*, 32(17), pp. 5853–5867. doi: 10.1523/JNEUROSCI.6495-11.2012.

Feng, J. *et al.* (2000) 'Spinophilin regulates the formation and function of dendritic spines', *Proceedings of the National Academy of Sciences of the United States of America*, 97(16), pp. 9287–9292. doi: 10.1073/pnas.97.16.9287.

Fenster, S. D. *et al.* (2000) 'Piccolo, a presynaptic zinc finger protein structurally related to Bassoon', *Neuron*, 25(1), pp. 203–214. doi: 10.1016/S0896-6273(00)80883-1.

Forloni, G. *et al.* (2016) 'Oligomeropathies and pathogenesis of Alzheimer and Parkinson's diseases', *Movement Disorders*, 31(6), pp. 771–781. doi: 10.1002/mds.26624.

Foust, A. J. *et al.* (2011) 'Somatic membrane potential and Kv1 channels control spike repolarization in cortical axon collaterals and presynaptic boutons', *Journal of Neuroscience*, 31(43), pp. 15490–15498. doi:

10.1523/JNEUROSCI.2752-11.2011.

Gerfen, C. R. *et al.* (1990) 'D1 and D2 dopamine receptor-regulated gene expression of striatonigral and striatopallidal neurons', *Science*, 250(4986), pp. 1429–1432. doi: 10.1126/science.2147780.

Gime, M. and Berna, J. (2012) 'Distribution of GABAergic Interneurons and Dopaminergic Cells in the Functional Territories of the Human Striatum', 7(1). doi: 10.1371/journal.pone.0030504.

Goedert, M., Jakes, R. and Spillantini, M. G. (2017) 'The Synucleinopathies: Twenty Years on', *Journal of Parkinson's Disease*, 7(s1), pp. S53–S71. doi: 10.3233/JPD-179005.

Goldstein, S. A. N. *et al.* (2005) 'Nomenclature and Molecular Relationships of Two-P Potassium Channels', *Pharmacological Reviews*, 57(4), pp. 527–540. doi: 10.1124/pr.57.4.12.1.

Graybiel, A. M. (1990) 'Neurotransmitters and modultaors of the basal ganglia', *Tins*, 13(7).

Gunn, B. G. *et al.* (2013) 'Dysfunctional astrocytic and synaptic regulation of hypothalamic glutamatergic transmission in a mouse model of early-life adversity: Relevance to neurosteroids and programming of the stress response', *Journal of Neuroscience*, 33(50), pp. 19534–19554. doi: 10.1523/JNEUROSCI.1337-13.2013.

Guo, Q. *et al.* (2015) 'Whole-Brain Mapping of Inputs to Projection Neurons and Cholinergic Interneurons in the Dorsal Striatum', pp. 1–15. doi: 10.1371/journal.pone.0123381.

Gutman, G. A. *et al.* (2005) 'Nomenclature and molecular relationships of voltage-gated potassium channels.', *Pharmacological Reviews*, 57(4), pp.

473–508. doi: 10.1124/pr.57.4.10.1.

Hardy, J. and Selkoe, D. J. (2002) ‘The amyloid hypothesis of Alzheimer’s disease: Progress and problems on the road to therapeutics’, *Science*, 297(5580), pp. 353–356. doi: 10.1126/science.1072994.

Harper, J. D. and Lansbury, P. T. (1997) ‘MODELS OF AMYLOID SEEDING IN ALZHEIMER’S DISEASE AND SCRAPIE:Mechanistic Truths and Physiological Consequences of the Time-Dependent Solubility of Amyloid Proteins’, *Annual Review of Biochemistry*, 66(1), pp. 385–407. doi: 10.1146/annurev.biochem.66.1.385.

Härtig, W. *et al.* (2007) ‘Hibernation model of tau phosphorylation in hamsters: Selective vulnerability of cholinergic basal forebrain neurons - Implications for Alzheimer’s disease’, *European Journal of Neuroscience*, 25(1), pp. 69–80. doi: 10.1111/j.1460-9568.2006.05250.x.

Hawkes, C. H., Del Tredici, K. and Braak, H. (2010) ‘A timeline for Parkinson’s disease’, *Parkinsonism and Related Disorders*. Elsevier Ltd, 16(2), pp. 79–84. doi: 10.1016/j.parkreldis.2009.08.007.

Hemmings, H. C. and Greengard, P. (1986) ‘DARPP-32, a dopamine-regulated phosphoprotein’, *Progress in Brain Research*, 69(C), pp. 149–159. doi: 10.1016/S0079-6123(08)61056-0.

Holt, D. J., Graybiel, A. M. and Saper, C. B. (1997) ‘Neurochemical architecture of the human striatum’, *Journal of Comparative Neurology*, 384(1), pp. 1–25. doi: 10.1002/(SICI)1096-9861(19970721)384:1<1::AID-CNE1>3.0.CO;2-5.

Hopp, S. C. (2020) ‘Targeting microglia L-type voltage-dependent calcium channels for the treatment of central nervous system disorders’, *Journal of*

Neuroscience Research, (January), pp. 1–22. doi: 10.1002/jnr.24585.

Hossain, M. M. *et al.* (2018) 'The anti-parkinsonian drug zonisamide reduces neuroinflammation: Role of microglial Na v 1.6', *Experimental Neurology*. Academic Press Inc., 308, pp. 111–119. doi: 10.1016/j.expneurol.2018.07.005.

Hsiao, K. *et al.* (1996) 'Amyloid Plaques in Transgenic Mice', *Science*, 274(October), pp. 99–102.

Huang, Y., Chan, P. and Halliday, G. (2007) 'Genetics of Parkinson's disease', *Oxidative Stress and Neurodegenerative Disorders*, pp. 663–697. doi: 10.1016/B978-044452809-4/50169-1.

Hunnicutt, B. J. *et al.* (2016) 'A comprehensive excitatory input map of the striatum reveals novel functional organization', pp. 1–32. doi: 10.7554/eLife.19103.

Jamebozorgi, K. *et al.* (2018) 'Cellular and Molecular Aspects of Parkinson Treatment : Future Therapeutic Perspectives'. Molecular Neurobiology.

Janezic, S. *et al.* (2013) 'Deficits in dopaminergic transmission precede neuron loss and dysfunction in a new Parkinson model', *Proceedings of the National Academy of Sciences of the United States of America*, 110(42). doi: 10.1073/pnas.1309143110.

Jiang, P. *et al.* (2013) 'hESC-derived Olig2+ progenitors generate a subtype of astroglia with protective effects against ischaemic brain injury', *Nature Communications*. Nature Publishing Group, 4, pp. 1–16. doi: 10.1038/ncomms3196.

Joers, V. *et al.* (2017) 'Microglial phenotypes in Parkinson's disease and animal models of the disease', *Progress in Neurobiology*, 155, pp. 57–75.

doi: 10.1016/j.pneurobio.2016.04.006.

John R.Giudicessi, BA.Michael J.Ackerman., 2013 (2008) '基因的改变NIH Public Access', *Bone*, 23(1), pp. 1–7. doi: 10.1038/jid.2014.371.

Kaczmarek, L. K. (2006) 'Non-conducting functions of voltage-gated ion channels', *Nature Reviews Neuroscience*, 7(10), pp. 761–771. doi: 10.1038/nrn1988.

Kaur, R., Mehan, S. and Singh, S. (2018) 'Understanding multifactorial architecture of Parkinson ' s disease : pathophysiology to management'.

Kawaguchi, Y. *et al.* (1995) 'Striatal interneurones: chemical, physiological and morphological characterization', *Trends in Neurosciences*, 18(12), pp. 527–535. doi: 10.1016/0166-2236(95)98374-8.

Kawaguchi, Y. (1997) 'Neostriatal cell subtypes and their functional roles', 27, pp. 1–8.

Kemp, J.M., and Powell, T. P. (1971) 'THE S T R U C T U R E OF THE C A U D A T E N U C L E U S OF TH E CAT : L IG H T AND E L E C T R O N M IC R O S C O P Y', 262(September), pp. 383–401.

Kemp, J. M. and Powell, T. P. S. (1970) 'The cortico-striate projection in the monkey', *Brain*, 93(3), pp. 525–546. doi: 10.1093/brain/93.3.525.

Kerti, K., Lorincz, A. and Nusser, Z. (2012) 'Unique somato-dendritic distribution pattern of Kv4.2 channels on hippocampal CA1 pyramidal cells', *European Journal of Neuroscience*, 35(1), pp. 66–75. doi: 10.1111/j.1460-9568.2011.07907.x.

De Kloet, E. R., Joëls, M. and Holsboer, F. (2005) 'Stress and the brain: From adaptation to disease', *Nature Reviews Neuroscience*, 6(6), pp. 463–475. doi: 10.1038/nrn1683.

Kotecha, S. A. and Schlichter, L. C. (1999) ‘A Kv1.5 to Kv1.3 Switch in endogenous hippocampal microglia and a role in proliferation’, *Journal of Neuroscience*, 19(24), pp. 10680–10693. doi: 10.1523/jneurosci.19-24-10680.1999.

Kumar, P., Kumar, D., Jha, S. K., Jha, N. K. and Ambasta, Rashmi K (2016) *Ion Channels in Neurological Disorders*. 1st edn, *Ion channels as therapeutic targets*. 1st edn. Elsevier Inc. doi: 10.1016/bs.apcsb.2015.10.006.

Kumar, P., Kumar, D., Jha, S. K., Jha, N. K. and Ambasta, Rashmi K. (2016) *Ion Channels in Neurological Disorders*. 1st edn, *Advances in Protein Chemistry and Structural Biology*. 1st edn. Elsevier Inc. doi: 10.1016/bs.apcsb.2015.10.006.

Lambert, M. P. *et al.* (2007) ‘Monoclonal antibodies that target pathological assemblies of Aβ’, *Journal of Neurochemistry*, 100(1), pp. 23–35. doi: 10.1111/j.1471-4159.2006.04157.x.

Lane, C. A., Hardy, J. and Schott, J. M. (2018) ‘Alzheimer’s disease’, *European Journal of Neurology*, 25(1), pp. 59–70. doi: 10.1111/ene.13439.

Larson, M. E. *et al.* (2012) ‘Soluble α-synuclein is a novel modulator of alzheimer’s disease pathophysiology’, *Journal of Neuroscience*, 32(30), pp. 10253–10266. doi: 10.1523/JNEUROSCI.0581-12.2012.

Lemos, J. C. *et al.* (2012) ‘Severe stress switches CRF action in the nucleus accumbens from appetitive to aversive’, *Nature*. Nature Publishing Group, 490(7420), pp. 402–406. doi: 10.1038/nature11436.

Li, Xiantao *et al.* (2015) ‘Overexpression of tau downregulated the mRNA levels of Kv channels and improved proliferation in N2A cells’, *PLoS ONE*, 10(1), pp. 1–15. doi: 10.1371/journal.pone.0116628.

Lorincz, A. and Nusser, Z. (2008) 'Cell-Type-Dependent Molecular Composition of the Axon Initial Segment', *Journal of Neuroscience*. Society for Neuroscience, 28(53), pp. 14329–14340. doi: 10.1523/jneurosci.4833-08.2008.

Lorincz, Andrea and Nusser, Z. (2008) 'Specificity of immunoreactions: The importance of testing specificity in each method', *Journal of Neuroscience*, 28(37), pp. 9083–9086. doi: 10.1523/JNEUROSCI.2494-08.2008.

Lorincz, A. and Nusser, Z. (2013) 'Europe PMC Funders Group Molecular Identity of Dendritic Voltage-Gated Sodium Channels', 328(5980), pp. 906–909. doi: 10.1126/science.1187958.Molecular.

Lotharius, J. and Brundin, P. (2002) 'Pathogenesis of parkinson's disease: Dopamine, vesicles and α-synuclein', *Nature Reviews Neuroscience*, pp. 932–942. doi: 10.1038/nrn983.

Luján, R. (2010) 'Organisation of potassium channels on the neuronal surface', *Journal of Chemical Neuroanatomy*, pp. 1–20. doi: 10.1016/j.jchemneu.2010.03.003.

Maroteaux, L., Campanelli, J. T. and Scheller, R. H. (1988) 'Synuclein: A neuron-specific protein localized to the nucleus and presynaptic nerve terminal', *Journal of Neuroscience*, 8(8), pp. 2804–2815. doi: 10.1523/jneurosci.08-08-02804.1988.

Mattson, M. P. (1997) 'Cellular actions of β-amyloid precursor protein and its soluble and fibrillogenic derivatives', *Physiological Reviews*, 77(4), pp. 1081–1132. doi: 10.1152/physrev.1997.77.4.1081.

McGeer, P. L. *et al.* (1971) 'Neostriatal choline acetylase and cholinesterase following selective brain lesions', *Brain Research*, 35(1), pp. 308–314. doi:

10.1016/0006-8993(71)90625-1.

Mcrae, D. (2003) ‘How to teach better teacher learning’, *Nature Neuroscience*, 15(11), pp. 1475–1484. doi: 10.1038/nn.3234.Neurobiology.

Michaely, P. *et al.* (2002) ‘Crystal structure of a 12 ANK repeat stack from human ankyrinR’, *EMBO Journal*, 21(23), pp. 6387–6396. doi: 10.1093/emboj/cdf651.

Miraglia, F. *et al.* (1997) ‘Subcellular localization of alpha-synuclein aggregates and their interaction with membranes’, 53. doi: 10.4103/1673-5374.235013.

Misonou, H., Mohapatra, D. P. and Trimmer, J. S. (2005) ‘Kv2.1: A voltage-gated K+ channel critical to dynamic control of neuronal excitability’, *NeuroToxicology*, 26(5), pp. 743–752. doi: 10.1016/j.neuro.2005.02.003.

Mitchell, S. J. *et al.* (2018) ‘Early-life adversity selectively impairs α2-GABAA receptor expression in the mouse nucleus accumbens and influences the behavioral effects of cocaine’, *Neuropharmacology*, 141(August), pp. 98–112. doi: 10.1016/j.neuropharm.2018.08.021.

Miura, E. *et al.* (2006) ‘Expression and distribution of JNK/SAPK-associated scaffold protein JSAP1 in developing and adult mouse brain’, *Journal of Neurochemistry*, 97(5), pp. 1431–1446. doi: 10.1111/j.1471-4159.2006.03835.x.

Miyazaki, T. *et al.* (2003) ‘Subtype switching of vesicular glutamate transporters at parallel fibre-Purkinje cell synapses in developing mouse cerebellum’, *European Journal of Neuroscience*, 17(12), pp. 2563–2572. doi: 10.1046/j.1460-9568.2003.02698.x.

Muñoz-Manchado, A. B. *et al.* (2018) ‘Diversity of Interneurons in the Dorsal

Striatum Revealed by Single-Cell RNA Sequencing and PatchSeq', *Cell Reports*, 24(8), pp. 2179-2190.e7. doi: 10.1016/j.celrep.2018.07.053.

Murphy, M. P. and Levine, H. (2010) 'Alzheimer's Disease and the Beta-Amyloid Peptide', *Journal of Alzheimer's Disease*, 19(1), pp. 1–17. doi: 10.3233/JAD-2010-1221.Alzheimer.

Muzerelle, A. *et al.* (2016) 'Conditional anterograde tracing reveals distinct targeting of individual serotonin cell groups (B5–B9) to the forebrain and brainstem', *Brain Structure and Function*, 221(1), pp. 535–561. doi: 10.1007/s00429-014-0924-4.

Myöhänen, T. T. *et al.* (2008) 'Spatial association of prolyl oligopeptidase, inositol 1,4,5-triphosphate type 1 receptor, substance P and its neurokinin-1 receptor in the rat brain: An immunohistochemical colocalization study', *Neuroscience*, 153(4), pp. 1177–1189. doi: 10.1016/j.neuroscience.2008.02.047.

Nemani, V. M. *et al.* (2010) 'Increased Expression of α-Synuclein Reduces Neurotransmitter Release by Inhibiting Synaptic Vesicle Reclustering after Endocytosis', *Neuron*. Elsevier Ltd, 65(1), pp. 66–79. doi: 10.1016/j.neuron.2009.12.023.

Nguyen, H. M. *et al.* (2017) 'Differential Kv1.3, KCa3.1, and Kir2.1 expression in "classically" and "alternatively" activated microglia', *Glia*, 65(1), pp. 106–121. doi: 10.1002/glia.23078.

O'Neil, J. N. *et al.* (2007) 'Catecholaminergic neuronal loss in locus coeruleus of aged female dtg APP/PS1 mice', *Journal of Chemical Neuroanatomy*, 34(3–4), pp. 102–107. doi: 10.1016/j.jchemneu.2007.05.008.

Osterhaus, A. *et al.* (1997) 'a -Synuclein in Lewy bodies Endogenous

proviruses as “ mementos ”?’, *Nature*, 388, pp. 839–840.

Perez, R. G. *et al.* (2002) ‘Erratum: “A role for α-synuclein in the regulation of dopamine biosynthesis” The Journal of Neuroscience (April 15, 2002) (3090-3099))’, *Journal of Neuroscience*, 22(20), p. 9142. doi: 10.1523/JNEUROSCI.22-20-09142.2002.

Polymeropoulos, M. H. *et al.* (1997) ‘Mutation in the α-synuclein gene identified in families with Parkinson’s disease’, *Science*, 276(5321), pp. 2045–2047. doi: 10.1126/science.276.5321.2045.

Rhodes, K. J. *et al.* (1997) ‘Association and colocalization of the Kvβ1 and Kvβ2 β-subunits with Kv1 α-subunits in mammalian brain K+ channel complexes’, *Journal of Neuroscience*, pp. 8246–8258. doi: 10.1523/jneurosci.17-21-08246.1997.

Rice, C. J. *et al.* (2008) ‘A novel mouse model for acute and long-lasting consequences of early life stress’, *Endocrinology*, 149(10), pp. 4892–4900. doi: 10.1210/en.2008-0633.

Rudy, B. (1988) ‘COMMENTARY DIVERSITY AND UBIQUITY OF K CHANNELS 6 . MODULATION OF K CHANNELS BY NEUROTRANSMITTERS AND’, 25(3), pp. 729–749.

Satake, W. *et al.* (2009) ‘Genome-wide association study identifies common variants at four loci as genetic risk factors for Parkinson’s disease’, *Nature Genetics*. Nature Publishing Group, 41(12), pp. 1303–1307. doi: 10.1038/ng.485.

Schock, S. C. *et al.* (2012) ‘Development of dissociated cryopreserved rat cortical neurons in vitro’, *Journal of Neuroscience Methods*. Elsevier B.V., 205(2), pp. 324–333. doi: 10.1016/j.jneumeth.2012.01.016.

Serrano-Pozo, A. *et al.* (2011) 'Neuropathological alterations in Alzheimer disease', *Cold Spring Harbor Perspectives in Medicine*, 1(1), pp. 1–23. doi: 10.1101/cshperspect.a006189.

Shah, N. H. and Aizenman, E. (2014) 'Voltage-Gated Potassium Channels at the Crossroads of Neuronal Function, Ischemic Tolerance, and Neurodegeneration', *Translational Stroke Research*, 5(1), pp. 38–58. doi: 10.1007/s12975-013-0297-7.

Tanzi, R. E. *et al.* (1987) 'Amyloid β protein gene: CDNA, mRNA distribution, and genetic linkage near the Alzheimer locus', *Science*, 235(4791), pp. 880–884. doi: 10.1126/science.2949367.

Tigner, M. and Cornell, U. (no date) 'Chapter 6 . ELECTRICAL CONSIDERATIONS'.

Trimmer, J. S. (2015) 'Subcellular localization of K+ channels in mammalian brain neurons: Remarkable precision in the midst of extraordinary complexity', *Neuron*. Cell Press, pp. 238–256. doi: 10.1016/j.neuron.2014.12.042.

Trimmer, J. S. and Rhodes, K. J. (2004) 'L OCALIZATION OF V OLTAGE -G ATED I ON C HANNELS IN M AMMALIAN B RAIN', (1), pp. 477–519. doi: 10.1146/annurev.physiol.66.032102.113328.

Truban, D. *et al.* (2017) 'PINK1, Parkin, and Mitochondrial Quality Control: What can we Learn about Parkinson's Disease Pathobiology?', *Journal of Parkinson's Disease*, 7(1), pp. 13–29. doi: 10.3233/JPD-160989.

Tzour, A. *et al.* (2017) 'KV7/M channels as targets for lipopolysaccharide-induced inflammatory neuronal hyperexcitability', *Journal of Physiology*, 595(3), pp. 713–738. doi: 10.1113/JP272547.

Vacher, H., Mohapatra, D. P. and Trimmer, J. S. (2008) 'Localization and Targeting of Voltage-Dependent Ion Channels in Mammalian Central Neurons', *Physiological Reviews*. American Physiological Society, 88(4), pp. 1407–1447. doi: 10.1152/physrev.00002.2008.

Vereczki, V. K. *et al.* (2016) 'Synaptic organization of perisomatic gabaergic inputs onto the principal cells of the mouse basolateral amygdala', *Frontiers in Neuroanatomy*, 10(MAR). doi: 10.3389/fnana.2016.00020.

Villa, C. *et al.* (2020) 'Potassium channels in the neuronal homeostasis and neurodegenerative pathways underlying Alzheimer's disease: An update', *Mechanisms of Ageing and Development*. Elsevier, 185(September 2019), p. 111197. doi: 10.1016/j.mad.2019.111197.

Viviani, B., Gardoni, F. and Marinovich, M. (2007) 'CYTOKINES AND NEURONAL ION CHANNELS IN', 82(07). doi: 10.1016/S0074-7742(07)82013-7.

Vizcaya-ruiz, A. De and Camacho, J. (2010) 'Ion channels in toxicology', (May), pp. 497–512. doi: 10.1002/jat.1556.

Wainer, B. H. *et al.* (1984) 'Cholinergic synapses in the rat brain: a correlated light and electron microscopic immunohistochemical study employing a monoclonal antibody against choline acetyltransferase', *Brain Research*, 308(1), pp. 69–76. doi: 10.1016/0006-8993(84)90918-1.

Watanabe, M. *et al.* (1998) 'Selective scarcity of NMDA receptor channel subunits in the stratum lucidum (mossy fibre-recipient layer) of the mouse hippocampal CA3 subfield', *European Journal of Neuroscience*, 10(2), pp. 478–487. doi: 10.1046/j.1460-9568.1998.00063.x.

Wei, A. D. *et al.* (2005) ' Nomenclature and Molecular Relationships of

Calcium-Activated Potassium Channels', *Pharmacological Reviews*, 57(4), pp. 463–472. doi: 10.1124/pr.57.4.9.1.

Weiser, M. *et al.* (1994) 'Differential expression of Shaw-related K+ channels in the rat central nervous system', *Journal of Neuroscience*, 14(3 I), pp. 949–972. doi: 10.1523/jneurosci.14-03-00949.1994.

Whitehouse, P. J. *et al.* (1981) 'Alzheimer disease: Evidence for selective loss of cholinergic neurons in the nucleus basalis', *Annals of Neurology*, 10(2), pp. 122–126. doi: 10.1002/ana.410100203.

Williams, D. R. and Litvan, I. (2013) 'Parkinsonian syndromes', *CONTINUUM Lifelong Learning in Neurology*, 19(5), pp. 1189–1212. doi: 10.1212/01.CON.0000436152.24038.e0.

Wilson, C. J., Chang, H. T. and Kitai, S. T. (1990) 'Firing patterns and synaptic potentials of identified giant aspiny interneurons in the rat neostriatum', *Journal of Neuroscience*, 10(2), pp. 508–519. doi: 10.1523/jneurosci.10-02-00508.1990.

Wilson, C. J. and Groves, P. M. (1980) 'Fine structure and synaptic connections of the common spiny neuron of the rat neostriatum: A study employing intracellular injection of horseradish peroxidase', *Journal of Comparative Neurology*, 194(3), pp. 599–615. doi: 10.1002/cne.901940308.

Wood, S. J. *et al.* (1999) 'α-Synuclein fibrillogenesis is nucleation-dependent: Implications for the pathogenesis of Parkinson's disease', *Journal of Biological Chemistry*, 274(28), pp. 19509–19512. doi: 10.1074/jbc.274.28.19509.

Wood, S. K. *et al.* (2015) 'Inflammatory factors mediate vulnerability to a social stress-induced depressive-like phenotype in passive Coping Rats',

Biological Psychiatry. Elsevier Inc., 78(1), pp. 38–48. doi: 10.1016/j.biopsych.2014.10.026.

Yanagi, M. *et al.* (2014) 'Kv3.1-containing K+ channels are reduced in untreated schizophrenia and normalized with antipsychotic drugs', *Molecular Psychiatry*. Nature Publishing Group, 19(5), pp. 573–579. doi: 10.1038/mp.2013.49.

Yang, R. *et al.* (2019) 'Neurodevelopmental mutation of giant ankyrin-G disrupts a core mechanism for axon initial segment assembly', *Proceedings of the National Academy of Sciences of the United States of America*, 116(39), pp. 19717–19726. doi: 10.1073/pnas.1909989116.

Yang, Z., You, Y. and Levison, S. W. (2008) 'Neonatal hypoxic/ischemic brain injury induces production of calretinin-expressing interneurons in the striatum', *Journal of Comparative Neurology*, 511(1), pp. 19–33. doi: 10.1002/cne.21819.

Zahm, D. S. (2000) 'An integrative neuroanatomical perspective on some subcortical substrates of adaptive responding with emphasis on the nucleus accumbens', in *Neuroscience and Biobehavioral Reviews*, pp. 85–105. doi: 10.1016/S0149-7634(99)00065-2.

Zeng, X. *et al.* (2018) 'Cellular and Molecular Basis of Neurodegeneration in Parkinson Disease', 10(April), pp. 1–16. doi: 10.3389/fnagi.2018.00109.

Zhao, Y. and Zhao, B. (2013) 'Oxidative stress and the pathogenesis of alzheimer's disease', *Oxidative Medicine and Cellular Longevity*, 2013. doi: 10.1155/2013/316523.

Appendix

FORM UPR16

Research Ethics Review Checklist

Please include this completed form as an appendix to your thesis (see the Research Degrees Operational Handbook for more information

UNIVERSITY OF PORTSMOUTH

Postgraduate Research Student (PGRS) Information				**Student ID:**	834849
PGRS Name:	Babajide Otuyemi				
Department:	PhBM		**First Supervisor:**	Dr Jerome Swinny	
Start Date: (or progression date for Prof Doc students)			**01.10.2016**		
Study Mode and Route:	Part-time ☐	Full-time ☒	MPhil ☐	PhD ☒	MD ☐ Professional Doctorate ☐

Title of Thesis:	Native expression of voltage-gated potassium channels in the mouse striatum and their plasticity in models of Parkinson's and Alzheimer's diseases
Thesis Word Count: (excluding ancillary data)	28,844

If you are unsure about any of the following, please contact the local representative on your Faculty Ethics Committee for advice. Please note that it is your responsibility to follow the University's Ethics Policy and any relevant University, academic or professional guidelines in the conduct of your study

Although the Ethics Committee may have given your study a favourable opinion, the final responsibility for the ethical conduct of this work lies with the researcher(s).

UKRIO Finished Research Checklist:
(If you would like to know more about the checklist, please see your Faculty or Departmental Ethics Committee rep or see the online version of the full checklist at: http://www.ukrio.org/what-we-do/code-of-practice-for-research/)

a) Have all of your research and findings been reported accurately, honestly and within a reasonable time frame?	YES ☒ NO ☐
b) Have all contributions to knowledge been acknowledged?	YES ☒ NO ☐
c) Have you complied with all agreements relating to intellectual property, publication and authorship?	YES ☒ NO ☐
d) Has your research data been retained in a secure and accessible form and will it remain so for the required duration?	YES ☒ NO ☐
e) Does your research comply with all legal, ethical, and contractual requirements?	YES ☒ NO ☐

Candidate Statement:

I have considered the ethical dimensions of the above named research project, and have successfully obtained the necessary ethical approval(s)

Ethical review number(s) from Faculty Ethics Committee (or from NRES/SCREC):	

If you have *not* submitted your work for ethical review, and/or you have answered 'No' to one or more of questions a) to e), please explain below why this is so:

All of the research described in this thesis was undertaken by Babajide Otuyemi under the project license of Dr Jerome Swinny (PPL 70/8459), and in accordance with the Animals (Scientific Procedures) Act 1986 and the European Directive 2010/63/EU on the protection of animals used for scientific purposes.

Signed *(PGRS)*:	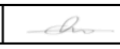	**Date:** 28.04.2020